

Self-similar orbit-averaged Fokker-Planck equation for isotropic spherical dense clusters (i) accurate pre-collapse solution

Yuta Ito^{a,b}

^a*Department of Physics, CUNY Graduate Center, [☆]*

^b*Department of Engineering and Physics, CUNY College of Staten Island^{☆☆}*

Abstract

This is the first paper of a series of our works on the self-similar orbit-averaged Fokker-Planck (OAFP) equation for distribution function of stars in dense isotropic star clusters. At the late stage of relaxation evolution of the clusters, standard stellar dynamics predicts that the clusters evolve in a self-similar fashion forming collapsing cores. However, the corresponding mathematical model, the self-similar OAFP equation, has never been solved on the whole energy domain ($-1 < E < 0$). The existing works based on kinds of finite difference methods provide solutions only on the truncated domain $-1 < E < -0.2$. To broaden the range of the truncated domain, the present work resorts to a (highly accurate and efficient) Gauss-Chebyshev pseudo-spectral method. We provide a spectral solution, whose number of significant figures is four, on the whole domain. Also, the solution can reduce to a semi-analytical form whose degree of polynomials is only eighteen holding three significant figures. We also provide the new eigenvalues; $c_1 = 9.0925 \times 10^{-4}$, $c_2 = 1.1118 \times 10^{-4}$, $c_3 = 7.1975 \times 10^{-2}$ and $c_4 = 3.303 \times 10^{-2}$, corresponding to the core collapse rate $\xi = 3.64 \times 10^{-3}$, scaled escape energy $\chi_{\text{esc}} = 13.881$ and power-law exponent $\alpha = 2.2305$. Since the solution on the whole domain is unstable against degree of Chebyshev polynomials, we also provide spectral solutions on truncated domains ($-1 < E < E_{\text{max}}$, where $-0.35 < E_{\text{max}} < -0.03$) to explain how to handle the instability. By reformulating the OAFP equation in several ways, we improve the accuracy of the spectral solution and reproduce an existing self-similar solution, which infers that existing solutions have only one significant figure at best.

Keywords: dense star cluster; core collapse; self-similar evolution; orbit-averaged Fokker-Planck model; isotropic; numerical; pseudo-spectral method; Gauss-Chebyshev polynomial

1. Introduction

The present paper is the first paper for a series of our works on the self-similar orbit-averaged Fokker-Planck (ss-OAFP) equation and shows an accurate Gauss-Chebyshev spectral solution for pre-collapse stage of relaxation evolution of isotropic star clusters. In the second paper (Ito, 2020a) and third paper (Ito, 2020b), we will discuss the physical properties of the ss-OAFP model focusing on the negative heat capacity of the core and application to the observed structural profiles of Galactic globular clusters with resolved cores.

The relaxation evolution of core-collapsing dense star clusters (e.g. globular clusters) can not result in a state of thermal equilibrium of stars due to the ‘negative’ heat capacity; as relaxation processes mostly in the core cause stars and kinetic energy to flow from the core to the halo, the core heats up and halo cools down. Once the core density reaches so high that the cluster undergoes the gravothermal instability (Antonov, 1985), it begins to show a self-similar density profile in the core and inner halo (Lynden-Bell and Eggleton, 1980). Without existence of primordial binary stars or formation and growth of binary stars, the most probable distribution of stars, still in sense of increment of Boltzmann entropy for distribution function (DF) of stars, is a core-collapsed (infinite-density) profile

[☆]365 Fifth Avenue, New York, NY 10016, USA

^{☆☆}2800 Victory Boulevard, Staten Island, NY 10314, USA

Email address: yito@gradcenter.cuny.edu (Yuta Ito)

that can be achieved during a finite time duration at the late stage of the self-similar evolution (Hénon, 1961; Cohn, 1980). While the core-collapsing self-similar profile of stars is just a mathematical idealization, it has been one's concern (e.g. Baumgardt et al., 2003; Szell et al., 2005; Pavlík and Šubr, 2018) since it can provide, in addition to conceptual understandings of the late stage of relaxation evolution, the (asymptotic value of) physical parameters to characterize the evolution; the core collapse rate ξ , the power-law index α in spatial density profile and scaled escape energy χ_{esc} in energy distribution function (Heggie and Stevenson, 1988). In the rest of the present section, we explain OAFP equation (Section 1.1), its self-similar form (Section 1.2) and numerical difficulty in integration of the ss-OAFP equation (Section 1.3).

1.1. Orbit-averaged Fokker-Planck (OAFP) equation

The ideal model of a dense star cluster would be a collection of N equal-mass stars that is isotropic in velocity space and spherical in configuration space; the model can provide a good qualitative understandings of relaxation evolution (Cohn, 1980; Takahashi, 1995).¹ Since the total number N of stars in a typical globular cluster is relatively high ($N \approx 10^4 \sim 10^6$), one may assume that the orbits of stars are dominated by the self-consistent mean field (m.f.) Newtonian potential $\psi(r)$ on crossing time scales (t_{dyn}) in zeroth-order of $1/N$ ($N \rightarrow \infty$) or *collisionless* limit (Jeans, 1902). Due to the nature of the long-range interacting stars, the DF of stars may be considered to reach a state of quasi-stationary equilibrium (Virial-equilibrium) through the rapid fluctuation in m.f. potential ('violent relaxation', phase- or chaotic- mixing, ...). Hence, by assuming that the m.f. potential is regular, the strong Jeans theorem (e.g. Binney and Tremaine, 2011) may allow one to simplify the phase-space probability DF at time t as $f(\mathbf{r}, \mathbf{v}, t) \approx f(\epsilon)$ for the isotropic system in which the energy of star per unit mass is as follows $\epsilon = \psi(\mathbf{r}, t) + \frac{\mathbf{v}^2}{2}$ where \mathbf{r} and \mathbf{v} are stellar position and velocity.

This collisionless dynamical-evolution scenario breaks down on relaxation time scales ($t_{\text{sec}} \sim N t_{\text{dyn}} / \ln[N]$) due to the effect of finiteness of total number N of stars; the 'smooth' orbits of stars are gradually changed due to (stochastic) irregular forces via many-body Newtonian interaction and the system could reach various quasi-stationary states. In this sense, the explicit time-dependence of DF may be retrieved ($f(\mathbf{r}, \mathbf{v}, t) \approx f(\epsilon, t)$) and the m.f. potential is to be determined by Poisson equation

$$\frac{\partial^2 \psi}{\partial r^2} + \frac{2}{r} \frac{\partial \psi}{\partial r} = \rho[\psi(r, t)] \equiv 16\pi^2 G m \int_{\psi(r, t)}^0 f(\epsilon, t) \sqrt{2\epsilon' - 2\psi(r, t)} d\epsilon'. \quad (1.1)$$

Stellar dynamicists have conventionally modeled the effect of many-body interaction, in first-order approximation of $1/N$,² as a (cumulative) weak two-body encounter with a homogeneous background approximation. The corresponding time-evolution model of DF is a (nonlinear) Fokker-Planck equation averaged over the radial period between the apocenter and pericenter of the orbits, which is known as the orbit-averaged Fokker-Planck (OAFP) equation (e.g. Hénon, 1961; Spitzer, 1988)

$$\frac{\partial f(\epsilon, t)}{\partial t} \frac{\partial q(\epsilon, t)}{\partial \epsilon} + \frac{\partial q(\epsilon, t)}{\partial t} \frac{\partial f(\epsilon, t)}{\partial \epsilon} = \Gamma \frac{\partial}{\partial \epsilon} \left\{ f(\epsilon, t) [f(\epsilon, t) q(\epsilon, t) - j(\epsilon, t)] + \frac{\partial f(\epsilon, t)}{\partial \epsilon} [i(\epsilon, t) + q(\epsilon, t) g(\epsilon, t)] \right\}, \quad (1.2a)$$

$$\Gamma \equiv (4\pi G m)^2 \ln N \quad (1.2b)$$

where G is the gravitational constant, and m the stellar mass. The q -integral (the integral associated with the radial action) reads

$$q(\epsilon, t) = \frac{1}{3} \int_0^{r_{\text{max}}(\epsilon, t)} [2\epsilon - 2\psi(r', t)]^{3/2} r'^2 dr', \quad (1.3)$$

¹More realistic star clusters must be modeled as anisotropic systems in velocity space based on statistical and dynamical principles (Polyachenko and Shukhman, 1982; Luciani and Pellat, 1987), numerical results (Cohn, 1979; Takahashi, 1995; Giersz and Spurzem, 1994; Baumgardt et al., 2002) and observation (Meylan, 1987; Meylan and Heggie, 1997).

²See (Gilbert, 1968; Ito, 2018a,b) for more statistically-exact treatment of $1/N$ -expansion in N -body Liouville equation which includes the effects of the inhomogeneity in encounter, gravitational polarization, statistical acceleration and/or strong encounter.

where $r_{\max}(\epsilon, t) = \psi^{-1}(\epsilon)$. The integrals associated with dynamical friction and energy diffusion read

$$i(\epsilon, t) \equiv \int_{-1}^{\epsilon} f(\epsilon', t) q(\epsilon', t) d\epsilon', \quad (1.4a)$$

$$j(\epsilon, t) \equiv \int_{-1}^{\epsilon} \frac{\partial f(\epsilon', t)}{\partial \epsilon'} q(\epsilon', t) d\epsilon', \quad (1.4b)$$

$$g(\epsilon, t) \equiv \int_{\epsilon}^0 f(\epsilon', t) d\epsilon', \quad (1.4c)$$

where $\psi(0) = -1$ is assumed.

1.2. Self-similar OAFP equation

The OAFP system (i.e. the system of OAFP equation (1.2a) and Poisson equation (1.1)) predicts that at the early stage of relaxation evolution the DF of stars may be characterized by a lowered-Maxwellian while at the late stage the cluster may undergo a self-similar evolution (Cohn, 1980). To reflect the self-similar evolution of a core-collapsing isotropic cluster, the following self-similar variables are employed in equations (1.2a) and (1.1) for independent variables concerned

$$E = \epsilon/E_c(t), \quad (1.5a)$$

$$R = r/r_c(t), \quad (1.5b)$$

and for dependent variables concerned

$$F(E) = f(\epsilon, t)/f_c(t), \quad (1.6a)$$

$$Q(E) = q(\epsilon, t)/q_c(t), \quad (1.6b)$$

$$\Psi(R) = \psi(r, t)/\psi_c(t), \quad (1.6c)$$

$$I(E) = i(\epsilon, t)/i_c(t), \quad (1.6d)$$

$$J(E) = j(\epsilon, t)/j_c(t), \quad (1.6e)$$

$$G(E) = g(\epsilon, t)/g_c(t), \quad (1.6f)$$

where suffice c means that the variables depend only on time t . Following (Heggie and Stevenson, 1988), one can obtain the ss-OAFP system; a system of four ordinary differential equations (4ODEs)

$$[I(E) + G(E)Q(E)] \frac{dF}{dE} = c_1 Q(E)F(E) + \frac{2c_1 - 3c_2}{4} J(E) - F(E) [F(E)Q(E) - J(E)], \quad (1.7a)$$

$$\frac{dG}{dE} = -F(E), \quad (1.7b)$$

$$\frac{dI}{dE} = Q(E)F(E), \quad (1.7c)$$

$$\frac{dJ}{dE} = Q(E) \frac{dF}{dE}, \quad (1.7d)$$

the Q -integral

$$Q(E) = \frac{1}{3} \int_0^{R_{\max}(E)} [2E - 2\Psi(R')]^{3/2} R'^2 dR', \quad (R_{\max}(E) = \Psi^{-1}(E)), \quad (1.8)$$

and Poisson equation

$$\frac{\partial^2 \Psi}{\partial R^2} + \frac{2}{R} \frac{\partial \Psi}{\partial R} = D[\Psi(R)] \equiv \int_{\Psi(R)}^0 F(E') \sqrt{2E' - 2\Psi(R)} dE'. \quad (1.9)$$

The self-similar parameters read

$$c_1 = \frac{1}{\Gamma f_c(t)} \frac{d}{dt} f_c(t), \quad (1.10a)$$

$$c_2 = \frac{1}{\Gamma f_c(t)} \frac{d}{dt} E_c(t), \quad (1.10b)$$

and the corresponding physical parameters concerned are

$$\alpha = \frac{2(3 + 2\beta)}{2\beta + 1}, \quad (1.11a)$$

$$\xi = \frac{c_1 + c_2}{0.167 \sqrt{\pi}}, \quad (1.11b)$$

$$\chi_{\text{esc}} = \frac{F_{\text{BC}}(F_{\text{BC}} - c_1)}{c_3}, \quad (1.11c)$$

where $c_3 (\equiv G(E = -1))$ is the third eigenvalue and the value F_{BC} is a boundary value to be assigned.³ The new eigenvalue $\beta (\equiv c_1/c_2)$ characterizes the power-law profile of stars in the halo for each of dependent variables in the following boundary conditions for the 4ODEs (1.7a)-(1.7d) and Q -integral (equation (1.2))

$$F(E \rightarrow 0) = c_4(\beta + 1)(-E)^\beta, \quad F(E = -1) = F_{\text{BC}}, \quad (1.12a)$$

$$G(E \rightarrow 0) = c_4(-E)^{\beta+1}, \quad G(E = -1) = c_3, \quad (1.12b)$$

$$I(E \rightarrow 0) = c_4 \frac{4(\beta + 1)}{2\beta - 7} (-E)^{\beta+1} Q(E \rightarrow 0), \quad I(E = -1) = 0, \quad (1.12c)$$

$$J(E \rightarrow 0) = -c_4 \frac{4\beta(\beta + 1)}{2\beta - 3} (-E)^\beta Q(E \rightarrow 0), \quad J(E = -1) = 0, \quad (1.12d)$$

$$Q(E \rightarrow 0) \propto (-E)^\sigma, \quad Q(E = -1) = 0, \quad (1.12e)$$

where $\sigma = -3(2\beta - 1)/4$ and c_4 is the fourth eigenvalue. The boundary condition for Poisson equation is

$$\frac{d\Psi(R=0)}{dR} = 0, \quad \Psi(R=0) = -1. \quad (1.13)$$

1.3. Numerical problems in integration of ss-OAFP equation and spectral methods

Solving the ss-OAFP system, i.e. solving equations (1.7)-(1.9) for the set of dependent variables $\{F, G, J, I, \Phi\}$ and four eigenvalues $\{c_1(\text{or } \beta), c_2, c_3, c_4\}$ based on the boundary conditions (1.12)-(1.13), is *supposed* to be a simple task compared to more exact models (e.g. time-dependent OAFP model and N -body direct simulations). However, it was studied only in a few works (Heggie and Stevenson, 1988; Takahashi and Inagaki, 1992; Takahashi, 1993) in which clear difficulties in numerical integration of the ss-OAFP system were reported. Although Heggie and Stevenson (1988); Takahashi (1993) found their self-similar solutions, their works are not complete due to the following reasons. First, the domains of their solutions are truncated in energy space, which means the solutions may depend on the extrapolation of power-law profile; they did not discuss the relationship between their solutions and a solution obtained on the whole domain. Second, Heggie and Stevenson (1988) reported the value of scaled escape energy χ_{esc} is 13.85 while this value is not compatible with a result of (Cohn, 1980) in which, at the same epoch of the energy ($=13.85$), the central density reaches *only* 10^{20} times higher than the initial density; if the value 13.85 is correct, the (Cohn, 1980)'s time-evolution model is supposed to reach an infinite density; one has yet to discuss which of their works is a more accurate result. Third, Takahashi and Inagaki (1992); Takahashi (1993) tried to reproduce the result of (Heggie and Stevenson, 1988) based on a variational principle though it was not a plentiful result; both the works

³Although the boundary condition for the DF in (Heggie and Stevenson, 1988; Takahashi and Inagaki, 1992) was set to $F(-1) = 1$, the present work specifies the value of F_{BC} when it is necessary.

reported that Newton iteration method did not well work unless the initial guess for solution was very close to the ‘true’ solution.

In the present work, we employ a Gauss-Chebyshev pseudo-spectral method to overcome the numerical difficulties associated with the ss-OAFP model and to obtain a solution on the whole domain. Spectral methods are a very accurate and efficient numerical scheme compared to finite difference (deferred correction) methods, also they can provide a closed form of solution different from finite element methods. Especially, Chebyshev spectral method has the advantages over other spectral methods in the sense that the explicit expression of Chebyshev nodes, numerical differentiation and integrals are known and that its numerical stability and efficiency have been extensively studied (e.g. Boyd, 2001). The ss-OAFP system is associated with infinite-domain problems through Poisson equation; the infinite domain problems have been a matter of concern in applied-mathematics and computational-physics communities as an end-point singularity problem last decades, especially which was discussed for Lane-Emden equations and the variants in astrophysical context (e.g. Parand and Shahini, 2010; Căruntu and Bota, 2013; Ito et al., 2018). The present work also aims at extending the numerical scheme developed in (Ito et al., 2018) to the ss-OAFP system.

The present paper is organized as follows. Section 2 explains the transformation of functions and change of variables for the ss-OAFP system that we made to avoid singularities of the functions and to adjust their domains for the spectral method. Section 3 explains the Gauss-Chebyshev pseudo-spectral method and also the numerical arrangements that we made to make the Newton iteration method converge. Sections 4 and 5 show the spectral solutions and eigenvalues obtained on whole- and truncated- domains respectively; the former provides the main result of the present work while the latter details the mathematical structure of the ss-OAFP system to validate the spectral solution on the whole domain. Section 6 reproduces the Heggie-Stevenson’s (HS’s) solution using the spectral method to see the consistency of our solution. Section 7 makes a conclusion.

2. Mathematical formulation

The domains of 4ODEs (1.7a) - (1.7d) and Q -integral (equation (1.2)) are finite ($E \in [-1, 0)$) while the domain of Poisson equation (1.9) is semi-infinite ($R \in [0, \infty)$). To employ the Chebyshev spectral method throughout the present work, in Section 2.1, we convert the domain of the latter to the same domain as the former employing an inverse function of the m.f. potential $\Psi(R)$ following the inverse-mapping method (Ito et al., 2018). Also, since all the dependent variables have power-law profiles forming large-scale gaps between terms in the 4ODEs and Poisson equation, we regularize the variables by the factor $(-E)^\beta$, DF $F(E)$ and/or the integral $Q(E)$ in Section 2.2. Lastly, the truncation of the domain is essential following (Heggie and Stevenson, 1988; Takahashi, 1993), hence Section 2.3 provides the explicit expression of the Q - and D - integrals on the whole- and truncated- domains.

2.1. Inverse form of Poisson equation

Using the inverse mapping R of Ψ through the local theorem

$$\frac{d\Psi}{dR} = \frac{1}{\frac{dR}{d\Psi}}, \quad \frac{d^2\Psi}{dR^2} = -\frac{d^2R}{d\Psi^2} \left(\frac{1}{\frac{dR}{d\Psi}} \right)^3, \quad (2.1)$$

we reduced Poisson equation (1.9) to

$$R(\Psi) \frac{d^2R}{d\Psi^2} - 2 \left(\frac{dR}{d\Psi} \right)^2 + R(\Psi) \left(\frac{dR}{d\Psi} \right)^3 D(\Psi) = 0. \quad (2.2)$$

The asymptotic approximation of the inverse form of Poisson equation (2.2) near $\Psi = -1$ (corresponding to the boundary condition (1.13) at $R = 0$) reads

$$R(\Psi \rightarrow -1) = (1 + \Psi)^{1/2}. \quad (2.3)$$

Also, the asymptotic approximation of the dependent variable R near $\Psi = 0$ is

$$R(\Psi \rightarrow 0) \propto (-\Psi)^\nu, \quad \left(\nu = -\frac{2\beta + 1}{4} \right). \quad (2.4)$$

2.2. Regularization of ss-OAFP system

We introduced the following independent variables x and y to employ Chebyshev polynomials (which are defined on $(-1, 1)$ to be explained in Section 3)

$$x \equiv 2(-E)^{1/L} - 1, \quad y \equiv 2(-\Psi)^{1/L} - 1, \quad (2.5)$$

where L is a numerical parameter introduced to deal with a certain kind of end-point singularities of Chebyshev polynomials (Ito et al., 2018). Making use of the known asymptotic approximation of dependent variables (i.e. equations (1.12), (2.3) and (2.4)), we regularized the dependent variables as follows

$$v_R(y) \equiv \ln \left[R(y) \left(\frac{1-y}{2} \right)^{-1/2} \left(\frac{1+y}{2} \right)^{-Lv} \right], \quad \left(v = -\frac{2\beta+1}{4} \right), \quad (2.6a)$$

$$v_S(y) \equiv \ln \left[-S(y) \left(\frac{1-y}{2} \right)^{1/2} \left(\frac{1+y}{2} \right)^{1-Lv} \right], \quad (2.6b)$$

$$v_Q(x) \equiv \left[Q(x) \left(\frac{1+x}{2} \right)^{-L\sigma} \right]^{1/3}, \quad \left(\sigma = -\frac{6\beta-3}{4} \right), \quad (2.6c)$$

$$v_F(x) \equiv \ln \left[F(x) \left(\frac{1+x}{2} \right)^{-\beta L} \right], \quad (2.6d)$$

$$v_G(x) \equiv \frac{G(x)}{F(x)}, \quad (2.6e)$$

$$v_I(x) \equiv \frac{I(x)}{F(x)Q(x)}, \quad (2.6f)$$

$$v_J(x) \equiv \frac{(2\beta-3)J(x)}{4\beta F(x)Q(x)}, \quad (2.6g)$$

where the following new dependent variable was introduced for convenience

$$S(y) \equiv 2 \frac{dR}{dy}. \quad (2.7)$$

The regularized variables provide more straightforward boundary conditions to understand the relation between the conditions and eigenvalues, compared to the original ones (equations (1.12a)-(1.12d));

$$v_F(x \rightarrow -1) = \ln c_4^*, \quad v_F(x = 1) = \ln F_{BC}, \quad (2.8a)$$

$$v_I(x \rightarrow -1) = 0, \quad v_I(x = 1) = 0, \quad (2.8b)$$

$$v_G(x \rightarrow -1) = 0, \quad v_G(x = 1) = c_3, \quad (2.8c)$$

$$v_J(x \rightarrow -1) = -1, \quad v_J(x = 1) = 0, \quad (2.8d)$$

where c_4^* is a newly-introduced eigenvalue for convenience and the relation of the eigenvalue c_4^* with c_4 in (Heggie and Stevenson, 1988)'s work is

$$c_4^* \equiv c_4(\beta + 1). \quad (2.9)$$

Since all the 4ODEs (1.7a)-(1.7d) are first order in differentiation, the eigenvalues (end-point values at $x = -1$) c_4^* and c_3 would be directly associated with the boundary conditions at the opposite ends ($v_F(x = 1)$ and $v_G(x \rightarrow -1) = 0$) while the eigenvalues c_1 and c_2 would be determined by two of the boundary conditions for $v_I(x)$ and $v_J(x)$.

The inverse form of Poisson equation (2.2) reduces to a system of the following two ODEs

$$2(1-y)(1+y) \frac{dv_R}{dy} + 2vL(1-y) - (1+y) + 4e^{v_S(y)-v_R(y)} = 0, \quad (2.10a)$$

$$2(1-y)(1+y) \frac{dv_S}{dy} + 2L(v-1)(1-y) + (1+y) + 8e^{v_S(y)-v_R(y)} - \frac{4}{L}e^{v_S(y)}v_D(y) = 0, \quad (2.10b)$$

where the regularized density $v_D(y)$ is

$$v_D(y) \equiv D(y) \left(\frac{1+y}{2} \right)^{-(\beta+3/2)L} = \frac{L}{2} \left(\frac{1+y}{2} \right)^{-L(\beta+3/2)} \int_{-1}^y A_L(y, x') e^{v_F(x')} \sqrt{\frac{x-x'}{2}} \left(\frac{1+x'}{2} \right)^{L(\beta+1)-1} dx', \quad (2.11)$$

where the factor $A_L(x, x')$ is

$$A_L(x, x') \equiv \sqrt{\left(\frac{1+x}{2} \right)^L - \left(\frac{1+x'}{2} \right)^L} \left(\frac{x-x'}{2} \right)^{-1/2}. \quad (2.12)$$

We did not need to employ any boundary conditions for equations (2.10a)-(2.10b) since the equations are completely regularized at each end point of the domains of $v_R(x)$ and $v_S(x)$; in other words; the equations themselves include their boundary conditions, which appears after the limits of $x \rightarrow \pm$ are taken at equation level.

We regularized the integral $Q(x)$ (equation (1.2)) as follows

$$[v_Q(x)]^3 = \frac{L}{6\sqrt{2}} \left(\frac{1+x}{2} \right)^{-\sigma L} \int_x^1 \left(\frac{1-y'}{2} \right)^{3/2} A_L(y', x) e^{3v_R(y')} \sqrt{y'-x} \left(\frac{1+y'}{2} \right)^{(3\nu+1)L-1} dy'. \quad (2.13)$$

4ODEs (1.7a) - (1.7d) reduce to

$$\frac{2}{L} \left(\frac{1+x}{2} \right)^{(\beta-1)L+1} \frac{dv_F}{dx} [v_I(x) + v_G(x)] + \left(\frac{1+x}{2} \right)^{(\beta-1)L} \left\{ \beta [v_I(x) + v_G(x)] + \left(\frac{1+x}{2} \right)^L \left(\frac{4\beta v_J(x)}{2\beta-3} - 1 \right) \right\} + c_1 e^{-v_F(x)} [1 + v_J(x)] = 0, \quad (2.14a)$$

$$\frac{1+x}{L} v_Q(x) \left(\frac{dv_I}{dx} + v_I(x) \frac{dv_F}{dx} \right) + v_I(x) \left[\frac{-2\beta+3}{4} v_Q(x) + \frac{3(1+x)}{L} \frac{dv_Q}{dx} \right] + \left(\frac{1+x}{2} \right)^L v_Q(x) = 0, \quad (2.14b)$$

$$\frac{1+x}{L} \frac{dv_G}{dx} + v_G(x) \left(\frac{1+x}{L} \frac{dv_F}{dx} + \beta \right) - \left(\frac{x+1}{2} \right)^L = 0, \quad (2.14c)$$

$$\frac{1+x}{L} v_Q(x) \left\{ \frac{dv_J}{dx} + \frac{dv_F}{dx} \left[v_J(x) - \frac{2\beta-3}{4\beta} \right] \right\} + v_J(x) \left[v_Q(x) \frac{-2\beta+3}{4} + 3 \frac{1+x}{L} \frac{dv_Q}{dx} \right] - \frac{2\beta-3}{4} v_Q(x) = 0. \quad (2.14d)$$

2.3. The integral formulations on the whole- and truncated- domains

When we solved the ss-OAFP system on the whole-domains $x, y \in (-1, 1)$, we numerically integrated the integrals $v_D(y)$ (equation (2.11)) and $v_Q(x)$ (equation (2.13)) using Fejér's first rule quadrature

$$v_D(y) = \frac{L}{2\sqrt{2}} \left(\frac{1+y}{2} \right)^{\frac{L}{2}} \int_{-1}^1 A_L \left[y, \frac{(y+1)(x'+1)}{2} - 1 \right] e^{v_F \left[\frac{(y+1)(x'+1)}{2} - 1 \right]} \sqrt{1-x'} \left(\frac{1+x'}{2} \right)^{L(\beta+1)-1} dx', \quad (2.15a)$$

$$[v_Q(x)]^3 = \frac{L}{24} \left(\frac{1-x}{2} \right)^3 \left(\frac{1+x}{2} \right)^{-\sigma L} \int_{-1}^1 A_L \left[1 - \frac{(1-x)(1-y')}{2}, x \right] e^{3v_R \left[1 - \frac{(1-x)(1-y')}{2} \right]} \sqrt{1+y'} (1-y')^{3/2} \left[1 - \frac{(1-x)(1-y')}{4} \right]^{(3\nu+1)L-1} dy'. \quad (2.15b)$$

On one hand, for numerical integration of the regularized ss-OAFP system on truncated domains $x, y \in (x_{\min}, 1)$ where $-1 < x_{\min} < 1$, we introduced new independent variables

$$z \equiv -2 \frac{1-x}{1-x_{\min}} + 1, \quad w \equiv -2 \frac{1-y}{1-x_{\min}} + 1. \quad (2.16)$$

Since the original domain of $v_F(x)$ in the integral $v_D(w)$ is $(-1, 1)$, one must extrapolate $v_F(x)$ on $(-1, x_{\min})$. The present work employed the following extrapolated DFs

$$v_F^{(\text{ex})}(x) \equiv \begin{cases} \ln \left\{ c_4^* + \frac{2c_4^*}{1-x_{\min}} \frac{dv_F(w=-1)}{dw} e^{d(1+x_{\min})-c} \left[1 - \left(\frac{1+x_{\min}}{1+x} \right)^c \right] (x-x_{\min}) \right\}, & (\text{smooth at } x = x_{\min}) \\ \ln[c_4^*], & (\text{non-smooth at } x = x_{\min} \text{ or } c \rightarrow \infty) \end{cases} \quad (2.17)$$

where c and d are numerical parameters. Hence, $v_D(w)$ is composed of the total of integrals $v_D^{(\text{nonex})}(w)$ and $v_D^{(\text{ex})}(w)$; the former is contribution to $v_D(w)$ from the (non-extrapolated) DF $v_F(x)$ and the latter is from an extrapolated DF $v_F^{(\text{ex})}(x)$ as follows

$$v_D(w) = v_D^{(\text{nonex})}(w) + v_D^{(\text{ex})}(w). \quad (2.18)$$

The non-extrapolated $v_F(x)$ on $x_{\min} < x < 1$ contributes to $v_D(w)$ as follows

$$v_D^{(\text{nonex})}(w) = \frac{1}{2\sqrt{2}} \left(\frac{1-x_{\min}}{2} \right)^{3/2} \left[\frac{1}{2} + \frac{2+x_{\min}(1-w)}{2(1+w)} \right]^{-3/2} \\ \times \int_{-1}^1 e^{v_F \left[\frac{(w+1)(z'+1)}{2} - 1 \right]} \sqrt{1-z'} \left\{ 1 - \frac{(1-z')(1+w)(1-x_{\min})}{2[3+x_{\min}+z'(1-x_{\min})]} \right\}^{\beta} dz', \quad (2.19)$$

where $L = 1$ is assumed for simplicity. On one hand, the contribution of $v_F^{(\text{ex})}(x)$ on $-1 < x < x_{\min}$ to $v_D(w)$ reads

$$v_D^{(\text{ex})}(w) \equiv \frac{1}{2} \int_{-1}^1 \left(\frac{1+x_{\min}}{1+y} \right)^{\beta+3/2} e^{v_F^{(\text{ex})} \left[\frac{(1+x_{\min})(1+z'')}{2} - 1 \right]} \sqrt{\frac{1+y}{1+x_{\min}} - \frac{1+z''}{2}} \left(\frac{1+z''}{2} \right)^{\beta} dz'', \quad (2.20)$$

where $y = \frac{1}{2} [1 + x_{\min} + w(1 - x_{\min})]$. Lastly, the integral $v_Q(z)$ on the truncated domain is

$$[v_Q(z)]^3 = \frac{1}{24} \left(\frac{1-x}{2} \right)^3 \left(\frac{1+x}{2} \right)^{-3/2} \\ \times \int_{-1}^1 e^{3v_R \left[1 - \frac{(1-z)(1-w')}{2} \right]} \sqrt{1+w'} (1-w')^{3/2} \left\{ 1 + \frac{(1-z)(1+w')(1-x_{\min})}{4(1+x)} \right\}^{3\nu} dw', \quad (2.21)$$

where $L = 1$ is assumed and $x = \frac{1}{2} [1 + x_{\min} + z(1 - x_{\min})]$.

3. Gauss-Chebyshev spectral method and numerical treatments of ss-OAFP system

Sections 3.1 and 3.2 explain Gauss-Chebyshev pseudo-spectral method and numerical treatment of the ss-OAFP system respectively.

3.1. The Gauss-Chebyshev pseudo-spectral method

Chebyshev polynomials of the first kind is defined on domain $x \in [-1, 1]$ as (e.g. Boyd, 2001; Mason and Handscomb, 2002)

$$T_n(x) = \cos \left[n \cos^{-1}(x) \right], \quad (n = 0, 1, 2, \dots, N) \quad (3.1)$$

Due to the singularities in 4ODES (2.14a)-(2.14a) and Poisson equation (2.10) at the endpoints $x = \pm 1$, we had to solve the equations as an open-interval problem $x \in (-1, 1)^4$. Hence, the discretized domain of the polynomials at Gauss-Chebyshev points is

$$x_k = \cos(t_k) \equiv \cos \left(\frac{2k-1}{2N} \right). \quad (k = 1, 2, 3 \dots N) \quad (3.2)$$

The discrete Gauss-Chebyshev polynomials $T_n(x_j)$ of the first kind satisfy the orthogonality condition (e.g. Mason and Handscomb (2002))

$$\sum_{j=1}^N T_n(x_j) T_m(x_j) = \begin{cases} 0, & (1 < n \neq m < N) \\ N, & (n = m = 0) \\ \frac{N}{2}, & (0 < n = j \leq N) \end{cases} \quad (3.3)$$

⁴The Poisson equation is regular singular at both the end points of the domain and the D - and Q -integral also have a singular property as $x \rightarrow -1$. In this sense, to handle the singularities, we employed Gauss-Chebyshev nodes by considering the domain to be an open interval (See e.g. Bhrawy and Alofi, 2012; Boyd, 2013, for application of Gauss-Chabyshev spectral methods).

Hence, the discrete Gauss-Chebyshev polynomial expansion of any function $h(x)$ and its derivative are

$$h(x_j) = \sum_{n=1}^n a_n T_{n-1}(x_j), \quad \frac{dh(x_j)}{dx} = \sum_{n=1}^n a_n \frac{n \sin(n \cos^{-1} x_j)}{\sin(\cos^{-1} x_j)}, \quad (3.4)$$

and the Chebyshev-Gauss expansion can be inverted to

$$a_1 = \frac{1}{n} \sum_{j=1}^n T_0(x_j) h(x_j), \quad (3.5a)$$

$$a_n = \frac{2}{n} \sum_{j=1}^n T_{n-1}(x_j) h(x_j). \quad (2 \leq n \leq n) \quad (3.5b)$$

3.2. Numerical treatments of the ss-OAFP equation

In a similar way to (Heggie and Stevenson, 1988)'s work, we had to carry out many numerical arrangements. First, Newton iteration method for the whole-domain formulation did not work at all. Hence we truncated the domain of v_Q and differentiation $\frac{d}{dx}$ in the 4ODEs employing equation (2.16). Then, this arrangement provided spectral solutions on $x_{\min} \approx -0.96 < x < 1$. Also, truncated-domain formulation did not work, hence, we regularized $v_I(x)$ and $v_J(x)$ by the factor $(1+x)/2$ so that $\lim_{x \rightarrow x_{\min}} 2v_I(x)/(1+x) = 4/(2a-7)$ and $\lim_{x \rightarrow x_{\min}} 2v_G(x)/(1+x) = 1/(a+1)$. This arrangement provided solutions on $x_{\min} \approx -0.2 < x < 1$. To broaden the range of the effective interval ($x_{\min} < x < 1$), following (Heggie and Stevenson, 1988), we shortened the Newton steps in the iteration process though, it did not work.

To overcome the difficulty in convergence of Newton method, we fixed the eigenvalue β to a certain value during iteration process. For the fixed β -value, once we found a solution at a specific x_{\min} , we chose a new β that is close to the old β . Then, we found a new solution for the new β using Newton iteration method. We repeated this process until $v_I(x=1)$ reached its minimum. Then, at a new x_{\min} that is *very* close to the old x_{\min} with new β that is *very* close to old β ,⁵ we repeated the whole process above. As a result, x_{\min} reached -1 for the whole-domain formulation while x_{\min} reached -0.96 for the domain-truncated formulation.

Also, since the eigenvalue β was fixed during the iteration process, we speeded up the numerical integration of the integrals $v_Q(x)$ and $v_D(x)$ by applying the Fejér's first rule quadrature to the integrals *before* the iteration process starts. For example, we discretized $v_D(y)$ as follows

$$v_D(y_j) = \sum_{n=1}^n F_n^{\text{linear}} \mathcal{D}_n(y_j) \quad (3.6)$$

where $\{F_n^{\text{linear}}\}$ is the Chebyshev coefficients of function $v_F^{\text{linear}}(x) (\equiv \exp[v_F(x)])$. One can obtain $\{F_n^{\text{linear}}\}$ from $v_F(x)$ by using equations (3.4) and (3.5). The matrix $\mathcal{D}_n(y_j)$ is a preset matrix to be integrated before the Newton-iteration (loop) process begins and explicitly reads

$$\mathcal{D}_n(y_j) = \frac{L}{2\sqrt{2}} \left(\frac{1+y_j}{2} \right)^{\frac{1-L}{2}} \times \int_{-1}^1 A_L \left[y_j, \frac{(y_j+1)(x'+1)}{2} - 1 \right] T_n \left[\frac{(y+1)(x'+1)}{2} - 1 \right] \sqrt{1-x'} \left(\frac{1+x'}{2} \right)^{L(\beta+1)-1} dx'. \quad (3.7)$$

We also prepared a similar preset matrix for $v_Q(x)$. As a result, the two preset matrices made the iteration process 10 ~ 100 times more efficient⁶ than the original iteration process in which we implemented the Fejér's first rule quadrature for each iteration.

⁵For example, to find the whole-domain solution, the change $\delta\beta$ in β was 0.03 from $x_{\min} = -0.94$ to -0.96 , $\delta\beta \approx 0.001$ from $x_{\min} = -0.9994$ to -0.9996 , and $\delta\beta \approx 0.000001$ from $x_{\min} = -0.999994$ to -0.999995 .

⁶Using a 2.4 GHz CPU processor, the resulting CPU time for 10^4 iterations was ~ a few min for $n = 70$, which was needed to find solutions near $x_{\min} = -1$.

4. Self-similar solution on the whole domain

As the main result, we provide the whole-domain solution, its semi-analytical form and eigenvalues (Section 4.1). Section 4.2 details the asymptotic approximation of the solution and the characteristics of the Chebyshev coefficients. Section 4.3 discusses the numerical stability of the solution and reports that the solution is unstable against degree n .

4.1. Numerical results (main results of the present paper)

We found the whole-domain solution compatible to the HS's solution. Figures 1(a) and 2 (a) depict DF $F(E)$ and m.f. potential $\Phi(R)$ obtained from the whole-domain spectral solution. In the figures, the HS's solution is also depicted. The spectral- and HS's solutions are visually almost identical on the figures. For the whole-domain solution, the optimal values of numerical parameters are $n = 70$, $F_{BC} = 1$, $L = 1$. The optimal eigenvalue of β is

$$\beta_o \equiv 8.1783711596581. \quad (4.1)$$

We chose the value of β_o so that $v_l(x = 1)$ reached its minimum value ($\sim 10^{-12}$). In order to make Newton iteration method work, we needed to correctly specify at least eight significant figures of β_o (Appendix B.1). Also, degree $n = 70$ is the minimum value among $70 \leq n \leq 400$ for which Newton iteration method worked (Section 4.3). Figures 1(b) and 2 (b) show the magnified figures for the solutions. The spectral solution slightly deviates from the HS's solution around $E = -0.3$

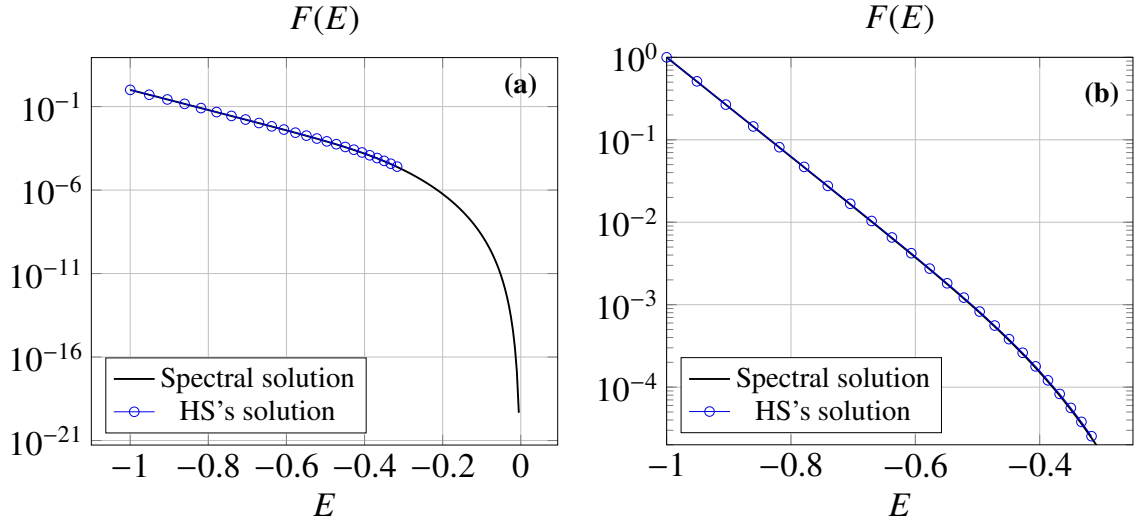


Figure 1: (a) Distribution function $F(E)$ of stars on the whole domain and (b) its magnified graph on $-1 \leq E < -0.25$. ($n = 70$, $F_{BC} = 1$, $L = 1$.)

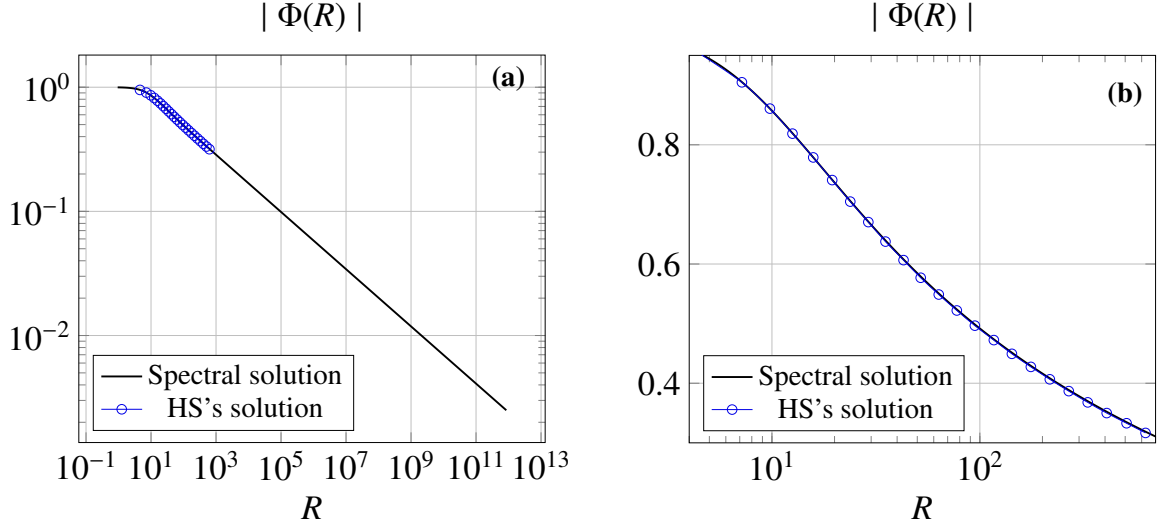


Figure 2: (a) Self-consistent m.f. potential $\Phi(R)$ of stars on the whole potential range and (b) its magnified graph on $-1 < \Phi(R) < -0.25$. ($n = 70$, $F_{BC} = 1$, $L = 1$.)

The eigenvalues we found are the same as one to two significant figures of the HS's eigenvalues. Table 1 lists the eigenvalues obtained from the spectral solution. Our eigenvalues c_1 , c_2 and c_3 are the same as two significant figures of the HS's values while c_4 is only one significant figure with relative error of 6.7%. On one hand, the physical parameters α , χ_{esc} and ξ are the same as three significant figures of the HS's values. The present value of χ_{esc} is greater than the HS's value 13.85. This is consistent with the result of (Cohn, 1980) that predicted $\chi_{\text{esc}} \approx 13.9$ at which a complete core-collapse (an infinite central density) occurs.

In the rest of sections, we call the following eigenvalues and β_o the *reference* eigenvalues for comparison with other solutions

$$c_{1o} = 9.09254120455 \times 10^{-4}, \quad (4.2a)$$

$$c_{4o}^* = 3.03155222 \times 10^{-1}. \quad (4.2b)$$

The reference eigenvalues were obtained from the whole-domain solution when $\beta = \beta_o$, $n = 70$, $L = 1$ and $F_{BC} = 1$.

Lastly, we report the semi-analytical solution of the ss-OAFP system. Since spectral-method studies generally provide a solution of equation concerned with a low degree of polynomials,⁷ Table 2 lists 'semi-analytical' forms of $F(E)$, $Q(E)$ and $R(\Phi)$. The degrees of polynomials are at most eighteen and % error is 0.1% compared to the whole-domain solution with degree $n = 70$.

4.2. The detail analyses regarding the whole-domain solution and its asymptotic feature

The present section details the mathematical characteristics of the whole-domain solution. We discuss the Chebyshev coefficients of the regularized functions (Section 4.2.1), regularized functions (Section 4.2.2) and detail structure of v_j (Section 4.2.3).

⁷Spectral methods can provide 'semi-analytical' solutions in the sense that the solutions can be expanded in terms of polynomials with degree of *a few to tens*; typical base functions are such as Legendre polynomials, Gegenbauer polynomials and Hermite functions. Sections 5 and 6 and Appendix B.4 show spectral solutions based on different formulations of the ss-OAFP system, hence we could construct variants of the semi-analytic solutions in the present work. However, they do not have an outstanding property. For example, the corresponding semi-analytical solutions on the truncated domain (Section 5) and contracted domain (Appendix B.4) need only 12 ~ 13 degrees to achieve a relative error of 10^{-4} , but they are not be practical since they depend on parameters L and x_{\min} . Also, the degrees of the exponential of the regularized solution $\exp[v_F(x)]$ still needs 16.

Eigenvalues	Spectral method	HS	T	% relative error [%]
c_1	9.0925×10^{-4}	9.10×10^{-4}	9.1×10^{-4}	0.1
c_2	1.1118×10^{-4}	1.12×10^{-4}	–	0.9
c_3	7.1975×10^{-2}	7.21×10^{-2}	–	0.1
c_4	3.303×10^{-2}	3.52×10^{-2}	–	6.7
α	2.2305	2.23	2.23	0
χ_{esc}	13.881	13.85	–	0.3
ξ	3.64×10^{-3}	3.64×10^{-3}	–	0

Table 1: Comparison of the present eigenvalues and physical parameters with the results of ‘HS’ (Heggie and Stevenson, 1988) and ‘T’ (Takahashi, 1993). The relative error between Heggie-Stevenson(HS)’s eigenvalues and the present ones are also shown. The present eigenvalues are based on the results for various combinations of numerical parameters ($13 < N < 560$, $10^{-4} < F_{\text{BC}} < 10^4$ and $L = 1/2, 3/4, 1$), different formulations (Sections 5 and 6 and Appendix B.4) and stability analyses (Appendix B).

index	Coefficients		
n	F_n	Q_n	R_n
1	−0.9793	0.7405	2.0588
2	0.4515	−0.2455	0.7337
3	0.3949	−0.2598	0.1589
4	0.1751	−0.1778	−0.0066
5	−0.0171	−0.0597	−0.0182
6	−0.0381	0.0003	0.0013
7	0.0076	0.0037	0.0038
8	0.0103	−0.0017	−0.0007
9	−0.0046	−0.0004	−0.0009
10	−0.0023	0.0006	0.0003
11	0.0023	−0.0001	0.0002
12	0.0001	−0.0001	−0.0001
13	−0.0009	0.0001	
14	0.0002		
15	0.0002		
16	−0.0002		
17	0.0000		
18	0.0001		

Function	semi-analytical expression
$F(E)$	$\exp\left[\sum_{n=1}^{18} F_n T_{n-1}(-2E-1)\right] (-E)^\beta$
$Q(E)$	$\left[\sum_{n=1}^{13} Q_n T_{n-1}(-2E-1)\right]^3 (-E)^\sigma$
$R(E)$	$\exp\left[\sum_{n=1}^{12} R_n T_{n-1}(-2E-1)\right] (-E)^\nu \sqrt{1+E}$
$E \in (-1, 0)$	$T_{n-1}(-2E-1) = \cos\left[(n-1) \cos^{-1}(-2E-1)\right]$
	$\beta = 8.178$
	$\sigma = -\frac{3}{2\beta-1}4 = -11.51$
	$\nu = -\frac{2\beta+1}{4} = -4.339$

Table 2: Semi-analytical forms of the Chebyshev spectral solution $F(E)$, $R(E)$ and $Q(E)$. The relative error of the semi-analytic form from the whole-domain solution is order of 10^{-4} .

4.2.1. Chebyshev coefficients

The Chebyshev coefficients of the regularized functions are depicted in Figure 3 in which the coefficients are divided by their own first ($n = 1$) coefficients. The minimum absolute values of all the coefficients reach $\sim 10^{-12}$ around at $n = 70$. This implies that possible relative error of the spectral solution is $\sim 10^{-10}\%$ at best. The coefficients show geometrical convergences; $|F_n/F_1| \sim |G_n/G_1| \sim |I_n/I_1| \sim |J_n/J_1| \sim \exp(-0.3n)$ and $|R_n/R_1| \sim |Q_n/Q_1| \sim \exp(-0.4n)$.

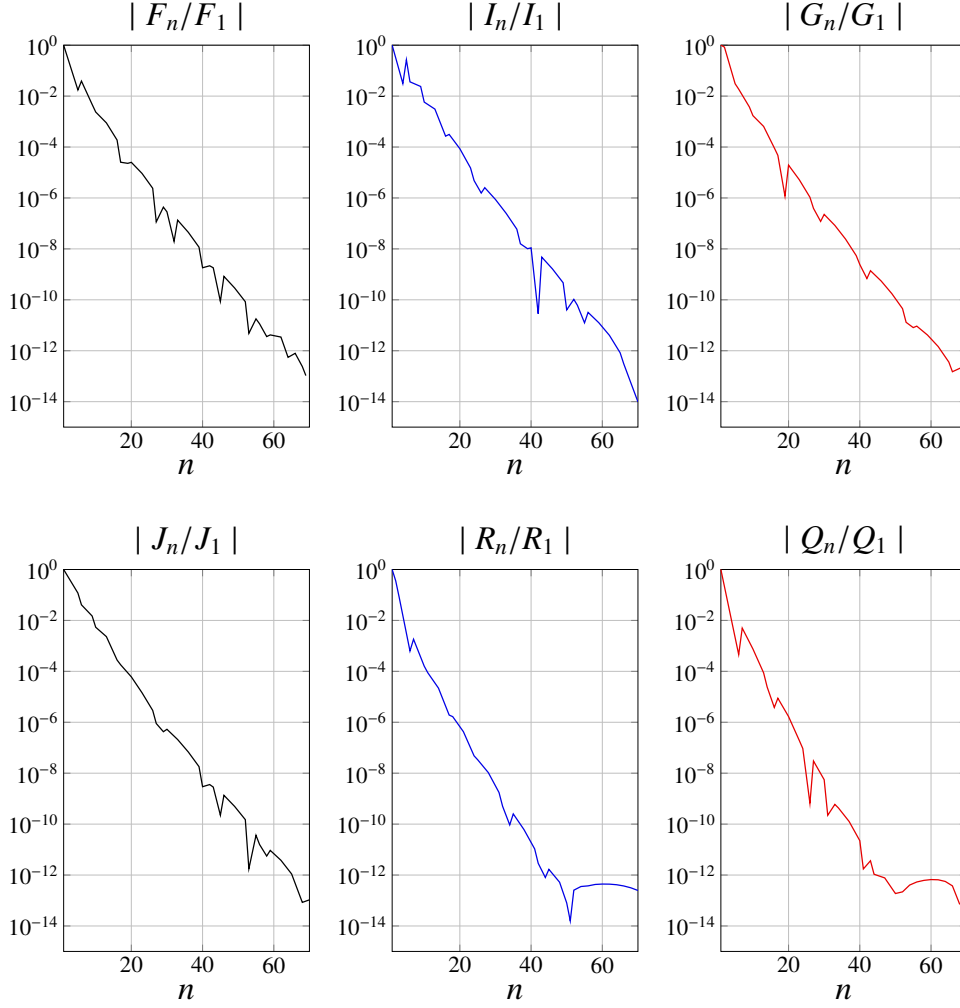


Figure 3: Absolute values of the normalized Chebyshev coefficients for the regularized functions. ($\eta = 70$, $F_{BC} = 1$ and $L = 1$). The coefficients are divided by their own first coefficients.

4.2.2. Regularized solution and its asymptotic approximation

To discuss the fine difference between the spectral and HS's solutions, Figure 4 compares the regularized functions obtained from the spectral solution and from the HS's work. One can find a discrepancy between the two works as $E \rightarrow 0$ for $v_F(E)$, $v_R(\Phi)$ and $v_Q(E)$. The figure indicates that the HS's functions were obtained *outside* the domain on which our functions asymptotically behave as constant functions. This implies that the actual number of significant figures of the HS's solution may not be more than one. This matter is discussed in detail in Section 6.3 (and also Appendix F).

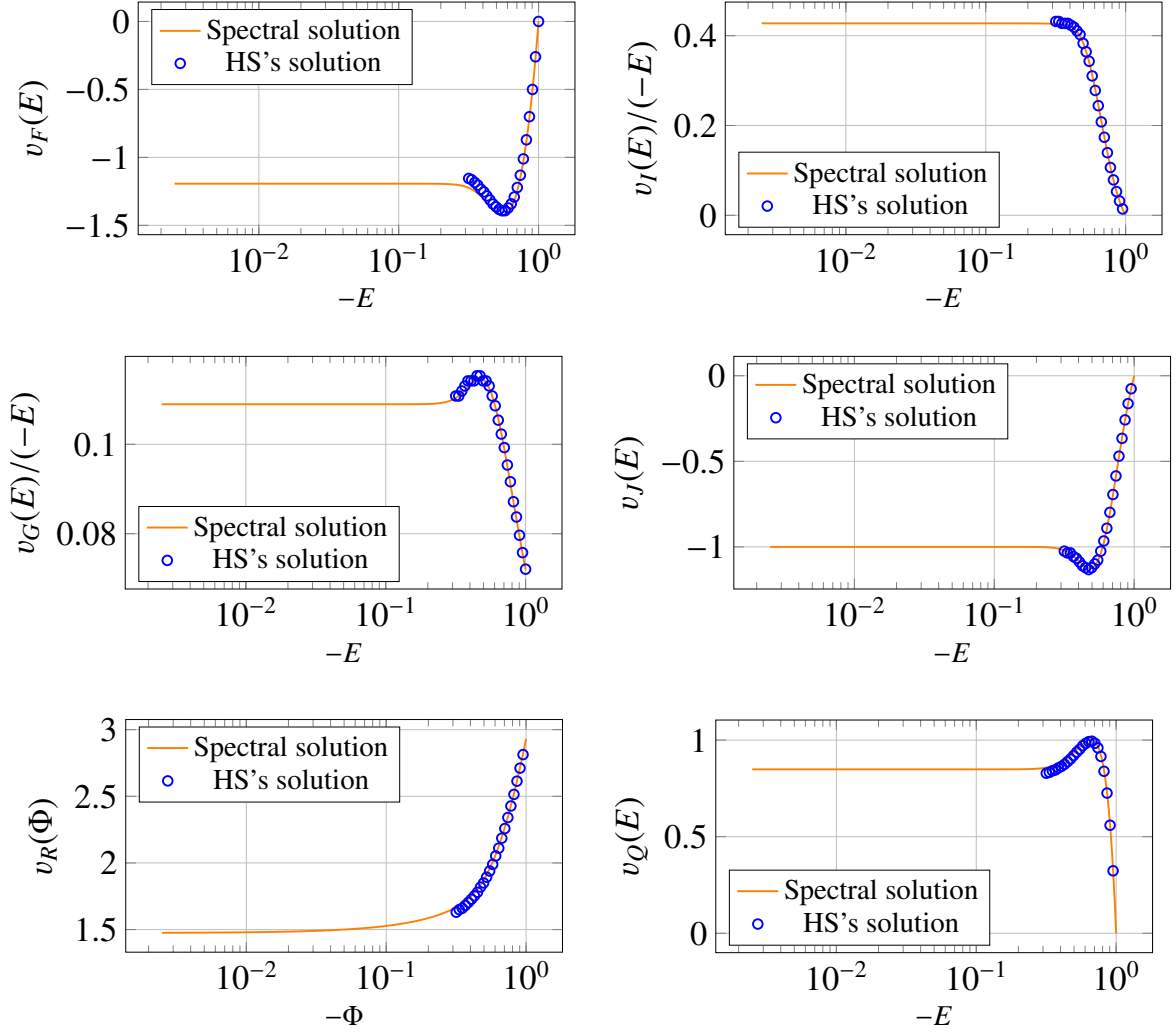


Figure 4: Regularized spectral functions ($n = 70$, $F_{BC} = 1$ and $L = 1$.)

Since the asymptotic approximations of $F(E)$, $G(E)$, $I(E)$ and $J(E)$ as $E \rightarrow 0$ read

$$F_{\text{asy}}(E) \equiv \ln[c_4^*](-E)^\beta, \quad (4.3a)$$

$$G_{\text{asy}}(E) \equiv \frac{1}{a+1}(-E)^{\beta+1}, \quad (4.3b)$$

$$I_{\text{asy}}(E) \equiv \frac{4}{2\beta-7}(-E)^{\beta+1}Q(E), \quad (4.3c)$$

$$J_{\text{asy}}(E) \equiv -\frac{4\beta}{2\beta-3}(-E)^\beta Q(E), \quad (4.3d)$$

we computed the relative errors between $\{F, G, I, J\}$ obtained from the spectral solution and $\{F_{\text{asy}}, G_{\text{asy}}, I_{\text{asy}}, J_{\text{asy}}\}$ (Figure 5). The figure also depicts the corresponding errors for the HS's functions. Both our and HS's functions show that $F_{\text{asy}}(E)$, $G_{\text{asy}}(E)$ and $J_{\text{asy}}(E)$ can well approximate $F(E)$, $G(E)$ and $J(E)$ near $E = -0.6$ or $E = -0.7$ and the relative errors between them are order of 10^{-3} . Since our value of c_4 is relatively different from the HS's value, one finds a discrepancy between the works for $|1 - F(E)/F_{\text{asy}}(E)|$.

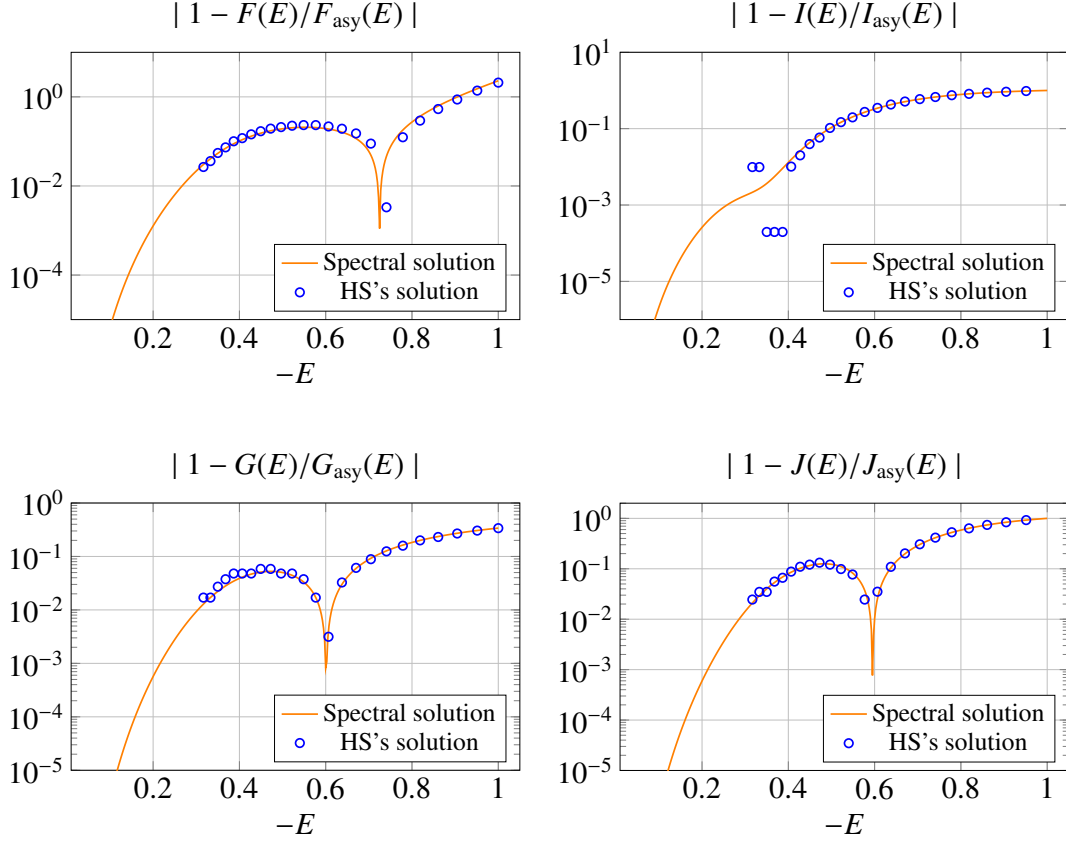


Figure 5: Relative error of the whole-domain spectral solution from the asymptotic approximation ($\eta = 70$, $F_{BC} = 1$, $L = 1$). The circles are the corresponding relative errors in the HS's solution. (Heggie and Stevenson, 1988) listed the numerical values of their solution rounded to the second decimal places, meaning the present solution can compare to their solutions at order of 5×10^{-3} at best.

4.2.3. Detail structure of v_J

Since the higher order of asymptotic approximation for $v_J(x)$ is analytically tractable, we discuss the feature qualitatively and quantitatively. First, we can qualitatively find a consistency of the spectral whole-domain solution by examining the asymptotic approximation of $J(E)$ that can be explicitly found from one of the 4ODEs (Appendix A.2);

$$|1 - J(E \rightarrow 0)/J_{\text{asy}}(E)| = -\frac{c_4^*}{c_1} \frac{(2\beta + 7)(6\beta - 3)}{(2\beta - 7)(2\beta - 3)(\beta + 1)} (-E)^\beta \equiv C_\beta(c_1, c_4^*) (-E)^\beta. \quad (4.4)$$

This $(-E)^\beta$ -dependence is numerically reproduced in Figure 6 (a). Figure 6 (b) depicts the characteristics of $|1 - J(E)/J_{\text{asy}}(E)| (-E)^{-\beta}$ that is still approximately constant on the interval $-4 \times 10^{-2} \lesssim E \lesssim -1 \times 10^{-1}$.

To quantitatively see the consistency of the spectral solution, we numerically calculated the values of β and $C_\beta(c_1, c_4^*)$ of equation (4.4). Figure 7 (a) shows the relative error between β_0 and the logarithmic derivative of $|1 - J(E)/J_{\text{asy}}(E)|$ and Figure 7 (b) depicts the error between $|1 - J(E)/J_{\text{asy}}(E)| (-E)^{-\beta}$ and $C_\beta(c_1, c_4^*)$. One can find the former is correct at order of 4.3×10^{-6} at best and the latter 2.0×10^{-7} . The logarithmic derivative and asymptotic approximation lose their accuracies at energies greater than $E = -0.07 \sim -0.05$. This is since the expression in equation 4.4 is correct under the limited condition that the factor $(0.5 + 0.5x)^\beta \frac{dv_E}{dx}$ in equation (2.14a) does not reach order of machine precision (See Appendix D for detail).

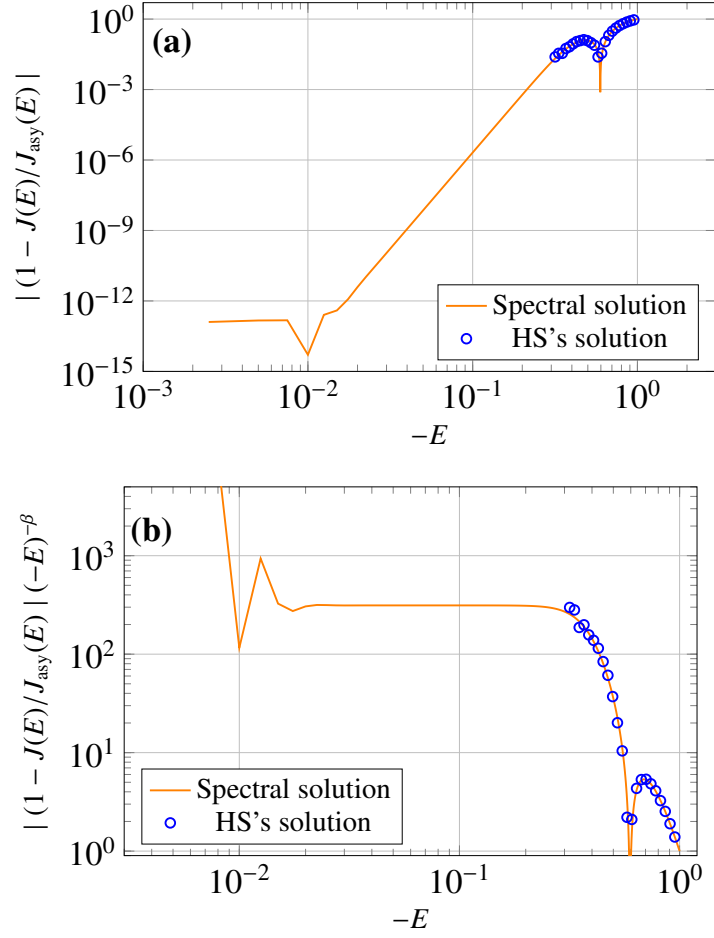


Figure 6: **(a)** Characteristics of $|1 - J(E)/J_{\text{asy}}(E)|$ and **(b)** characteristics of $|1 - J(E)/J_{\text{asy}}(E)| (-E)^{-\beta}$ ($n = 70$, $F_{\text{BC}} = 1$, $L = 1$). The circles are the corresponding characteristics of (Heggie and Stevenson, 1988)'s work.

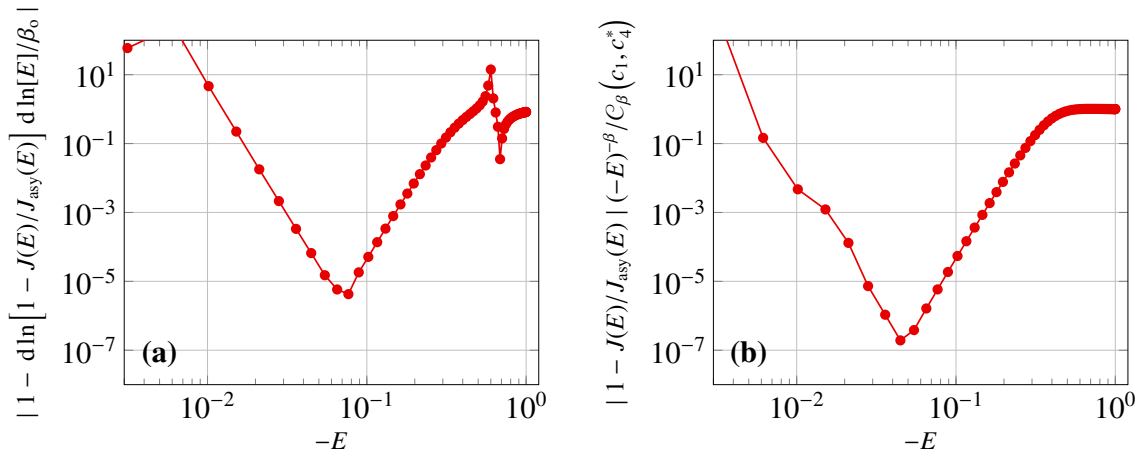


Figure 7: **(a)** Logarithmic derivative of $|1 - J(E)/J_{\text{asy}}(E)|$ with respect to E and **(b)** characteristics of $|1 - J(E)/J_{\text{asy}}(E)| (-E)^{-\beta}$ ($n = 70$, $F_{\text{BC}} = 1$, $L = 1$).

4.3. Numerical instability of the whole-domain solution

The present section explains the numerical instability of the whole-domain solution. As explained in detail in Appendix B, the whole-domain solution is stable against various numerical parameters. For a broad range of β , F_{BC} , L and the total number of nodes for the Fejér's rule quadrature, the eigenvalues c_1 and c_4^* can preserve seven- and five-significant figures compared to the reference values c_{10} and c_{40}^* . On one hand, the whole-domain solution is unstable against degree \mathcal{N} . The Newton iteration method well worked only for $70 \leq \mathcal{N} \lesssim 400$. It did not work at all for \mathcal{N} less than 70 while it still worked for $\mathcal{N} > 400$ but high \mathcal{N} increased $|v_I(x = 1)|$ and the condition number of the Jacobian Matrix for the 4ODE and Q -integral in Newton method, costing an unfeasible CPU time.

Figure 8 (a) shows that $|v_I(x = 1)|$ increases with \mathcal{N} but the rate of change becomes calm for higher \mathcal{N} and Figure 8 (b) depicts the condition number of the Jacobian matrix and the number monotonically increases with \mathcal{N} . Both $|v_I(x = 1)|$ and the condition number reach their lowest values when $\mathcal{N} = 70$. Hence, we compared the DF $F(E)$ for $\mathcal{N} = 70$ to the DFs with different degrees \mathcal{N} (Figure 8 (c)). The figure shows that the accuracy of DFs lowers with increasing \mathcal{N} and it reaches order of 10^{-4} at $\mathcal{N} = 400$. Also, Figure 9 shows the power-law profiles under the asymptotic approximations (that appear if the displayed domain in Figure 5 is extended to $E \rightarrow 0$) lose their characteristics as \mathcal{N} increases. In the figure, the power-law profiles for $\mathcal{N} = 400$ and $\mathcal{N} = 70$ are shown.

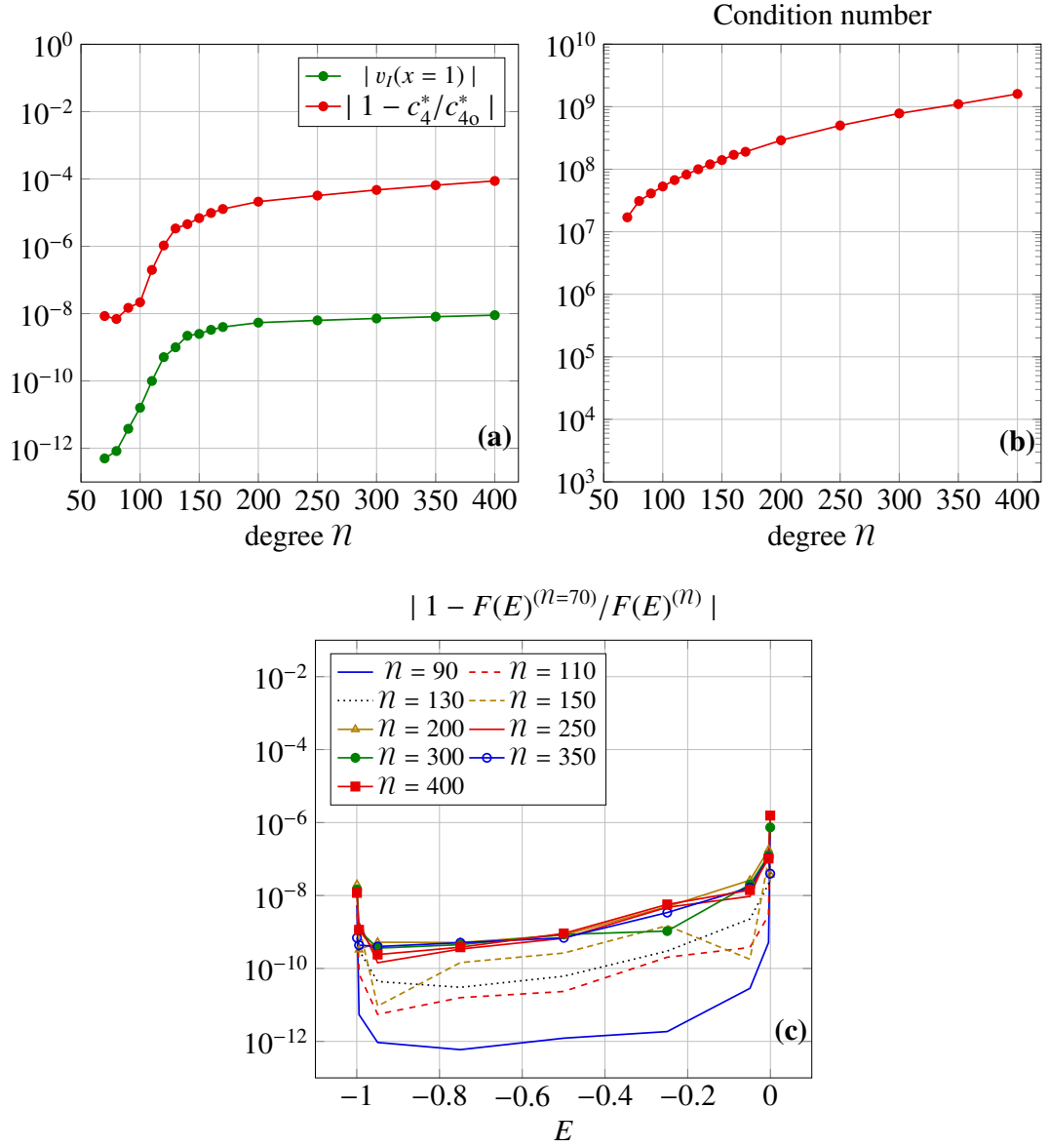


Figure 8: (a) Relative error between c_4 and c_{40}^* and the value of $v_I(x=1)$, (b) Condition number of the Jacobian matrix for the 4ODEs and Q -integral. The condition number was computed when $\{a_q\}^{\text{old}} - \{a_q\}^{\text{new}}$ reached order of 10^{-13} in Newton iteration process. (c) Relative error between DFs with different n and the DF with $n=70$. ($L=1$ and $F_{\text{BC}}=1$)

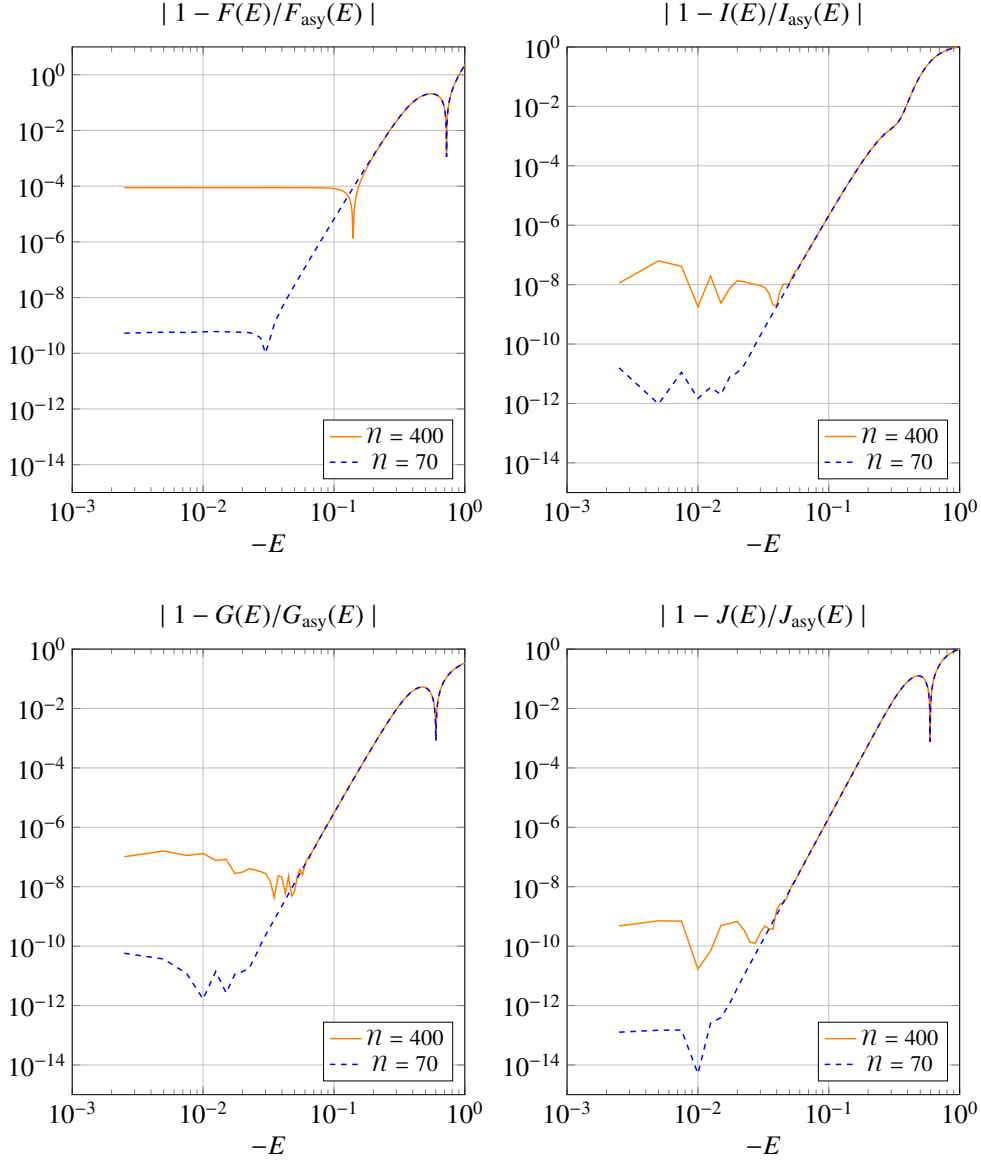


Figure 9: Relative error of the whole-domain spectral solution from the asymptotic approximation for $n = 70$ and $n = 400$. ($F_{BC} = 1$, $L = 1$.)

5. Self-similar solutions on truncated domains

The present section provides spectral solutions on several truncated domains and show that the relative error of an optimal truncated-domain solution from the whole-domain solution with $n = 70$ can achieve order of 10^{-9} on certain truncated domains. Since the spectral solution on the whole domain is unstable against degree n and also since the present work relies on a collocation method, it is imperative for us to construct a spectral solution whose accuracy improves with increasing n . To find such a solution, we truncated the domain of the ss-OAFP system following the approach of (Heggie and Stevenson, 1988). According to Section 4, we extrapolated the domain of $v_F(x)$ so that it turns into $v_F^{(ex)}(x)$ (equation (2.17)) on $-0.2 \lesssim E \lesssim 0$ on which the regularized functions obtained from the whole-domain solution behave like constant functions of E . This means one may expect to obtain several kinds of solutions for different maximum energy E_{\max} . The following classification lists kinds of solutions based on the absolute value

of each term in equation (2.14a) (Refer to Appendix D for the details of the classification.)

- (i) $E_{\max} \lesssim -0.25$ (Incorrect solution)
Solutions and eigenvalues significantly differ from existing results.
- (ii) $-0.25 \lesssim E_{\max} \lesssim -0.05$ (Stable solution)
Chebyshev coefficients are relatively stable against degree \mathcal{N} .
- (iii) $-0.05 \lesssim E_{\max} \lesssim -0.005$ (Semi-stable solution)
Chebyshev coefficients are stable against up to a certain degree \mathcal{N}_c .
- (iv) $-0.005 \lesssim E_{\max}$ (unstable solution)
Chebyshev coefficients are unstable against degree \mathcal{N} .

The goal of the present section is, based on four cases (i) - (iv), to show some optimal truncated-domain solution compatible to the whole-domain solution and to explain the cause of numerical instability of the whole-domain solution. First, Section 5.1 explains the condition to obtain a truncated solution by examining cases (i) and (ii). Sections 5.2 and 5.3 discuss cases (ii) and (iii) to find an optimal truncated-domain solution. Especially, Section 5.2 shows solutions on truncated domains with optimal values of β . Section 5.3 discusses the difference between the solutions obtained on whole- and truncated- domains for fixed $\beta = \beta_o$.

For comparison in the rest of sections, we call the whole-domain solution with $\mathcal{N} = 70$, $L = 1$, F_{BC} and $\beta = \beta_o$ (shown in Section 4.1) the *reference* solution. The solution is labeled with subscript symbol "o"; hence the corresponding functions obtained from the solution are described as $F_o(E)$, $\Phi_o(R_o)$, $v_{Fo}(x)$, $v_{Go}(x)$... and so on.

5.1. Stable solutions on truncated domains with $-0.35 < E_{\max} < -0.05$

While Newton iteration method itself worked for $E_{\max} < -0.1$, spectral solutions obtained on the truncated domains have a transition point around at $E_{\text{soln}} (= -0.225)$ that separates the solutions into incorrect and stable solutions. To see this, the present section shows truncated-domain solutions obtained near E_{soln} for $L = 1$, $F_{BC} = 1$ and $\beta = 8.1783$.⁸ Figure 10 (a) shows the values of $|1 - c_1/c_{1o}|$, $|1 - c_4^*/c_{4o}^*|$ and $|v_I(x = 1)|$ for $-0.35 < E_{\max} < -0.1$ and Figure 10 (b) depicts the condition number of the Jacobian matrix of the 4ODEs and Q -integral. All the values show significant changes around at E_{soln} . Heggie and Stevenson (1988) reported this transition as a difficulty in convergence of Newton method. Since the eigenvalues for $E_{\text{soln}} > E_{\max}$ significantly deviate from both the previous and reference eigenvalues and the value of $|v_I(x = 1)|$ is large ($\gtrsim 10^{-2}$), solutions on $-1 < E < E_{\text{soln}}$ may be considered as incorrect solutions.

⁸The value of β is set to five digits, meaning if one applies the same accuracy relation discussed in Appendix B to this case, the relative error of solutions would be $|1 - c_4^*/c_{4o}^*| \sim 10^{-1}$.

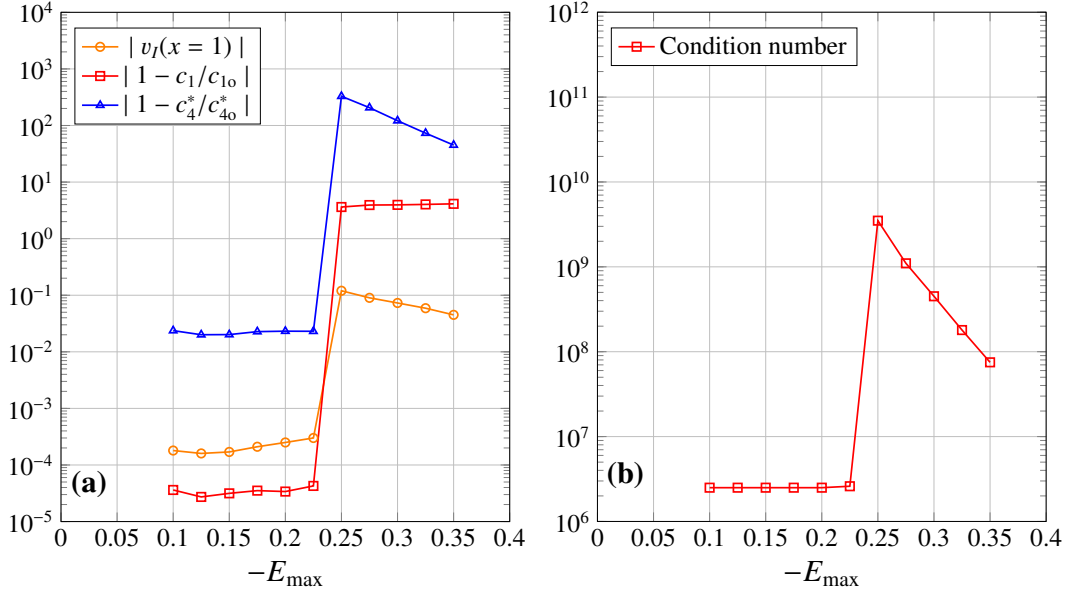


Figure 10: (a) Characteristics of $|v_l(x=1)|$ and relative error of c_1 and c_4^* from their reference eigenvalues for different E_{\max} . ($\mathcal{N} = 40$, $\beta = 8.1783$, $F_{\text{BC}} = 1$ and $L = 1$.) (b) Condition number of the Jacobian Matrix calculated when $\{a_q\}^{\text{new}} - \{a_q\}^{\text{old}}$ reached order of 10^{-13} in Newton iteration.

Spectral solutions for $-0.225 \leq E_{\max} < -0.05$ are relatively stable against degree \mathcal{N} . Especially at $E_{\max} = -0.225$ the solution is the most stable. For $E_{\max} = -0.225$ and $\beta = 8.17837$, Figure 11(a) shows the characteristics of $|1 - c_1/c_{10}|$, $|1 - c_4^*/c_{40}^*|$ and $|v_l(x=1)|$ against degree \mathcal{N} . The Newton iteration worked well even for $\mathcal{N} = 360$ and the accuracy improves with increasing \mathcal{N} in the sense that the eigenvalues approach the reference eigenvalues. Also, higher \mathcal{N} provides smaller absolute values of Chebyshev coefficients. Figure 11 (b) shows the coefficients for $\mathcal{N} = 50$ and $\mathcal{N} = 360$. The reason why the coefficients do not decay rapidly with high index n would be that the rapid decay was hindered by the discontinuous behavior of the Q -integral (Appendix E.1). Possible causes of the discontinuity are that one can not correctly specify the value of β with high accuracy or even an accurate solution does not exist when E_{\max} is not close to zero. In fact, the discontinuous behavior disappears for semi-stable solutions with $E_{\max} \approx 0.05$ (Section 5.2).

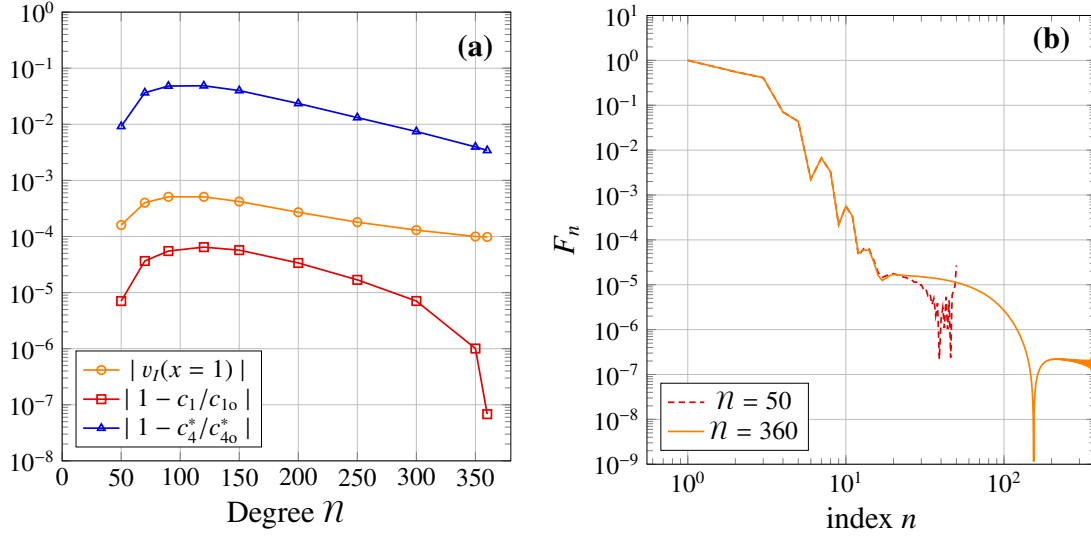


Figure 11: (a) Relative error of c_1 and c_4^* from the reference eigenvalues and the absolute value of $v_I(x = 1)$ for different n . (b) Chebyshev coefficients for v_F with $n = 50$ and $n = 360$. ($E_{\max} = -0.225$ and $\beta = 8.17837$.)

5.2. Optimal eigenvalues of semi-stable solutions on truncated domains with $-0.08 < E_{\max} < -0.03$

On truncated domains with $-0.08 < E_{\max} < -0.03$, Newton iteration method well worked for different n and we found truncated-domain solutions and eigenvalues that are close to the reference- solution and eigenvalues. Especially, the present section provides an optimal value of β on the truncated domains. Table 3 shows optimal eigenvalues for the semi-stable solutions with $-0.08 < E_{\max} < -0.03$ and the maximum significant figures of β is limited to ten.⁹ Also, the table presents the values of $|1 - c_1/c_{10}|$, $|1 - c_4^*/c_{40}^*|$ and $|v_I(x = 1)|$ to show the accuracy of the solutions. On $-0.07 < E_{\max} < -0.03$, the optimal value of β was the same as up to eight significant figures ($= 8.1783712$) of β_o . On one hand, at $E_{\max} = -0.08$ the optimal value of β is relatively large. This would be since $n = 25$ is not large enough to provide an accurate solution (while Newton iteration did not work over $n = 25$). Also, we could not find solutions for small $E_{\max} < -0.07$ whose eigenvalues are as close to β_o as the solutions for $-0.07 < E_{\max} < -0.03$.

The truncated-domain solutions have an advantage over the whole-domain solution. The former needs low degrees ($n = 25 \sim 55$) of polynomials to make Newton method work. Also, even the lowest degrees provide reasonable results in accuracy; $v_I(x = 1) = 10^{-8} \sim 10^{-9}$ and $|1 - c_4^*/c_{40}^*| = 10^{-4} \sim 10^{-6}$. The result of the present section confirms that the eigenvalues of the truncated-domain solutions for $-0.08 < E_{\max} < -0.03$ are the same as those of the whole-domain solution with the prescribed accuracies.

5.3. Optimal semi-stable solutions on truncated domains with $-0.1 < E_{\max} < -0.03$ for fixed $\beta = \beta_o$

To see the direct relationship between the reference and truncated-domain solutions, we show the truncated-domain solutions with fixed $\beta = \beta_o$ for $-0.1 < E_{\max} < -0.03$. The result of Section 5.2 shows that the optimal eigenvalues for semi-stable solutions are close to the reference eigenvalues, hence we fix β to the reference value β_o . We report semi-stable solutions with $\beta = \beta_o$ (Section 5.3.1), show the relation of the solutions with numerical instability against change in degree n (Section 5.3.2) and propose an optimal semi-stable solution that is compatible to the reference solution in accuracy (Section 5.3.3).

5.3.1. Semi-stable solutions with $\beta = \beta_o$

Semi-stable solutions with $\beta = \beta_o$ approach the reference solution as the degree of polynomials increases but they lose accuracy beyond certain degrees. We found truncated-domain solutions with $\beta = \beta_o$ for $-0.1 \leq E_{\max} < -0.03$. In

⁹The condition number of the Jacobian is order of 10^7 in Newton iteration process for the whole-domain solution. This means one can obtain approximately five significant-figure solution since the minimum of the ‘practical’ machine precision is order of 10^{-12} (Appendix D). Considering that the gap in accuracy is order of 10^{-5} between c_1 (or β) and c_4 , the ten maximum significant figures are a reasonable choice for β .

$$E_{\max} = -0.03 \quad \text{or} \quad (-E_{\max})^\beta \approx 3.5 \times 10^{-13}$$

\mathcal{N}	Eigenvalue β	$ 1 - c_1/c_{10} $	$ 1 - c_4^*/c_{40}^* $	$v_I(x=1)$
55	8.178371160	6.5×10^{-10}	2.6×10^{-6}	1.6×10^{-8}
50	8.178371160	7.1×10^{-10}	2.9×10^{-6}	1.7×10^{-8}
40	8.178371165	2.4×10^{-9}	<u>6.9×10^{-7}</u>	<u>4.3×10^{-9}</u>
30	8.178370376	1.3×10^{-7}	9.8×10^{-6}	8.1×10^{-10}
25	8.1783436	8.1×10^{-7}	1.3×10^{-4}	1.1×10^{-9}

$$E_{\max} = -0.05 \quad \text{or} \quad (-E_{\max})^\beta \approx 2.2 \times 10^{-11}$$

\mathcal{N}	Eigenvalue β	$ 1 - c_1/c_{10} $	$ 1 - c_4^*/c_{40}^* $	$v_I(x=1)$
50	8.178371158	2.8×10^{-9}	1.0×10^{-5}	6.8×10^{-8}
40	8.178371165	5.5×10^{-9}	<u>9.7×10^{-7}</u>	<u>3.0×10^{-9}</u>
30	8.1783723	2.1×10^{-8}	3.7×10^{-6}	3.1×10^{-8}
25	8.178373	1.5×10^{-6}	1.9×10^{-5}	4.0×10^{-9}

$$E_{\max} = -0.07 \quad \text{or} \quad (-E_{\max})^\beta \approx 3.6 \times 10^{-10}$$

\mathcal{N}	Eigenvalue β	$ 1 - c_1/c_{10} $	$ 1 - c_4^*/c_{40}^* $	$v_I(x=1)$
35	8.178371159	8.6×10^{-9}	2.3×10^{-6}	<u>1.4×10^{-9}</u>
30	8.1783717	2.2×10^{-7}	1.9×10^{-5}	9.7×10^{-8}
25	8.178382	1.1×10^{-6}	5.0×10^{-5}	9.8×10^{-8}

$$E_{\max} = -0.04 \quad \text{or} \quad (-E_{\max})^\beta \approx 3.7 \times 10^{-12}$$

\mathcal{N}	Eigenvalue β	$ 1 - c_1/c_{10} $	$ 1 - c_4^*/c_{40}^* $	$v_I(x=1)$
55	8.178371160	5.1×10^{-10}	2.1×10^{-6}	1.3×10^{-8}
50	8.178371160	1.9×10^{-10}	8.3×10^{-7}	5.1×10^{-9}
40	8.178371170	1.4×10^{-10}	<u>7.1×10^{-7}</u>	<u>4.0×10^{-9}</u>
30	8.17837159	1.8×10^{-7}	4.7×10^{-6}	6.7×10^{-9}
25	8.1783585	1.7×10^{-6}	6.8×10^{-5}	5.2×10^{-9}

$$E_{\max} = -0.06 \quad \text{or} \quad (-E_{\max})^\beta \approx 1.0 \times 10^{-10}$$

\mathcal{N}	Eigenvalue β	$ 1 - c_1/c_{10} $	$ 1 - c_4^*/c_{40}^* $	$v_I(x=1)$
40	8.178371160	8.3×10^{-10}	<u>8.7×10^{-7}</u>	<u>2.2×10^{-9}</u>
30	8.17837225	1.5×10^{-7}	5.0×10^{-6}	8.1×10^{-9}
25	8.1783813	2.4×10^{-7}	1.6×10^{-5}	2.3×10^{-9}

$$E_{\max} = -0.08 \quad \text{or} \quad (-E_{\max})^\beta \approx 1.1 \times 10^{-9}$$

\mathcal{N}	Eigenvalue β	$ 1 - c_1/c_{10} $	$ 1 - c_4^*/c_{40}^* $	$v_I(x=1)$
25	8.1783768	2.8×10^{-6}	<u>4.7×10^{-5}</u>	<u>7.9×10^{-9}</u>

Table 3: Numerical results for the truncated-domain formulation at different E_{\max} ($L = 1$ and $F_{\text{BC}} = 1$). The minimum values of $|1 - c_4^*/c_{40}^*|$ and $v_I(x=1)$ are underlined to highlight the accuracy for each \mathcal{N} . The results do not include some data in which the value of $v_I(x=1)$ are greater than of the order of $\sim 10^{-7}$ for convenience. The Newton iteration method was very hard to work for $\mathcal{N} < 25$ and the degrees beyond the maximum values of \mathcal{N} for each E_{\max} ; those conditions provided the change $|\{a_n\}^{(\text{new})} - \{a_n\}^{(\text{old})}| \gtrsim 10^{-9}$ while the data in the table are the results when it reached order of $\sim 10^{-12}$.

order to see the accuracy of the solutions, Figure 12 shows the characteristics of $v_I(x = 1)$ against \mathcal{N} and the relative errors of c_1 and c_4^* from the reference values. For $E_{\max} > -0.07$, $|v_I(x = 1)|$, $|1 - c_1/c_{10}|$ and $|1 - c_4^*/c_{40}^*|$ show an ideal characteristics under change in \mathcal{N} . They decrease with increasing \mathcal{N} and can reach very small values ($\approx 10^{-9} \sim 10^{-13}$) at certain degrees. Beyond the degrees, the Newton iteration method, however, did not work or the solutions significantly lose their accuracies. On one hand, for $E_{\max} < -0.07$ the characteristics of the \mathcal{N} -dependence are less ideal. The values of $|v_I(x = 1)|$, $|1 - c_1/c_{10}|$ and $|1 - c_4^*/c_{40}^*|$ stall with increasing \mathcal{N} while the minimum values still can be found at relatively-low degrees ($\mathcal{N} = 27 \sim 35$). This would be since the optimal value of β is not close to β_0 as found in Table 3; near $E_{\max} = -0.08$ the optimal value may be larger than β_0 .

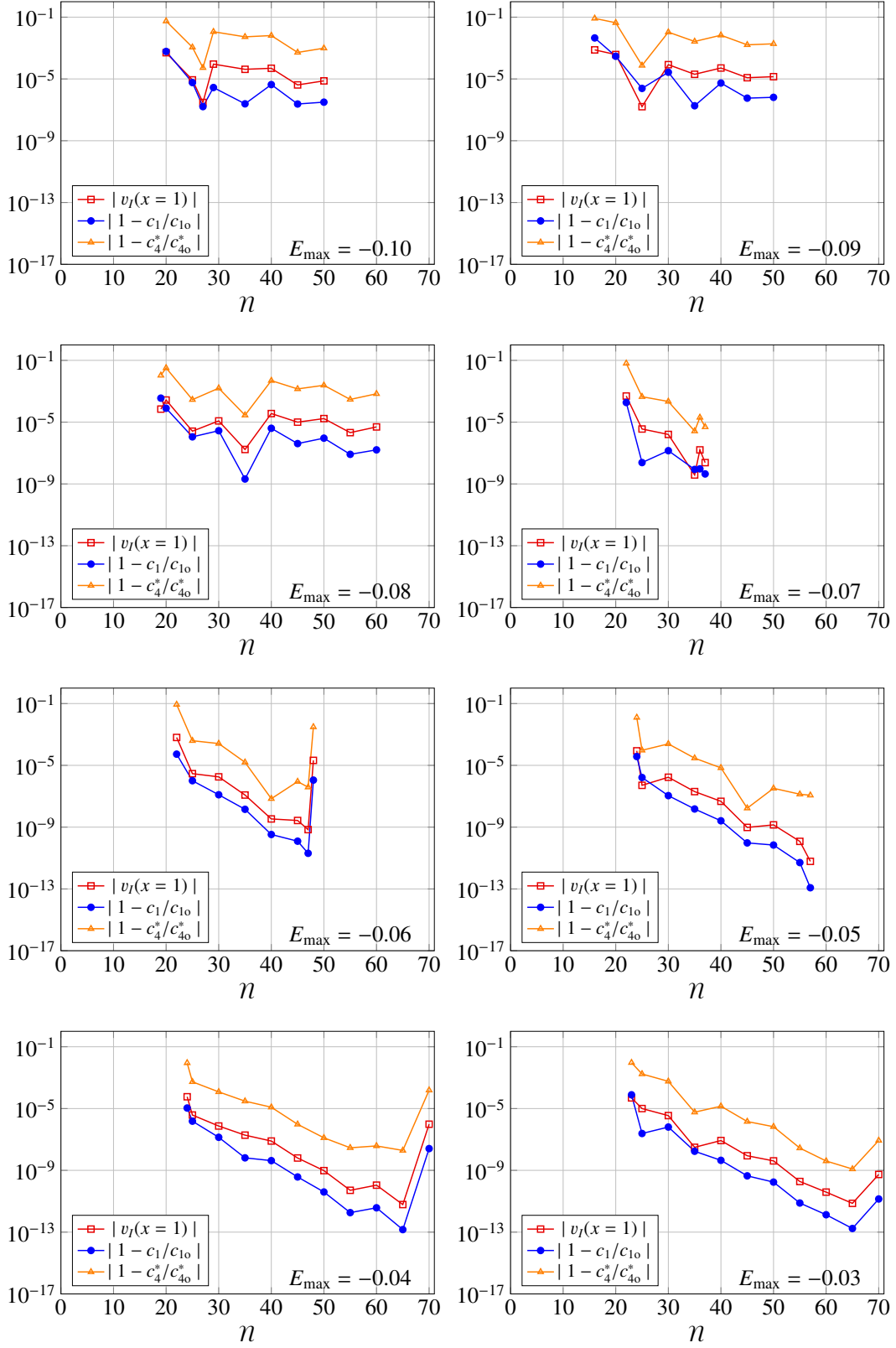


Figure 12: Relative errors of c_1 and c_4^* from the reference eigenvalues and characteristics of $v_I(x=1)$ against n for the truncated-domain solutions with $\beta = \beta_o$. ($-0.1 \leq E_{\max} \leq -0.03$, $L = 1$ and $F_{BC} = 1$.)

5.3.2. Truncated domains and numerical instability against change in degree \mathcal{N}

We consider the numerical stability that occurred to the semi-stable solutions and reference solution originates from the property that ss-OAFP system may not have a solution when the terms of the system reach order of machine precision at equation level and beyond the accuracy. In Figure 12, the minimum of $|v_I(x=1)|$ occurs at degrees $\mathcal{N}_{\text{best}} = \{27, 25, 35, 35, 47, 57, 65, 65\}$ for $E_{\text{max}} = \{-0.10, -0.09, -0.08, -0.07, -0.06, -0.05, -0.04, -0.03\}$. To consider why the truncated-domain solutions lose their accuracy beyond $\mathcal{N}_{\text{best}}$, Figure 13 depicts the E_{max} -dependence of $|v_I(x=1)|$, $|1 - c_1/c_{10}|$ and $|1 - c_4^*/c_{40}^*|$ obtained at each $\mathcal{N}_{\text{best}}$. The value of $|1 - c_4^*/c_{40}^*|$ decreases in a power-law-like fashion with increasing E_{max} . One may understand this characteristics by introducing a power-law profile $c_{10}(-E_{\text{max}})^{\beta_0}/c_{40}^*$. This profile originates from the power-law dependence of the last term in equation (2.14a) (See Appendix D). In Figure 13, the decrease of $c_{10}(-E_{\text{max}})^{\beta_0}/c_{40}^*$ is similar to that of $|1 - c_4^*/c_{40}^*|$. On one hand, $|1 - c_1/c_{10}|$ and $|v_I(x=1)|$ stops decreasing at E_{max} larger than -0.05 . This may be understood as the limit of double precision. In addition to $c_{10}(-E_{\text{max}})^{\beta_0}/c_{40}^*$ that characterizes the accuracy of c_{40}^* (correspondingly the solution), the infinity norm of $|\{F_n\}^{(\text{old})} - \{F_n\}^{(\text{new})}|$ for Newton method reaches order of 10^{-13} at best (Appendix D). Under these circumstances, $c_{10}(-E_{\text{max}})^{\beta_0}/c_{40}^*$ reaches order of 10^{-13} at $E_{\text{max}} \approx -0.0523$ that is the maximum value of E_{max} to preserve numerical accuracy. This result implies that, for the truncated-domain solutions for $E_{\text{max}} \lesssim -0.05$, machine precision is not enough precise to obtain more accurate solution. On one hand, in case of the reference solution, the solution is not truncated on large E , meaning the power-law boundary conditions in the ss-OAFP system can be satisfied only when they reach order of machine precision. Hence, the reference solution does not improve accuracy with increasing low degrees of polynomials unlike the semi-stable solution and it only loses its accuracy with increasing large degree. One can find more detail discussion for machine precision and the convergence of Newton iteration method in Appendix D.

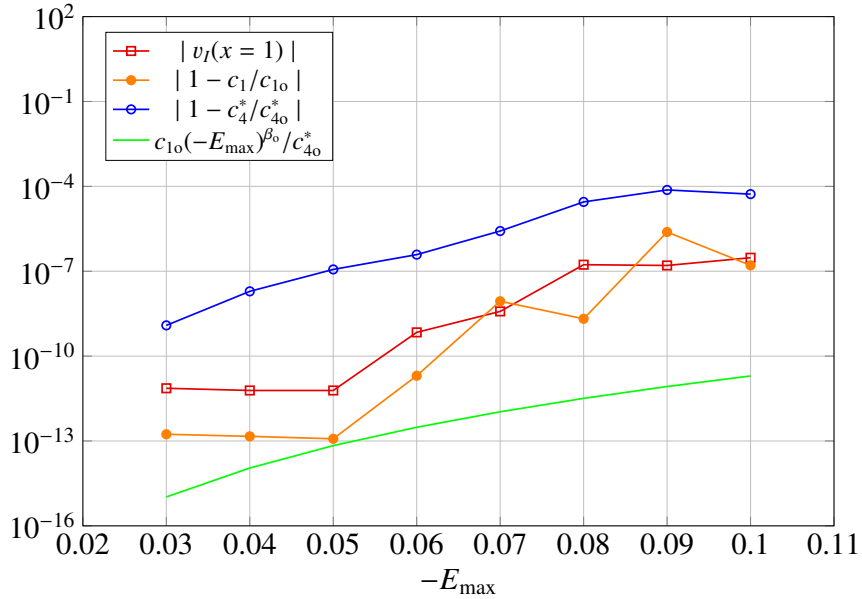


Figure 13: Relative error of c_1 and c_4^* from the reference values and characteristics of $|v_I(x=1)|$ that are obtained at each $\mathcal{N}_{\text{best}}$. The guideline $c_{10}(-E_{\text{max}})^{\beta_0}/c_{40}^*$ is shown for comparison. ($L = 1$, $F_{\text{BC}} = 1$ and $\beta = \beta_0$.)

5.3.3. An optimal semi-stable solution

Lastly, we propose an optimal truncated-domain solution that is compatible to the reference solution. For $E_{\text{max}} = -0.03$ in Figure 12, the order of $|1 - c_4^*/c_{40}^*|$ reaches 10^{-9} . This is the same order as the minimum value of $|1 - c_4^*/c_{40}^*|$ computed against different β in Section B.1. Also, $|v_I(x=1)| \approx 6.1 \times 10^{-12}$ for $\mathcal{N} = 65$ is one of the least values among the values of $|v_I(x=1)|$ calculated for semi-stable truncated solutions. Hence we calculated the relative errors between the DF with $\mathcal{N} = 65$ and DFs with different \mathcal{N} for $E_{\text{max}} = -0.03$ (Figure 14 (a)). We obtained the ideal tendency that as \mathcal{N} increases the DFs gradually converge to the DF with $\mathcal{N} = 65$. Hence the truncated-domain solution

with $E_{\max} = -0.03$, $n = 65$ and $\beta = \beta_o$ is the optimal truncated-domain solution in the present work. Figure 14 (b) shows the relative error between DFs between the optimal solution and the reference solution at points that are less associated with the Gauss-Chebyshev nodes. The optimal truncated-domain solution validates the reference solution and the largest relative error between them is order of 10^{-9} at the prescribed points.

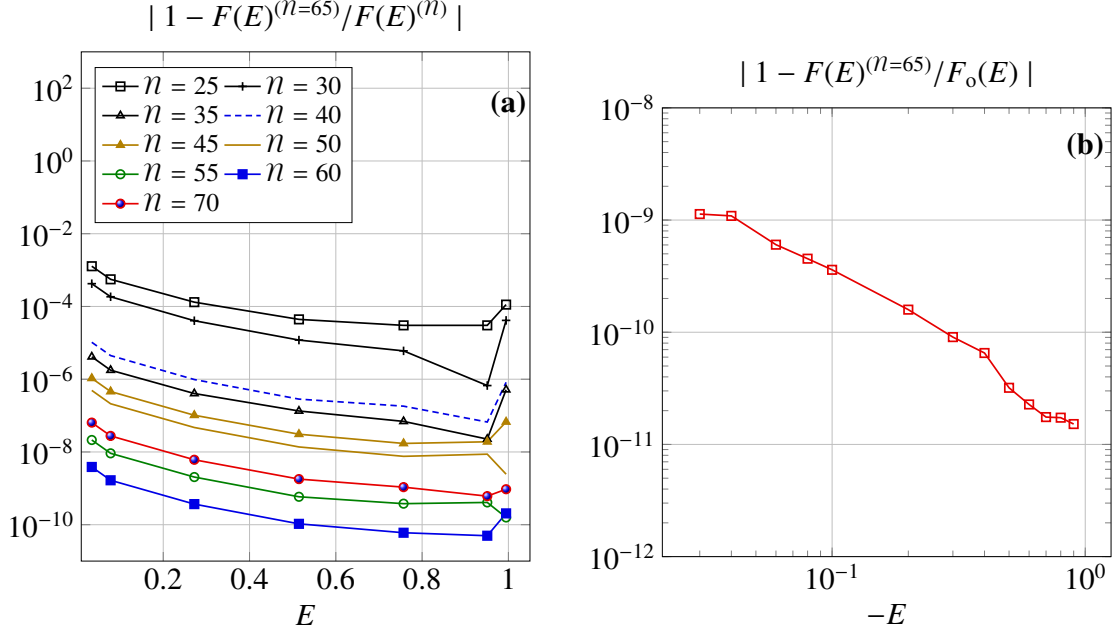


Figure 14: (a) Relative errors between DFs with different n and DF with $n = 65$ for $E_{\max} = -0.03$. ($L = 1$ and $F_{BC} = 1$) (b) Relative error between the reference solution $F_o(E)$ and the optimal truncated-domain solution. ($L = 1$, $F_{BC} = 1$ and $\beta = \beta_o$.)

6. Discussion: Modifying the mathematical formulation of the ss-OAFP system to reproduce the HS's solution

The present section discusses how to improve the whole-domain solution and reproduce the solution of (Heggie and Stevenson, 1988) using the spectral method to discuss the accuracy of the reference solution. The result of Section 5.1 shows that the stable truncated-domain solutions on $-0.35 < E < -0.1$ are closer to the reference solution rather than the HS's solution that was obtained on almost the same domain. Our goal of the present section is to show that the discrepancy between our and the HS's solutions originates from the difference in mathematical formulation of the ss-OAFP system between the two works. In order to explain the discrepancy and also see the consistency of our result compared to the HS's solution, we discuss several classes of ss-OAFP solutions by modifying the regularized independent variables. We found that only modification of $v_J(x)$, $v_R(x)$ and $v_F(x)$ provides significant change in ss-OAFP solution while that of the rest of the regularized function does not change the solution. Sections 6.1 and 6.2 detail the effect of modifying the regularization of $v_J(x)$ and $v_R(x)$ to improve the asymptotic behavior of $v_J(x)$ and to discuss the effect of discontinuity in $v_R(x)$. Based on the modification of $v_R(x)$, Section 6.3 reproduces the HS's solution with limited degrees of Chebyshev polynomials and shows that the formulation can provide both the HS's and reference- solutions only by controlling x_{\min} (or E_{\max}). For brevity, further detail discussion on reproducing the HS's solution is included into Appendix F in which we discuss how to take off the limitation on the degrees of polynomial; this can be done by modifying the regularization of $v_R(x)$ and $v_F(x)$.

6.1. Modification of function $v_J(x)$ and its asymptotic behavior

The present section shows that one can improve the reference solution by modifying the regularization of the regularized function $v_J(x)$. Even after all the independent variables of the ss-OAFP system are completely regularized (so that the variables reach certain constant values at the end points of the domain), the terms of the regularized

ss-OAFP system significantly change at equation level. All the terms in the 4ODEs (equations (2.14a) and (2.14d)) change like at least $\sim (0.5 + 0.5x)^\beta$ as $x \rightarrow -1$. The result of Section 4 shows the consequence of the large-scale gap in Figure 7 in which the accuracy in the logarithmic derivative and higher order of $\sim (0.5 + 0.5x)^\beta$ in v_J are divergent as $x \rightarrow -1$. One can weaken the divergence by modifying the regularization of $v_J(x)$ as follows

$$v_J^{(m)}(x) \equiv (v_J(x) + 1) \left(\frac{1+x}{2} \right)^{-bL}, \quad (6.1)$$

where b is a real number. In equation (2.14a) the highest order of $(0.5 + 0.5x)^\beta$ is the term $\frac{dv_J(x)}{dx} \left(\frac{1+x}{2} \right)^\beta$, hence the function $v_J^{(m)}(x)$ can reduce it to $\frac{dv_J(x)}{dx} \left(\frac{1+x}{2} \right)^{\beta-b}$. We solved the ss-OAFP system again following the procedure of Section 3.2, but this time for $v_J^{(m)}(x)$ (in place of v_J) and the rest of unchanged regularized independent variables on both truncated and whole domains.

We found solutions for $1 \leq b \leq 6$ on both whole and truncated domains and $b = 6$ provided the best result in accuracy. The results are quite well; the modification of v_J improved the asymptotic behaviors of the logarithmic derivative of $v_J(x)$ and the approximation $C_\beta(c_1, c_4^*)$ as $x \rightarrow -1$ on the whole domain (Figure 15). Also, the eigenvalues that were obtained for $b = 6$ on the truncated and whole domains are almost identical to the reference eigenvalues (Table 4). The relative error between stellar DFs obtained from the reference solution and the truncated-domain solution is at most order of $\sim 3 \times 10^{-8}$ for $b = 6$ at $E_{\max} = -0.025$ (Figure 16). This result infers that one can obtain a *suitable* solution that is less divergent in higher order of $\sim (0.5 + 0.5x)^\beta$ as $x \rightarrow -1$ by correctly regularizing function $J(E)$.

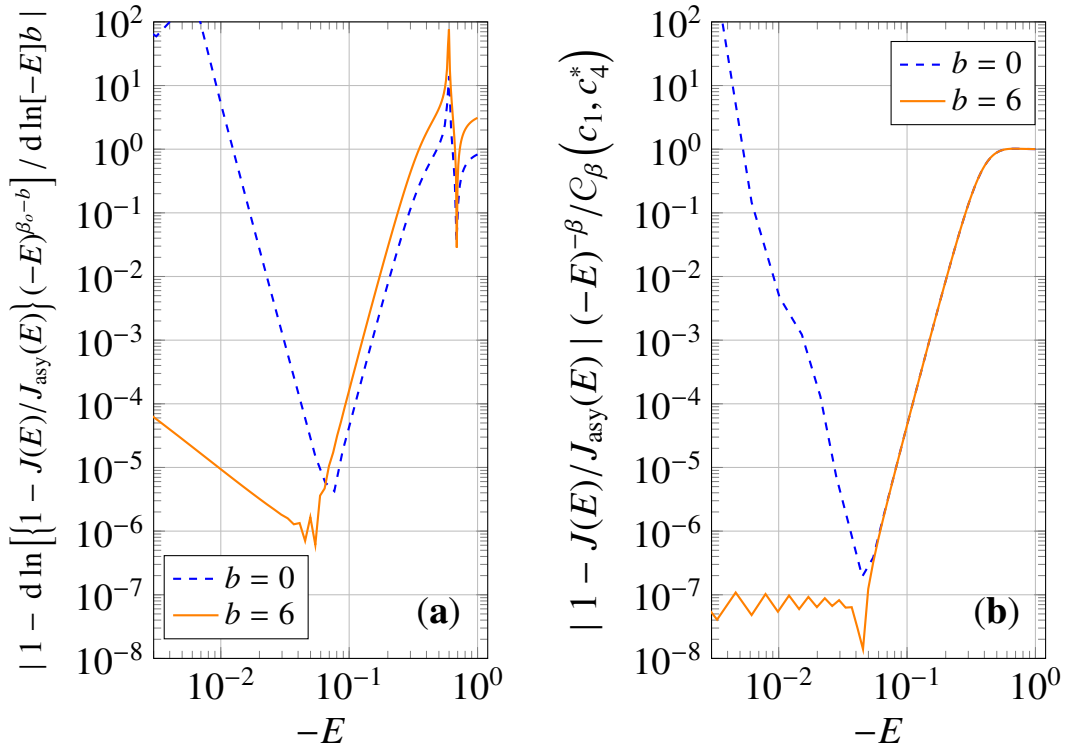


Figure 15: (a) Logarithmic derivative of $|1 - J(E)/J_{\text{asy}}(E)|$ with respect to E and (b) Characteristics of $|1 - J(E)/J_{\text{asy}}(E)| (-E)^{-\beta}$ on the whole domain for $b = 6$. ($\mathcal{N} = 150$, $F_{\text{BC}} = 1$, $L = 1$). The solution with $b = 0$ corresponds to the reference solution.

domain	n	optimal β	$ 1 - c_1/c_{10} $	$ 1 - c_4^*/c_{40}^* $	$v_I(x=1)$	condition number
whole	150	β_0	2.4×10^{-11}	7.7×10^{-8}	1.6×10^{-9}	8.8×10^7
truncated ($x_{\min} = -0.95$)	55	$\beta_0 + 3.0 \times 10^{-12}$	1.6×10^{-12}	2.6×10^{-8}	3.0×10^{-12}	1.2×10^8

Table 4: Numerical results for the integration of the ss-OAFP system for $b = 6$. ($L = 1$ and $F_{BC} = 1$). The eigenvalues are compared to the reference eigenvalues.

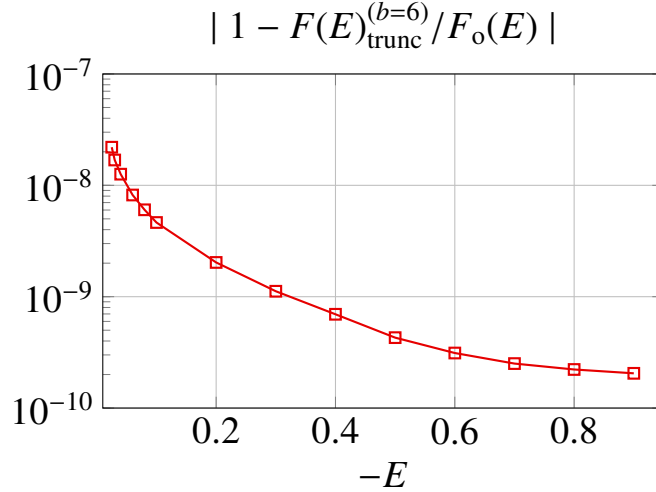


Figure 16: Relative error between DFs obtained from the reference solution and from the truncated-domain solution with $x_{\min} = -0.95$, $b = 6$ and $n = 55$. ($F_{BC} = 1$ and $L = 1$).

6.2. Modification of function $v_R(x)$ and its discontinuous behavior

The asymptotic behavior of $v_R(x)$ as $x \rightarrow -1$ is important to see the effect of discontinuity in the ss-OAFP solutions and the discontinuity clearly appears in the solutions that are obtained without the assumption that $v_R(x)$ is regular at $x = -1$ (this assumption is made implicitly in Section 2 by regularizing R with $(1 - E)$). We show this by modifying the regularization of $v_R(x)$ as follows

$$v_R^{(m)}(x) = [v_R(x)]^2 \left(\frac{1-x}{2} \right). \quad (6.2)$$

The square of $v_R(x)$ can avoid the endpoint singularity at the branch point $x = 1$. Again we solved the ss-OAFP system but this time for $v_R^{(m)}(x)$ and for the rest of independent variables (without including $v_J^{(m)}(x)$), following the procedure of Section 3.2.

We found spectral solutions with high degrees (e.g. $n = 540$) for $E_{\max} = -0.05$. The computed functions $v_F(x)$ and $v_R^{(m)}(x)$ well explain the feature of discontinuity in the ss-OAFP system. Figures 17 shows the maximum relative errors of $v_R^{(m)}(x)$ and v_F are order of 2×10^{-5} and 5×10^{-5} from their reference solutions $v_{R0}(x)$ and $v_{F0}(x)$. The order of errors well reflects the relative error of the solutions from their asymptotic approximations (Figure 18). Figure 19 depicts the Chebyshev coefficients of $v_F(x)$ and $v_R^{(m)}(x)$. A slow decay appears in both the coefficients for $v_F(x)$ and $v_R^{(m)}(x)$. The former apparently flattens (more exactly, decays like $7 \times 10^{-8} n^{-0.1}$) and the latter decays like $1.5 \times 10^{-9} n^{-1}$. It is not easy for one to find the cause of the flattening and slow decay due to the mathematically complex structure of the ss-OAFP system. Yet, the asymptotic behavior $a_n \sim 1/n$ ($n \rightarrow \infty$) has approximately the same decay rate as Chebyshev coefficients for discontinuous functions (Boyd, 2001; Xiang, 2013). Hence, Appendices E.1 and E.2 show the numerical results that we obtained by integrating the Q integral for a fixed discontinuous v_R and also by solving

the Poisson equation for a fixed discontinuous v_D . The former provides a slow decay of Chebyshev coefficients like $1/n$ or much slower (Figure E.29) and the latter a flattening of Chebyshev coefficients for large n (Figure E.30). These unique behaviors occur only when the point of discontinuity is very close to either of endpoints on the domain (See Appendices E.1 and E.2 for detail).

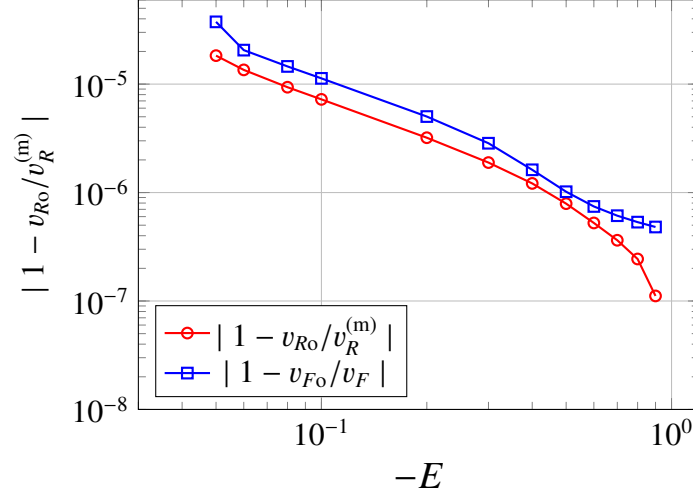


Figure 17: Relative error of $v_R^{(m)}$ and v_F from their reference solutions v_{R0} and v_{F0} . ($E_{\max} = -0.05$, $\mathcal{N} = 540$, $L = 1$ and $F_{BC} = 1$.)

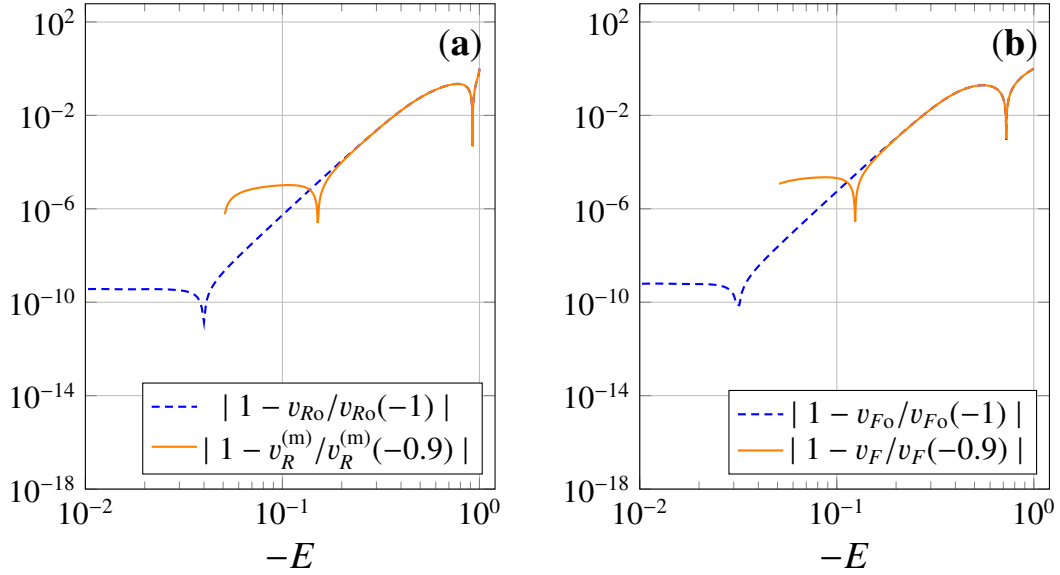


Figure 18: (a) Comparison of asymptotic behaviors between $v_R^{(m)}$ and v_{R0} . On the graph, the relative errors between them and the corresponding end values $v_R^{(m)}(x = -0.9)$ and $v_{R0}(x = -1)$ are shown. (b) Comparison of asymptotic behaviors between v_{F0} and v_F . On the graph, the relative errors between them and the corresponding end values $v_F(x = -0.9)$ and $v_{F0}(x = -1)$ are shown.

6.3. Reproducing the HS's solution and eigenvalues with limited degrees

The present section reproduces the HS's solution with low degrees ($\mathcal{N} < 20$) of polynomials by modifying the regularization of v_R . According to (Heggie and Stevenson, 1988), the numerical values of their solutions are “thought

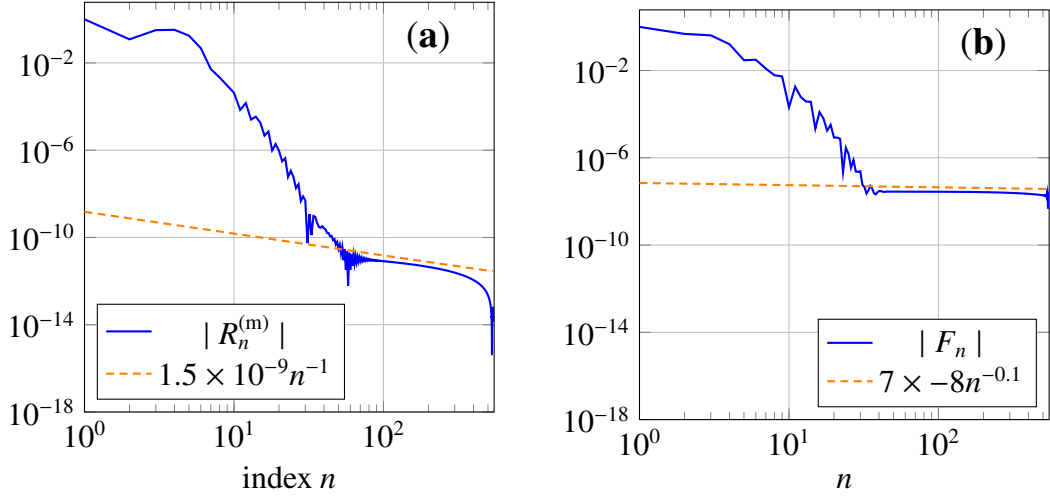


Figure 19: (a) Absolute value of Chebyshev coefficients for $v_R^{(m)}$. (b) Absolute value of the Chebyshev coefficients for v_F . Dashed guidelines are also depicted for measure of slow decay.

to be accurate about three significant figures”. On one hand, they described the value of χ_{esc} as “ ~ 13.85 ” and reported three significant figures for the eigenvalues c_1 , c_2 , c_3 and c_4 . Due to these ambiguous expressions and lack of detail description for their error analysis in (Heggie and Stevenson, 1988), the present section aims to reproduce *at least two significant figures* of the HS’s solutions and eigenvalues. We show the results obtained by reformulating the ss-OAFP system based on $v_R^{(m)}$ (explained in Section 6.2) and by using the numerical procedure of Section 3.2. However, the results reproduced only either of the HS’s solution and eigenvalues for a certain \mathcal{N} , not both of them. To understand the reproduced solutions, the present section examines two kinds of solutions. In section 6.3.1, the first kind of solution reproduces the HS’s solution but the eigenvalues are the same as only two significant figures of the HS’s eigenvalues. In section 6.3.2 the second kind reproduces the HS’s eigenvalues but the solution is the same as only two significant figures of the HS’s solution. For comparison, the HS’s solution is labeled hereafter by subscript ‘HS’, such as F_{HS} for stellar DF.

6.3.1. Reproducing the same solution as HS’s work

We found spectral solutions with low degrees ($\mathcal{N} = 13 \sim 19$) that can provide the same numerical values of $\ln[F(E)]$ as (Heggie and Stevenson, 1988)’s work, however the obtained eigenvalues are different from the HS’s eigenvalues (Table 5). Only two significant figures of the eigenvalues are stable against E_{max} ; $\beta = 8.2$, $c_1 = 9.1$ and $c_4 = 3.5$ and three significant figures of the physical parameters; $\chi_{\text{esc}} = 13.8$ and $\alpha = 2.23$. The measures of accuracy, $\min(\{F_n\})$ and $v_I(x=1)$, hold approximately the same order for different E_{max} and \mathcal{N} , that is, $\min(\{F_n\}) \approx 10^{-4}$ and $|v_I(x=1)| \approx 10^{-4} \sim 10^{-5}$.

Available degrees \mathcal{N} that can reproduce the HS’s solution are limited. Figure 20 shows the \mathcal{N} -dependence of relative error between the calculated DF and HS’s DF for $E_{\text{max}} = -0.275$. Since the HS’s work reported their solution rounded to the second decimal places, we also show the values of $0.005/\ln[F_{\text{HS}}]$ in the figure as reference. The spectral solution reproduced the HS’s solution for $\mathcal{N} = 15$ and $\mathcal{N} = 17$; in Figure 20 all the relative errors are below $0.005/\ln[F_{\text{HS}}]$. However, beyond $\mathcal{N} = 17$, our DF deviates from the HS’s DF.

6.3.2. Finding solution whose eigenvalues are the same as the HS’s eigenvalue

We found spectral solutions whose eigenvalues are the same as the HS’s eigenvalues ($c_1 = 9.10$ and $c_4 = 3.52$) with $\mathcal{N} = 15$ near $E_{\text{max}} = -0.225$. For the solutions, Table 6 shows β , χ_{esc} and measures of accuracy ($\min(\{F_n\})$ and $|v_I(x=1)|$). The measures of accuracy are approximately the same order as the reproduced HS’s solution (shown in Table 5); $\min(\{F_n\}) \sim |v_I(x=1)| \sim 10^{-4}$. Interestingly, for $E_{\text{max}} = -0.225$, χ_{esc} reaches the HS’ value ($= 13.85$). The numerical values of $\ln[F]$ reproduced 2 \sim 4 significant figures of $\ln[F_{\text{HS}}]$. The relative error between $\ln[F]$ and

E_{\max}	n	β	$c_1(\times 10^{-4})$	$c_4(\times 10^{-2})$	χ_{esc}	$\min(\{F_n\})$	$ v_I(x=1) $
-0.300	19	8.17370	9.101	3.449	13.838	3.5×10^{-4}	4.0×10^{-4}
-0.290	17	8.17050	9.110	3.451	13.837	3.2×10^{-4}	3.3×10^{-4}
-0.275	17	8.17316	9.103	3.495	13.837	3.4×10^{-5}	3.2×10^{-5}
-0.260	15	8.16900	9.112	3.497	13.835	1.3×10^{-4}	2.6×10^{-5}
-0.250	15	8.17188	9.105	3.526	13.836	3.5×10^{-4}	1.7×10^{-4}
-0.240	13	8.16110	9.137	3.485	13.832	1.1×10^{-4}	7.2×10^{-6}
-0.230	13	8.16060	9.130	3.497	13.832	2.8×10^{-4}	9.0×10^{-5}
-0.220	13	8.16020	9.123	3.514	13.832	4.7×10^{-4}	1.8×10^{-4}
-0.210	13	8.15800	9.124	3.489	13.835	3.8×10^{-4}	1.3×10^{-4}
-0.200	13	8.15850	9.122	3.529	13.834	7.0×10^{-4}	3.0×10^{-4}

Table 5: Eigenvalues obtained when the spectral solution reproduced the HS's solution. Heggie and Stevenson (1988) reported the numerical values of their solution on $-1 \lesssim E \leq -0.317$. They mentioned that their Newton iteration method worked up to $E_{\max} \approx -0.223$ and it could work beyond -0.223.

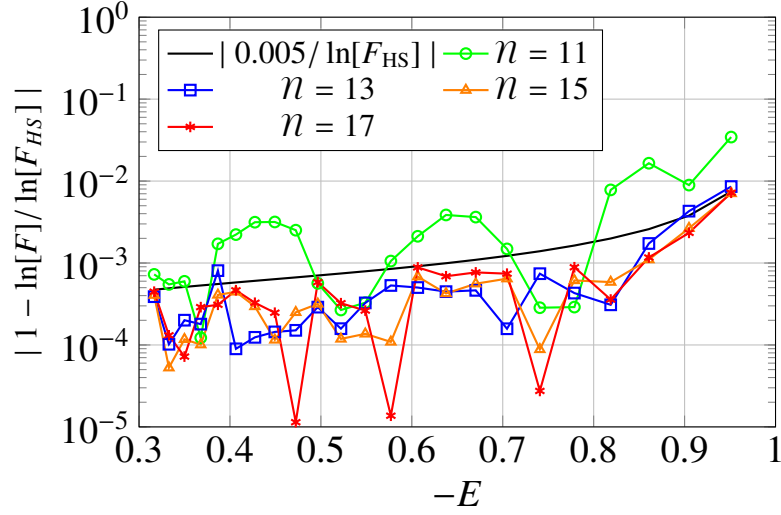


Figure 20: Degree- n -dependence of relative error of $\ln[F]$ obtained from the spectral and HS's solutions for $E_{\max} = -0.275$.

E_{\max}	β	χ_{esc}	$\min(F_n)$	$v_I(x=1)$
-0.240	8.17310	13.840	4.1×10^{-4}	2.1×10^{-4}
-0.225	8.17460	13.845	4.5×10^{-4}	2.3×10^{-4}
-0.215	8.17536	13.847	4.7×10^{-4}	2.4×10^{-4}
-0.200	8.17560	13.850	4.6×10^{-4}	2.3×10^{-4}

Table 6: Eigenvalues of the reproduced HS's solution with eigenvalues $c_1 = 9.10 \times 10^{-4}$ and $c_4 = 3.52 \times 10^{-2}$ for $n = 15$. (Heggie and Stevenson, 1988) reported the numerical values of their solution on $-1 \lesssim E \leq -0.317$. They mentioned that their Newton iteration method worked up to $E_{\max} \approx -0.223$ and it could work beyond -0.223.

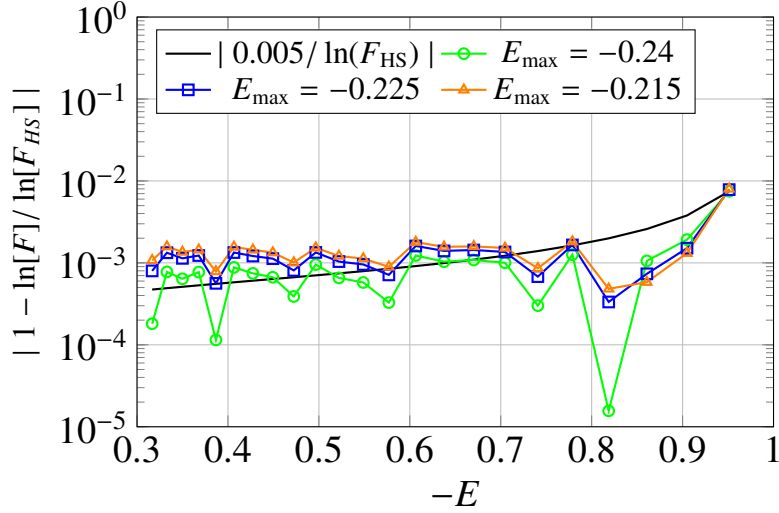


Figure 21: Relative error between DFs obtained from the spectral solution with $n = 15$ and HS's solution for different truncated domains.

$\ln[F_{\text{HS}}]$ is at most order of 1×10^{-3} for $E \geq -0.9$ (Figure 21). This result would infer that the spectral solution reproduced “about three significant figures” of the HS's solution with the same eigenvalues.

6.3.3. Successfully reproducing HS's solution and accuracy of the reference solution

We briefly explain the condition to obtain the both reference- and HS's solution on truncated domains based on only a single mathematical formulation of the ss-OAFP model. For brevity the detail discussion is made in Appendix F and we explain only the results. The most important result in Appendix F is that one can find the HS's solution if the absolute value of the coefficients $\{I_n\}$ for $v_I(x)$ reach approximately $10^{-4} \sim 10^{-5}$ for $E_{\max} \approx -0.25$ and also the reference solution if the coefficients reach order of $10^{-6} \sim 10^{-7}$ for $E_{\max} \approx -0.05$ (Figure F.34). We believe the reason why we could not find out the condition in the present section is that the decay rate of the Chebyshev coefficients is too rapid and provided only limited degrees to obtain the HS's solution for $E_{\max} \approx -0.25$. Hence, for numerical calculation in the Appendix F, we intentionally included the effect of the non-analytic and non-regular properties into dependent variables by modifying the regularization of v_R (with a discontinuity) and v_F (with a logarithmic dependence).

We believe our numerical accuracy of the reference solution is at least four significant figures based on the detail analyses that we carried out for the various formulations in the present section, Sections 4 and 5 and Appendixes B and F. What we made the most efforts in the majority of the present work is to find a truncated-domain solution which is close to HS's solution for small E_{\max} but still close to the reference solution for large E_{\max} based on only a single formulation. Among the variant formulations, the $v_R^{(m)}$ -formulation of the present section not only reproduced both the HS's and reference- solutions but also provided the smallest relative error ($\sim 4 \times 10^{-5}$) from the reference solution (See Figure 17). This error corresponds with the relative error of c_4 from the reference eigenvalue. Hence, Table 1 lists four significant figures for c_4 and five for the rest of eigenvalues (since c_1 , c_2 and c_3 were more stable against numerical parameters than c_4 for any formulations in our work.)

7. Conclusion

The self-similar OAFP equation to model core-collapsing star clusters is important in the sense that it provides a conceptual understanding of the late stage of the relaxation evolution of isotropic-spherical dense star clusters and useful physical parameters. The equation, however, has never been solved with an agreeable accuracy and existing solutions were domain-truncated, whose domain is $-0.2 < E < 1$. Accordingly, the detail physical feature and application of the model have never been discussed; those are the topics we discuss in our follow-up papers. This work is the first paper of our works on the ss-OAFP equation focusing on finding an accurate solution of the equation using a Gauss-Chebyshev pseudo-spectral method.

We first applied the pseudo-spectral method to the ss-OAFP equation on the whole domain ($-1 < E < 0$). Section 4 provided the whole-domain solution whose degree of Chebyshev polynomials is 70. The minimum of the normalized Chebyshev coefficients reaches order of 10^{-12} for all the regularized independent variables in the equation. We obtained the corresponding eigenvalues more consistently compared to existing works as follows $c_1 = 9.0925 \times 10^{-4}$, $c_2 = 1.1118 \times 10^{-4}$, $c_3 = 7.1975 \times 10^{-2}$ and $c_4 = 3.303 \times 10^{-2}$. The eigenvalues result in the following physical parameters; the power-law index α is 2.230, the collapse rate $\xi = 3.64 \times 10^{-3}$ and the scaled escape energy $\chi_{\text{esc}} = 13.89$. Also, we provided a semi-analytical form of the whole-domain solution whose degree of polynomials is at most 18.

Since the whole-domain solution depends on degree n of polynomials in an undesirable way, in Section 5 we aimed at finding truncated-domain solutions whose accuracy improves with increasing degree n . We obtained truncated-domain solutions whose numbers of significant figures are up to 8 for $-0.08 \leq E_{\text{max}} < -0.04$ and the degrees of the polynomials are only $N \approx 25 \sim 55$. To find an optimal truncated-domain solution that is close to the whole-domain solution, we obtained the truncated-domain solutions with $\beta = \beta_o$ for $-0.05 \leq E_{\text{max}} < -0.02$ and those solutions are stable against up to specific degrees of polynomials. At point $E_{\text{max}} = -0.03$, the truncated-domain solution has the same order of accuracy in c_4^* as the whole-domain solution. Hence, we compared the reference solution and the truncated-domain solution with $N = 65$ at $E_{\text{min}} = -0.03$; the relative error between the solutions are approximately 10^{-9} at certain energy-domain points.

Also, in Section 6 by modifying the regularization of independent variable v_J , we improved the divergent asymptotic behavior as $E \rightarrow 0$ in differentiation of the whole-domain and truncated-domain solutions. Also, the new regularization of v_R and v_F helped us to reproduce the (Heggie and Stevenson, 1988)'s solution around at $E_{\text{max}} = -0.225$ while it still can provide the whole domain solution around at $E_{\text{max}} = -0.05$ with accuracy of order of 10^{-5} . We consider that one can find the HS's solution as a result of low accuracy with small E_{max} and that the actual number of significant figures of the HS's solution is one.

We will discuss the physical properties and application of the ss-OAFP model in the follow-up papers; the second paper (Ito, 2020a) is for thermodynamic property of the model focusing the negative heat capacity in the core and the third (Ito, 2020b) for application of the model to globular clusters in Milky Way. We are also planning to extend our numerical code to post-core-collapse solutions in future work. The present model can be meaningful only to the clusters that (i) have already reached in complete-core-collapsed state (if possible) and (ii) are undergoing core collapse as an approximation of more exact models (time-dependent OAFP model and N -body simulations). Our numerical code can extend to post-core-collapse models such as the ss-OAFP model (Heggie and Stevenson, 1988) and a FP model that follows the approach of self-similar conductive gaseous model (Goodman, 1984).

Acknowledgements

The present work is partial fulfillment of the degree of Philosophy at CUNY graduate center. Spectral method and part of regularization for independent variables were encouraged to use by my advisor Carlo Lancellotti.

Appendix A The asymptotic approximations of function in the 4ODEs

We detail the asymptotic approximations of the regularized functions $v_I(x)$ and $v_J(x)$ (Appendix A.1) and $v_J(x) + 1$ (Appendix A.2).

A.1 The asymptotic approximation of the functions $v_I(x)$ and $v_J(x)$

The function $v_I(x)$ is important to determine the eigenvalue β and the asymptotic approximation of $v_I(x)$ is related to the boundary condition of the ss-OAFP system. Equation (2.14b) for $v_I(x)$ does not include c_1 at first-order differential equation level and even the asymptotic approximations in first-order differentiation do not include c_1 around endpoints

$$v_I(x \rightarrow -1) = \frac{4}{2\beta - 7} \left(\frac{x+1}{2} \right)^L + \dots, \quad (\text{A.1})$$

$$v_I(x \rightarrow 1) = \frac{L}{4} \left[1 - \left(\frac{1+x}{2} \right)^L \right] + \dots. \quad (\text{A.2})$$

On one hand, the eigenvalue c_1 is associated with $v_J(x)$ since equation (2.14d) for $v_J(x)$ includes c_1 in its asymptotic approximation

$$v_J(x \rightarrow -1) = - \left(\frac{x+1}{2} \right)^L + \dots, \quad (\text{A.3})$$

$$v_J(x \rightarrow 1) = \frac{v_F(x \rightarrow 1)}{L} - \frac{\beta}{2} = \frac{1}{2F_{BC}} \frac{2\beta - 3}{4\beta} \left(\frac{F_{BC} - c_1}{c_3} \right) \left[1 - \left(\frac{1+x}{2} \right)^L \right] + \dots. \quad (\text{A.4})$$

The relation between the eigenvalues and boundary conditions can be confirmed by fixing the value of β during iteration process and by seeing how the value of $v_I(x)$ reaches the expected boundary numerical value, i.e. 0, for different values of β (See Appendix B.1).

A.2 The asymptotic approximation of the factor $[v_J(x) + 1]$

Careful readers would realize that 4ODEs (2.14a) - (2.14d) do not *apparently* include an equation to describe the asymptotic approximation of $v_F(x)$ in the limit of $x \rightarrow -1$ while they include the corresponding approximations of v_I , v_J and v_G . To see this, take the limit of $x \rightarrow -1$ in equation (2.14a); one can see that the factor $[1 + v_J(x)]$ is proportional to $(1/2 + x/2)^\beta$. Hence, one may introduce a new dependent variable

$$\overline{v_J}(x) \equiv \frac{1 + v_J(x)}{\left(\frac{1+x}{2} \right)^{\beta L}}. \quad (\text{A.5})$$

By the new variable, equations (2.14a) and (2.14d) can be rewritten as

$$\left[\frac{1+x}{L} \frac{d\overline{v_F}}{dx} \left(\frac{1+x}{2} \right)^{\beta L} + \beta \right] [v_I(x) + v_G(x)] + \left(\frac{1+x}{2} \right)^L \frac{4\beta}{2\beta - 3} \left[\overline{v_J}(x) \left(\frac{1+x}{2} \right)^{\beta L} - 1 \right] + \beta c_2 e^{-v_F(x)} \overline{v_J}(x) \left(\frac{1+x}{2} \right)^L = 0, \quad (\text{A.6a})$$

$$\frac{1+x}{L} v_Q(x) \frac{d\overline{v_J}}{dx} + \overline{v_J}(x) \left(\frac{1+x}{2} \right)^{\beta L} \left\{ 3 \frac{2\beta + 1}{4} v_Q(x) + \frac{1+x}{2L} \left[v_Q(x) \frac{dv_F}{dx} + 3 \frac{dv_Q}{dx} \right] \right\} - \frac{1+x}{2L} v_Q(x) \frac{dv_F}{dx} \frac{3(2\beta - 1)}{2} - \frac{6}{L} \frac{dv_Q}{dx} = 0. \quad (\text{A.6b})$$

Taking the limit of $x \rightarrow -1$ in equation (A.6a) provides the asymptotic approximation;

$$\overline{v_J}(x \rightarrow -1) = - \frac{c_4^*}{c_2} \frac{(2\beta + 7)(6\beta - 3)}{\beta(2\beta - 7)(2\beta - 3)(\beta + 1)}, \quad (\text{A.7})$$

Hence, we can find from equations (A.6b) and (A.7) the equation for v_F as $x \rightarrow -1$; $-\frac{1+x}{2L} v_Q(x) \frac{dv_F}{dx} \frac{3(2\beta - 1)}{2} - \frac{6}{L} \frac{dv_Q}{dx} = 0$. However, this expression is false since our numerical result showed that derivatives $\frac{dv_F}{dx}$, $\frac{dv_I}{dx}$ and $\frac{dv_Q}{dx}$ behave like power-law $(0.5 + 0.5x)^{\beta-1}$ as $x \rightarrow -1$ (such power-law behaviors are shown graphically in Figure 9). This means, equation (A.6b) is still the equation to determine the behavior of v_J as $x \rightarrow -1$. Accordingly, the expression for the asymptotic approximation of v_J (equation (A.7)) is correct only when the first term in (A.6a) is greater than order of double precision (as explained in Appendix D); strictly speaking the first term should be always included in numerical calculation to consistently solve the 4ODEs.

Appendix B Stability analyses of the whole-domain solution

The present appendix shows the numerical stability of the whole-domain solution. We detail the dependence of the solution on eigenvalue β (Appendix B.1), the nodes of Fejér's quadrature (Appendix B.2), the boundary condition for $v_F(x)$ (Appendix B.3) and the numerical parameter L (Appendix B.4).

B.1 Stability of the whole-domain solution against the eigenvalue β

Throughout the present work the boundary value $v_I(x = 1)$ is important since it determines the eigenvalue β ; the present appendix shows its stability. We solved the ss-OAFP system for different β between $\beta_o - 10^{-8}$ and $\beta_o + 10^{-8}$. Figure B.22 shows the β -dependence of $v_I(x = 1)$, $|1 - c_1/c_{10}|$ and $|1 - c_4^*/c_{40}^*|$. All the values are almost symmetric about β_o and minimized around at $\beta = \beta_o$. Also, the eigenvalues consistently converge to their reference values, $c_1 \approx c_{10}$ and $c_4^* \approx c_{40}^*$ when β reaches β_o . One can find the following approximate relationship in the order of values

$$|1 - c_1/c_{10}| \sim |1 - \beta/\beta_o| \sim \frac{|v_I(x = 1)|}{10^2} \sim \frac{|1 - c_4^*/c_{40}^*|}{10^5}. \quad (\text{B.1})$$

This relationship implies that one needs 5 ~ 6 significant figures of β and c_1 to determine one significant figure of c_4^* .

The Newton iteration did not work when the value of β deviated from the reference value β_o by $1.3 \times 10^{-6}\%$ in the lower limit while we gave up at the relative error of $2.5 \times 10^{-7}\%$ in the upper limit due to an expensive CPU cost¹⁰. Hence, the condition that Newton iteration method works for the whole-domain formulation is that one must correctly specify the eight or nine significant figures of β ($8.17837105 \leq \beta \lesssim 8.17837119$).

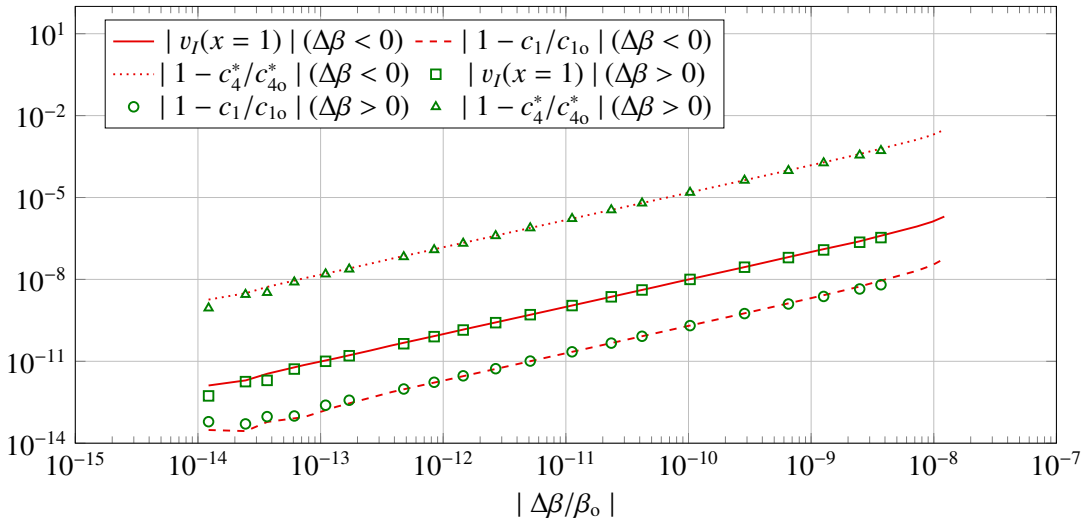


Figure B.22: Values of $|v_I(x = 1)|$, $|1 - c_1/c_{10}|$ and $|1 - c_4^*/c_{40}^*|$ against change $\Delta\beta$ around β_o ($\Delta\beta \equiv \beta - \beta_o$). Numerical parameters $n = 70$, $L = 1$ and $F_{BC} = 1$ are employed.

B.2 Stability of the whole-domain solution against the number of nodes in Fejér's first-rule quadrature

Figure B.23 shows the dependence of the eigenvalues c_1 and c_4 and boundary value $v_I(x = 1)$ on the number of nodes in Fejér's first-rule quadrature. The total number of nodes are chosen between 150 to 10^4 for fixed $\beta = \beta_o$ and $n = 70$; the Newton iteration did not work for the number of nodes less than 150. The eigenvalues get stable for the nodes over ~ 580 points; c_1 and c_2 approach the reference eigenvalues c_{10} and c_{40}^* . Also, the boundary value $v_I(x = 1)$ is qualitatively similar to $|1 - c_1/c_{10}|$ and $|1 - c_4^*/c_{40}^*|$.

¹⁰Over one million iterations were needed when the eigenvalue β deviated more than $1 \times 10^{-7}\%$ above the reference value β_o

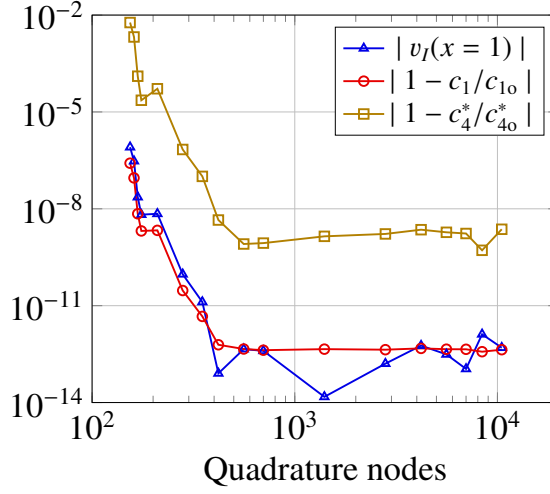


Figure B.23: Dependence of the eigenvalues c_1 and c_4^* and boundary value $|v_I(x=1)|$ on the number of nodes in Fejér's first-rule quadrature. The eigenvalues are compared to their reference eigenvalues c_{1o} and c_{4o}^* and the following numerical parameters are employed; $n = 70$, $L = 1$ and $F_{BC} = 1$.

B.3 Stability of the whole-domain solution against F_{BC}

While the boundary condition $F(E = -1) = 1$ was employed in (Heggie and Stevenson, 1988; Takahashi, 1993), there is no specific reason to choose the value 1 unless one needs to change the central density. Hence, we employed different boundary values of $F(E = -1)$ to see the consistency of the eigenvalues. The left panel in Figure B.24 shows the values of c_1 and c_4^* against the different values of F_{BC} between 0.0001 and 10000. We found that c_1 and c_4^* are proportional to F_{BC} while the eight significant figures of β and c_3 are constant. Also, as F_{BC} increases, a similar characteristics was found in the condition number of the Jacobian matrix for the 4ODEs and the number reached $\sim 10^{12}$ for $F_{BC} = 10^4$. Due to the linear relation between the eigenvalues and the boundary value, we divided c_1 and c_4^* by F_{BC} and compared to the reference values c_{1o} and c_{4o}^* obtained for $F_{BC} = 1$. We confirmed the eigenvalues (c_1 and c_4^*) are proportional to F_{BC} with a relative accuracy of $\sim 10^{-8}$ for c_4^* and $\sim 10^{-13}$ for c_1 while the high condition number did not interfere the accuracies (Figure B.24, right panel).

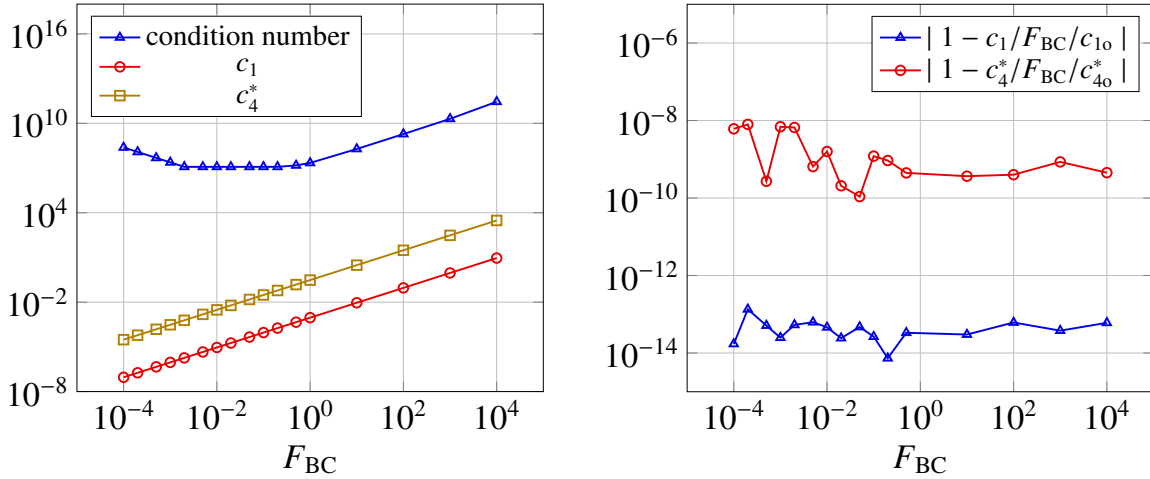


Figure B.24: (Left panel) Dependence of the eigenvalues c_1 and c_4^* on the boundary condition $F(x=1)$ compared to the condition number of the Jacobian matrix for the 4ODEs. (Right panel) Relative error of the regularized eigenvalues c_1/F_{BC} and c_4^*/F_{BC} from the reference eigenvalues c_{1o} and c_{4o}^* . ($F_{BC} = 1$, $L = 1$ and $n = 70$)

To avoid the significant change in the condition number for high values of F_{BC} , we regularized the ss-OAFP system by dividing the function $F(E)$ by F_{BC} . This regularization corresponds with that only the density $D(E)$ in the system is proportional to F_{BC} . We again solved the regularized ss-OAFP system for different F_{BC} . As expected, the condition number does not change significantly against change in F_{BC} (Figure B.25). Also, the eigenvalues are stable against F_{BC} ; $\mathcal{O}(10^{-14}) < |1 - c_1/F_{BC}/c_{10}| < \mathcal{O}(10^{-13})$ and $\mathcal{O}(10^{-10}) < |1 - c_4^*/F_{BC}/c_{40}^*| < \mathcal{O}(10^{-8})$.

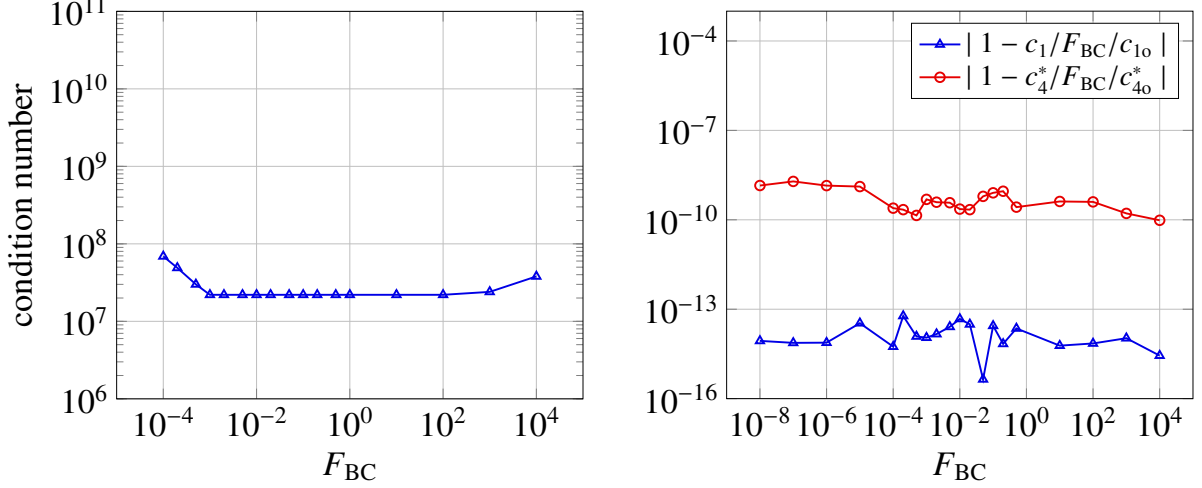


Figure B.25: (Left panel) Condition number of the Jacobian matrix for the Q -integral and 4ODEs regularized by dividing $F(E)$ by F_{BC} . (Right panel) Relative error of the regularized eigenvalues c_1/F_{BC} and c_4^*/F_{BC} from the reference eigenvalues c_{10} and c_{40}^* for the 4ODEs regularized through $F(E)/F_{BC}$. ($F_{BC} = 1$, $L = 1$ and $N = 70$.)

In conclusion, the eigenvalues are less sensitive to high condition number and the eigenvalues β (or α) and c_3 have a numerically intrinsic property against change in F_{BC} while c_1 , c_2 and c_4^* are extrinsic;

$$c_1(F_{BC}) \propto (c_{10} + \mathcal{O}(10^{-13})) F_{BC}, \quad c_4^*(F_{BC}) \propto (c_{40}^* + \mathcal{O}(10^{-8})) F_{BC}, \quad \beta(F_{BC}) = \beta_0 + \mathcal{O}(10^{-8}), \quad (\text{B.2})$$

where $-10^{-4} < F_{BC} < 10^4$.

B.4 Stability of the whole-domain solution against the numerical parameter L

The parameter- L -dependence of the solutions provides an understanding of the ss-OAFP equation. We found spectral solutions of the ss-OAFP system with the mapping parameters $L = 1/2$ and $L = 3/4$ (Table B.4) while Newton method with $L > 1$ was hard to work¹¹. In this sense, we call a solution with $L < 1$ the 'contracted-domain' solution of the ss-OAFP system. The contracted-domain solutions provide some advantages over the reference solution; they are still whole-domain solutions (since they are not truncated) while they need less degrees of polynomials and are compatible to the reference solution. The convergence rate of Chebyshev coefficients for large n is apparently¹² characterized by $a_n \propto n^{-1-2L}$ due to the end-point singularity $(1 \pm x)^L$ at branch points $x = 1$. The characteristics of the low convergence rate for the function $v_F(x)$ clearly appears when the degree n is greater than 65 and 75 for $L = 0.75$ and $L = 0.5$ respectively. The Newton iteration converged only when the Chebyshev coefficients reach as low as order of 10^{-9} for $L = 3/4$ and 10^{-6} for $L = 1/2$. Recalling the Newton iteration worked only when the Chebyshev

¹¹Choosing high numbers for L (e.g. $L = 1.5$ and $L = 2$) resulted in much more difficulty in Newton interaction convergence. We had to shorten the Newton steps from 1 to a fraction less than 0.01. On one hand, low numbers of L less than $1/2$ did not work; this is perhaps because contracted-domain formulation provides slow decay of Chebyshev coefficients, accordingly low accuracy of the solutions. As discussed in Section 6.3 solutions with low accuracy can not provide the reference solution.

¹²The slow convergence does not originate from the branch point. This is since the regularized function v_F behaves like $c_4^*(1 + b(0.5 + 0.5x)^\beta)$ as $x \rightarrow -1$ where b is a constant. In fact, as we increased the digits of β by correctly specifying the value, the coefficients decayed rapidly and reached order of 10^{-13} at the maximum degree ($n = 65$).

$L = 0.75$

n	Eigenvalue β	$ 1 - c_1/c_{10} $	$ 1 - c_4^*/c_{40}^* $	$v_I(x=1)$
60	8.178371160	2.1×10^{-10}	6.6×10^{-7}	9.4×10^{-9}
55	8.178371160	2.1×10^{-10}	1.3×10^{-6}	1.7×10^{-9}
50	8.178371160	8.0×10^{-10}	9.8×10^{-6}	1.3×10^{-9}

$L = 0.5$

n	Eigenvalue β	$ 1 - c_1/c_{10} $	$ 1 - c_4^*/c_{40}^* $	$v_I(x=1)$
35	8.17837104	4.9×10^{-8}	2.3×10^{-6}	2.1×10^{-10}

Table B.7: Numerical results for the contracted-domain formulation with $L = 1/2$ and $L = 3/4$ and $F_{BC} = 1$.

coefficients of the whole-domain solution with $L = 1$ reach order of 10^{-12} (Table 3), we infer a *rule-of-thumb* for the relationship between the coefficients and iteration method that *Newton iteration method could work when the minimum absolute value of Chebyshev coefficients reaches as low as order of 10^{-12L} .*

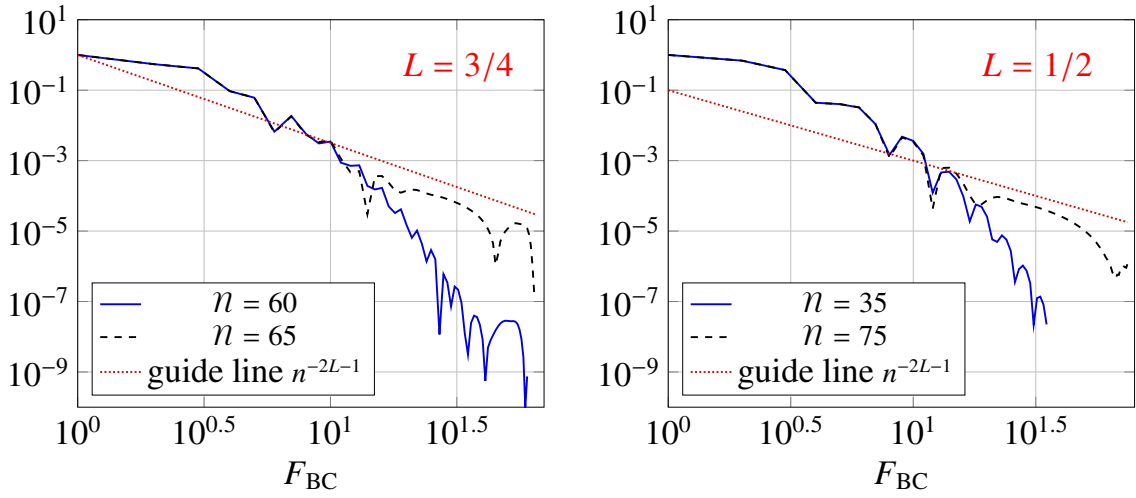


Figure B.26: (Left Panel) Chebyshev coefficients of $v_F(x)$ for $L = 0.75$ in the following cases (a) $n = 60$ and $\beta = 8.178371160$ and (ii) $n = 65$ and $\beta = 8.178371275$. The iteration method for the latter did not work satisfactorily since $|\{a\}^{\text{new}} - \{a\}^{\text{old}}| \approx 7 \times 10^{-10}$ (resulting in $|1 - c_4^*/c_{40}^*| \approx 6.0 \times 10^{-3}$ and $v_I = 4.4 \times 10^{-6}$). Yet, it is shown here for comparison. (Right panel) Chebyshev coefficients of $v_F(x)$ for $L = 0.5$ in the following cases (a) $n = 35$ and $\beta = 8.178371160$ and (ii) $n = 75$ and $\beta = 8.1783712$.

Appendix C Stability of the truncated-domain solution against change in extrapolated DF

We found that the truncated-domain solutions is little sensitive to the the expression of the extrapolated DF (equation (2.17)). We compared the effects of change in the extrapolated DF on the eigenvalues (Table C.8). The set of parameters $(c, d) = (1, 10)$ provided the best accuracy in the sense that $|v_I(x)|$ reaches the minimum value (7.3×10^{-12}) among the chosen parameters (c, d) , hence we compared the eigenvalues obtained for (c, d) to the eigenvalues for $(c, d) = (1, 10)$. For combinations of different sets of parameters among $0.01 < c < 10$ and $0.01 < d < 10$, the relative error of eigenvalues are order of 10^{-13} in c_1 compared to its reference value and 10^{-9} in c_4^* at most, holding small values of $|v_I(x=1)| \approx 1 \times 10^{-11}$. Even the effect of discontinuity in derivative of the extrapolated DF at $E = E_{\min}$ ($c \rightarrow \infty$) is not significant compared to the effect of large value of c ($= 5, 10$).

Appendix D Why is Newton iteration method hard to work for the ss-OAFP system?

The difficulty in numerical integration of the ss-OAFP system may originate from the complicated mathematical structure of the 4ODEs (2.14a) - (2.14d). To understand the structure, one must refer to the values of the infinity norms of the difference between ‘new’ and ‘old’ Chebyshev coefficients associated with 4ODEs in the process of Newton

c	d	$ 1 - c_1/c_{1\text{ex}} $	$ 1 - c_4^*/c_{4\text{ex}}^* $	$v_I(x=1)$	c	d	$ 1 - c_1/c_{1\text{ex}} $	$ 1 - c_4^*/c_{4\text{ex}}^* $	$v_I(x=1)$
∞	N/A	1.2×10^{-13}	5.3×10^{-10}	1.0×10^{-11}	10	10	9.4×10^{-14}	5.3×10^{-10}	1.0×10^{-11}
10	1	1.2×10^{-13}	5.3×10^{-10}	1.0×10^{-11}	2	10	2.1×10^{-14}	3.1×10^{-11}	7.5×10^{-12}
5	1	7.7×10^{-14}	5.3×10^{-10}	1.0×10^{-11}	1	5	4.0×10^{-14}	2.6×10^{-10}	8.8×10^{-12}
1	1	1.0×10^{-13}	4.5×10^{-10}	9.8×10^{-12}	1	0.1	1.1×10^{-13}	8.7×10^{-10}	1.1×10^{-11}
0.1	1	1.6×10^{-13}	9.6×10^{-10}	1.2×10^{-11}	1	0.01	1.2×10^{-13}	9.6×10^{-10}	1.1×10^{-11}
0.01	1	1.4×10^{-13}	9.1×10^{-10}	1.1×10^{-11}	0.1	0.1	1.2×10^{-13}	8.4×10^{-10}	1.0×10^{-11}

Table C.8: Numerical results for different extrapolated DF ($L = 1$ and $F_{\text{BC}} = 1$). The eigenvalues are compared to $c_{1\text{ex}} \equiv c_{10}$ and $c_{4\text{ex}}^* \equiv 3.03155223 \times 10^{-1} (= c_{40}^* + 1 \times 10^{-1})$ obtained for $(c, d) = (1, 10)$ and the value of $|v_I(x=1)|$ is 7.3×10^{-12} . The combination $(c, d) = (\infty, N/A)$ means the extrapolated function is constant.

iteration method. We found the following values were universally output for all the truncated-domain-, whole-domain- and contracted-domain- formulations

$$\|\{F_n\}^{\text{new}} - \{F_n\}^{\text{old}}\|_{\infty} \approx \mathcal{O}(10^{-13}), \quad (\text{D.1a})$$

$$\|\{G_n\}^{\text{new}} - \{G_n\}^{\text{old}}\|_{\infty} \sim \|\{I_n\}^{\text{new}} - \{I_n\}^{\text{old}}\|_{\infty} \sim \|\{J_n\}^{\text{new}} - \{J_n\}^{\text{old}}\|_{\infty} \approx \mathcal{O}(10^{-16}) \approx \text{eps}. \quad (\text{D.1b})$$

$$\|c_1^{\text{new}} - c_1^{\text{old}}\|_{\infty} \sim \mathcal{O}(10^{-16}), \quad \|c_4^{*\text{new}} - c_4^{*\text{old}}\|_{\infty} \approx \mathcal{O}(10^{-13}), \quad (\text{D.1c})$$

where *eps* means the machine precision of MATLAB ($\approx 2.2 \times 10^{-16}$). Only the norms for $\{F_n\}$ and c_4^* are approximately 10^3 higher than the others, implying that equation (2.14a) associated with v_F may have a mathematically internal conflict. Equation (2.14a) has the following mathematical structure

$$4L \left(\frac{1+x}{2} \right)^{\beta+1} \frac{dv_F(x)}{dx} \eta(x; v_G, v_I) + \left(\frac{1+x}{2} \right)^{\beta} \mu(x; v_G, v_I) + c_1 e^{-v_F(x)} (v_J + 1) = 0, \quad (\text{D.2})$$

where $\eta(x; v_G, v_I)$ and $\mu(x; v_G, v_I)$ are functionals of $v_G(x)$ and $v_I(x)$ and their absolute values are order of unity on the whole domain. We explain possible relationships of the Newton's method with the mathematical structures focusing on problems in equation (D.2) in the limit of $x \rightarrow 1$ (Section D.1) and $x \rightarrow -1$ (Section D.2) for v_F , and in the derivative of v_F (Section D.3). Also, we show equation (D.2) is important in integration of the 4ODE at equation level (Section D.4) and explain some other numerical difficulties in integrating the ss-OAFP system (Section D.5).

D.1 A problem in solving equation for v_F in the limit of $x \rightarrow 1$

A problem in solving equation (D.2) is that the factor c_1 forms a numerical gap between terms at equation level. First, take the limit of $x \rightarrow 1$ in equation (D.2)

$$4c_3 \frac{dv_F(x \rightarrow 1)}{dx} + \beta c_3 - 1 + \frac{c_1}{F_{\text{BC}}} = 0. \quad (\text{D.3})$$

where $L = 1$ is chosen for simplicity. In equation (D.3), since βc_3 is approximately unity (≈ 0.59), the largest gap is order of 10^{-3} between the third and fourth terms regardless of the value of F_{BC} (since c_1 is proportional to F_{BC} as explained in Appendix B.3). Hence, the equation can turn into an overdetermined problem at equation level greater than order of 10^{-3} , which would be one of the reasons why the Newton method is hard to work. Also, the smallness of the gap could explain the large value of the norms for c_4^* and $\{F_n\}$ (equation (D.1)); the boundary value $F_{\text{BC}} (= \ln(v_{DF}(x=1)))$ is effective only up to 13 digits in the sense that it consistently determine the differentiation $\frac{dv_F(x)}{dx}$; digits more than 13 would be counted as rounding error due to the gap in $1 - c_1/F_{\text{BC}}$. Due to this mathematical structure, we call order of 10^{-13} 'practical' machine precision at equation level as comparison to Matlab machine precision $\approx 2.2 \times 10^{-16}$.

D.2 A problem in solving equation for v_F in the limit of $x \rightarrow -1$

Another problem in solving equation (D.2) is that the factors $\left(\frac{1+x}{2}\right)^\beta$, $\frac{dv_F(x)}{dx}$ and $(v_J + 1)$ form power law profiles as $x \rightarrow -1$, which limits the effective domain on which we can consistently solve the 4ODE. Take the limit of $x \rightarrow -1$ in equation (D.2)

$$\begin{aligned} \frac{6(2\beta-1)}{(2\beta-7)(\beta+1)} \left(\frac{1+x}{2}\right)^{\beta+1} \frac{dv_F(x)}{dx} (x \rightarrow -1) + \left(\frac{1+x}{2}\right)^\beta \frac{4\beta^2 - 4\beta + 37}{(2\beta-7)(\beta+1)(2\beta-3)} + \frac{c_1}{c_4^*} [v_J(x \rightarrow -1) + 1] = 0. \quad (D.4) \\ \sim \left(\frac{1+x}{2}\right)^{2\beta} \qquad \qquad \qquad \sim \left(\frac{1+x}{2}\right)^\beta \qquad \qquad \qquad \sim \left(\frac{1+x}{2}\right)^\beta \end{aligned}$$

where the second line represents the power-law dependence of each term; the differentiation $\frac{dv_F(x)}{dx}(x \rightarrow -1)$ behaves like $\left(\frac{1+x}{2}\right)^{\beta-1}$ according to the result of Section 4.2 and $[v_J(x \rightarrow -1) + 1]$ is explicitly proportional to $\left(\frac{1+x}{2}\right)^\beta$ as explained in Section A.2. The first term in equation (D.4) describes the 'time-evolution' equation with respect to x in the sense that the equation is first order in differentiation or an initial value problem. Hence, one may consider the first term in equation (D.4) is important to determine the interval on which one can solve the equation satisfactorily beginning from $x = 1$. The factor $\left(\frac{1+x}{2}\right)^{2\beta}$, of course, does not contribute to the numerical integration of equation (D.4) if it reaches order of machine precision $\sim 10^{-16}$. Hence, by equating the first term to machine precision of Matlab $\frac{6(2\beta-1)}{(2\beta-7)(\beta+1)} \left(\frac{1+x}{2}\right)^{\beta+1} \frac{1-c_1}{c_3} = 2.2 \times 10^{-16}$, where $\frac{1-c_1}{c_3} = \frac{dv_F(x)}{dx}(x = -1)$, we can estimate the lower limit of the interval is $x_{\text{const}} \approx -0.82$ (or the upper limit $E_{\text{const}} \approx -0.09$). This discussion implies that one can not effectively determine the value of c_4^* at equation level with a numerical accuracy better than 10^{-9} ($= (0.5 + 0.5x_{\text{const}})^\beta$) (Since c_4^* is related to the third term in equation D.4). This order of values well reflects the result in Figure B.22 in which $|1 - c_4^*/c_{40}^*|$ is stable at order of 10^{-9} at best against change in β . Also, it may explain the reason that the relative error of the optimal truncated solution to the reference solution is at best $\sim 10^{-9}$ as shown in Figure 14.

D.3 Absolute values of terms in equation for v_F and classification of truncated-domain solutions

The present appendix compares the orders of absolute values of terms in equation (2.14a) to detail the mathematical structures and explains the classification of the truncated-domain solutions employed in Section 5. Figure D.27 depicts the absolute values of the first through third terms in equation (2.14a) together with relative error $|1 - v_F(x)/\ln[c_4^*]|$ and practical machine precision ($\sim 10^{-13}$). Also, the sum of the three terms is depicted. The absolute value of the first term reaches the total of the three terms approximately at $E = -0.05$ while the second and third terms reach it at $E = -0.005$. Since we expect that we can satisfactorily solve equation (2.14a) at $E < -0.05$, we name the solutions that we can obtain on interval $E < -0.05$ as the 'stable solution' (The incorrect solution is discussed later in the present appendix). This well reflects the result for the reference solution in Figure 7 in which the asymptotic behavior in differentiation of $v_J(x)$ loses accuracy at $E > -0.05$. Also, the truncated-domain solution holds accuracy beyond $E = -0.05$ as shown in Figure 13. On one hand, we call solutions obtained for $-0.05 < E_{\text{max}} < -0.005$ as 'semi-stable' solutions. This is since as $x \rightarrow -1$ the second and third terms, in place of the derivative of v_F , can determine the value of v_F , which results in that the accuracy of c_4 does not change with increasing E_{max} . The practical machine precision well describes the constancy of the accuracy of c_4 . Lastly, beyond $E_{\text{max}} > -0.005$ there does not exist a meaningful term below machine precision, hence we can not solve the equation consistently. Since we could reasonably solve 4ODEs with fixed Q -integral (Appendix E.3), we believe the essential cause of the numerical instability originates from the relationship between v_F and the integrals v_Q and v_D ; one can not integrate the integrals for $E_{\text{max}} > -0.005$ holding a high accuracy since one needs more than double-precision to integrate them on their domains $(-1, E)$ and $(-E, 0)$ ¹³. We call solutions that we could obtain for $E_{\text{max}} > -0.005$ as the 'unstable' solution.

We can show Figure D.27 has two more important characteristics of equation (2.14a) focusing on the second and third terms. First, we can obtain solutions that are close to the reference solution and HS's solution only for

¹³One may consider the similarity in mathematical structure between the v_Q and v_D integrals and Dawson's integral; the latter exponentially loses accuracy (e.g. Cody et al., 1970; Boyd, 2008) and the former algebraically with increasing argument of them. As a result one needs more than double precision to find numerical values on broader truncated-domain (corresponding $E \rightarrow 0$).

$E_{\max} < -0.25$ (Section 5.1). This nature appears when the second and third terms reach the same order of value and cancel out each other. Around at $E = -0.25$, the absolute values of the terms are order of 10^{-5} . This reflects the order of value under which $|1 - c_4/c_4^*|$ is stable against change in β (Figure B.1). Also, this infers that, in order to make Newton's method work, one must prepare an accurate 'initial guess' for solution whose accuracy is order of 10^{-5} to effectively determine the *first* digit of the eigenvalue c_4 , which would make the Newton method hard to work. Another important characteristics is that the value of $|1 - v_F(x)/\ln[c_4^*]|$ multiplied by the maximum value of the third term is greater than that of the first term. This means the reason why v_F can behave like a constant function as $E \rightarrow 0$ is *not* because the first term reaches machine precision and lose its significance. This property is important to secure the consistency of our solution.

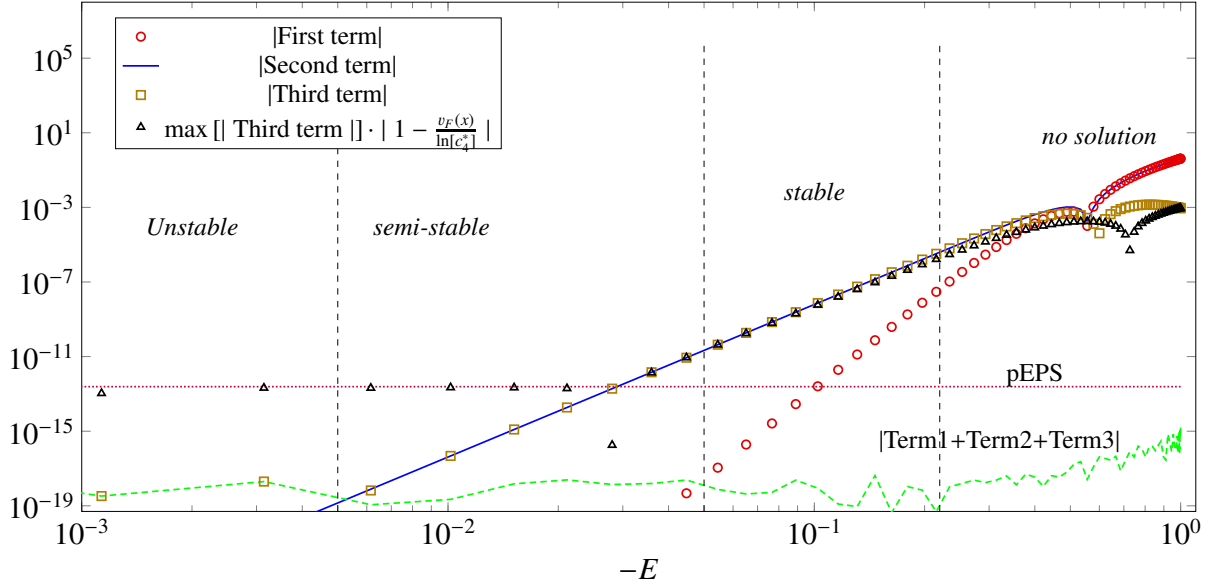


Figure D.27: Absolute values of terms appearing in equation (2.14a). The horizontal line represents the limit of precision and the deviation $|1 - v_F(x)/\ln[c_4^*]|$.

D.4 A problem in solving the 4ODE at machine precision level

Appendixes D.1, D.2 and D.3 only focuses on equation (2.14a) among the 4ODEs; to emphasize the importance of equation (2.14a) we compare the equation to the rest of the equations. To analyze the mathematical structures of the 4ODEs, we rewrite the 4ODE with new functions for convenience

$$O_1(E) \equiv 0, \quad O_2(E) \equiv 0, \quad O_3(E) \equiv 0, \quad O_4(E) \equiv 0, \quad (D.5)$$

where $O_1(x)$ through $O_4(x)$ are functions that read the left hand sides of equations (2.14a)-(2.14d). Figure D.28 (top panel) depicts the absolute values of O_1 through O_4 at Gauss-Chebyshev nodes on the whole domain. In the figure only O_1 is regularized by dividing O_1 by c_1 . All the functions $O_1(x)$ through $O_4(x)$ lose accuracy on the unstable region increasing their absolute values as $x \rightarrow -1$. One can see the absolute values of $O_1(x)$ and $O_4(x)$ are very alike around the semi-stable region, which well describes the fact that O_1 and O_4 'switch' their roles; they determine v_J and v_F respectively as $x \rightarrow -1$ while v_F and v_J as $x \rightarrow +1$, as explained in Appendix A.2. Since the absolute values of the functions in Figure D.28 are not regularized consistently to compare their absolute values, Figure D.28 (Bottom panel) shows the regularized functions $O_1(x) - O_4(x)$; we regularized the absolute values of $O_1(x) - O_4(x)$ by dividing each function by the term whose value is the largest in the corresponding equation in the limit of $E \rightarrow -1$. As expected, $O_2(x)$, $O_3(x)$ and $O_4(x)$ stalls near the machine precision except for the unstable region. On one hand, $O_1(x)$ significantly loses accuracy as x approaches -1 and it well reflects the relation of $O_1(x)$ with $|1 - v_F(x)/\ln[c_4^*]|$ in a similar way to Figure 7. In Figure D.28 (Bottom Panel) $|1 - v_F(x)/\ln[c_4^*]|$ is also regularized by the same term

for equation (2.14a). This result highlights the dominant effect of equation (2.14a) to determine the accuracy of the 4ODE as $x \rightarrow -1$.

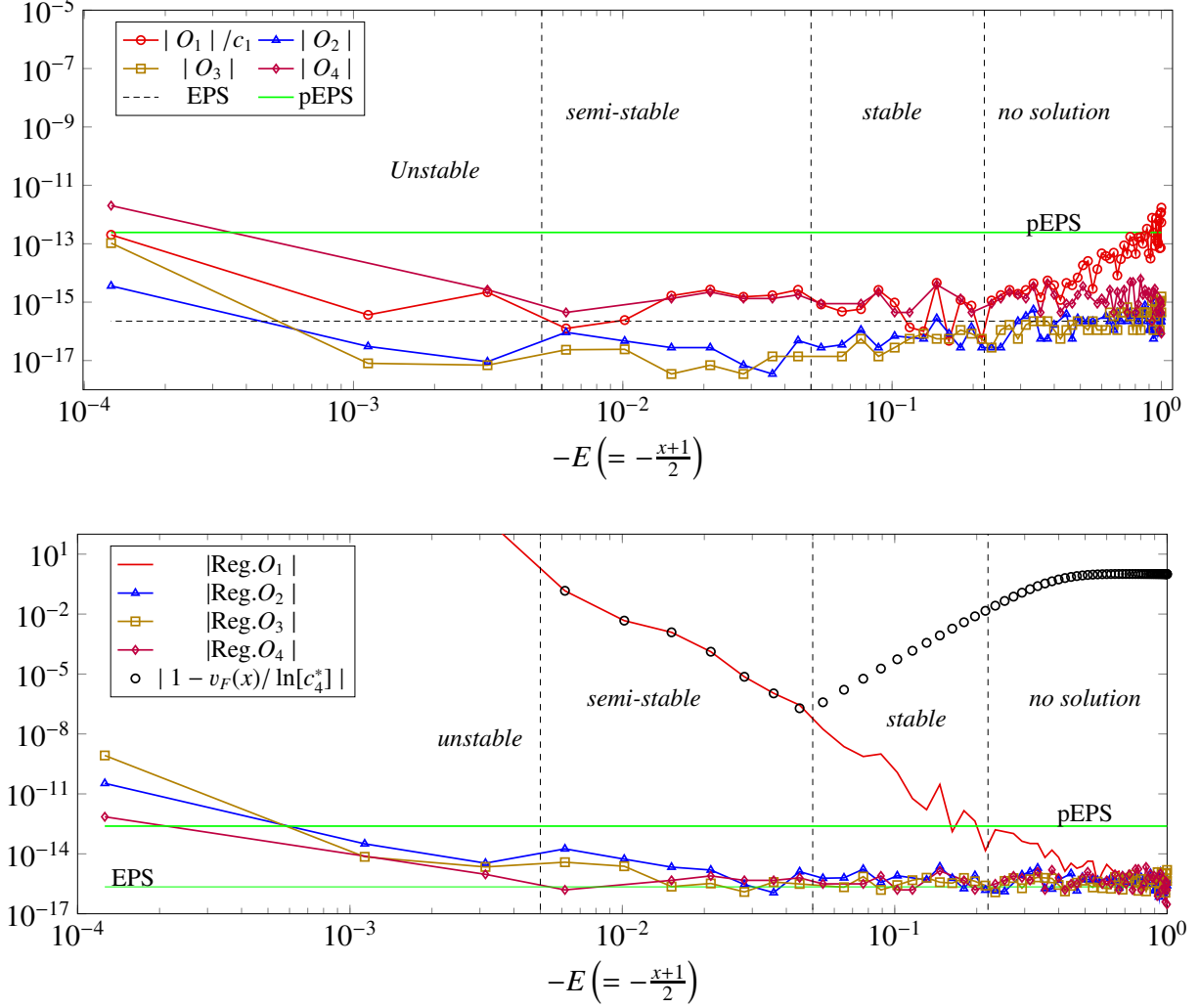


Figure D.28: Values of the regularized functions O_1 through O_4 in 4ODEs (2.14a)- (2.14d) at Gauss-Chebyshev nodes. (Top) only O_1 is divided by c_1 (Bottom panel) All the functions are normalized so that the largest value of terms in each equation approaches unity as $E \rightarrow -1$. The horizontal lines represent limits of precision. On the bottom panel, $|1 - v_F(x)/\ln[c_4^*]|$ is further regularized by the first term of equation (2.14a).

D.5 Some problems in numerical integration of ss-OAFP system

Lastly, we summarize the three more difficulties that we faced in numerical integration of the ss-OAFP system. (i) The effect of discontinuity in solutions was an issue for truncated-domain formulation (see some discussion in Appendix E), which would have made harder guessing a ‘good’ initial solutions in Newton iteration process. (ii) We also employed the Radau-Chebyshev spectral method and boundary condition $v_I(x = 1) = 0$ so that we can determine a spectral solution when the value $v_I(x = -1)$ is minimized by changing the value of β , but such solution included very strong discontinuous property in both whole- and truncated-domain solutions. This could be due to the gap $|1 - c_1/c_{1\text{ex}}| / |v_I(x = 1)| \approx 10^{-2}$ that prevents us from imposing the boundary condition $v_I(x = 1) = 0$. If one would like to determine 15 significant digits for $v_I(x = 1)$, one must find 17 significant digits of eigenvalue c_1 , which is beyond the limit of double-precision. (iii) The Newton iteration was hard to work for truncated-domain solutions for $-0.1 < E_{\text{max}} < -0.4$. This would simply reflect the fact that an extrapolation of DF by the power-law profile on the domain is not a proper treatment.

Appendix E Solving part of the ss-OAFP system with a fixed independent variable

The present appendix shows the results of numerical integration of part of the ss-OAFP system that we solved including some fixed independent variables (without self-consistently solving the entire system). Appendices E.1 and E.2 show the effect of discontinuities in independent variable on the convergence rate of Chebyshev coefficients for integration of the Poisson equation and Q -integral respectively. The results possibly explain the slow convergence rate of the truncated-domain solutions (Section 5). Also, Appendix E.3 shows that the numerical instability (reported in Section 4.3) does not occur for integration of 4ODE with a fixed $\{Q_n\}$. This infers that the instability may originate from the relation between the 4ODE and the integrals Q and D rather than 4ODE itself.

E.1 Solving Q -integral with fixed discontinuous v_R

In the present work, all the spectral solutions that we obtained with *truncated-domain* formulations include a certain flattening in their Chebyshev coefficients as index n becomes large. To find a possible cause of the flattening, we calculated the Chebyshev coefficients of the Q -integral for the following discontinuous test function v_R

$$v_R^{(\text{tes})} = 0.1 \Theta\left(\frac{1+x-x_{\text{trans}}}{2}\right) + 1, \quad (\text{E.1})$$

where x_{trans} is a small positive number and $\Theta(\cdot)$ the Heaviside function. When the point of discontinuity is relatively close to order of unity, say $x_{\text{trans}} = 0.1$, the Chebyshev coefficients for Q -integral slowly decay like $\sim 1/n^2$ for large n (Left panel, Figure E.29) in a similar way to Chebyshev coefficients for discontinuous functions and for the integral of them (e.g. Boyd, 2001; Xiang, 2013). However, once the discontinuity point more closely approaches the end point of the domain such as $x_{\text{trans}} = 0.001$ (Right panel, Figure E.29), the coefficients show a flattening with large n . Since for $x_{\text{trans}} = 0.001$ the majority of domain is covered by a constant function, one can find a rapid decay for small n . One can also observe for very large n that the coefficients reach the same order of value regardless of the value of x_{trans} .

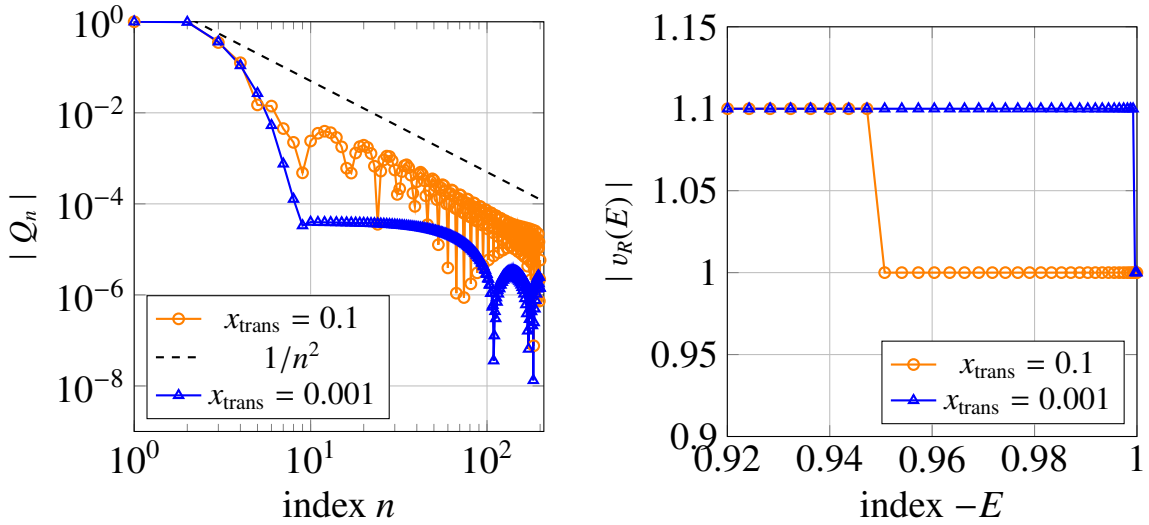


Figure E.29: Chebyshev coefficients of Q -integral for a discontinuous test function $v_R^{(\text{tes})} = 0.1\Theta(0.50+0.5[x-x_{\text{trans}}])+1$. Recall $E = -(0.5+0.5x)^L$, here $L = 1$.

E.2 Solving Poisson equation with fixed discontinuous v_D

In Section 6.2 the modification of function from v_R to $v_R^{(m)}$ changes the numerical result significantly; especially, a slow decay of the Chebyshev coefficients is observed. This also may be associated with the effect of discontinuous behavior of independent variable v_D on $v_R^{(m)}$ in Poisson equation. We tested the following test function

$$v_D^{(\text{tes})} = v_{D0}(x) \left(A_{\text{trans}} \Theta\left[\frac{1+x-0.001}{2}\right] + 1 \right), \quad (\text{E.2})$$

where A_{trans} is a small positive number and $v_{D0}(x)$ is the regularized density of the reference solution. We solved the Poisson equation with the fixed $v_D^{(\text{tes})}$ and different A_{trans} . When the value of A_{trans} is very small such as 0.00001, Figure E.30(Right panel) compares the solutions $\sqrt{v_R^{(m)}}$ and $\exp(v_R) \sqrt{0.5 + 0.5x}$ (that are supposed to be the same if the Poisson equation is successfully integrated) and shows the difference appears only at order of 10^{-4} . On one hand, when A_{trans} is close to unity such as 0.1, not only the difference appears in the value of coefficients at order of 0.1 but also $v_R^{(m)}$ shows a slower decay compared to v_R (Left Panel, Figure E.30).

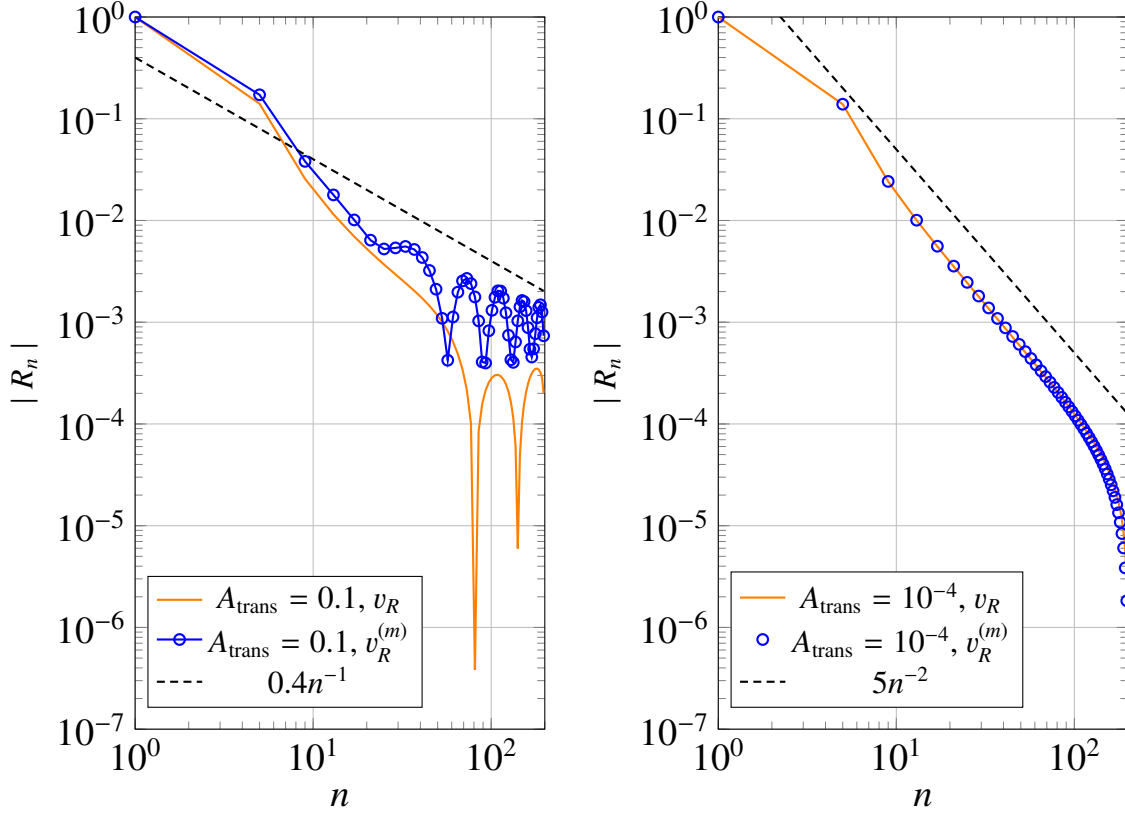


Figure E.30: Chebyshev coefficients of $\sqrt{v_R^{(m)}}$ and $\exp(v_R) \sqrt{0.5 + 0.5x}$ for discontinuous test function $v_D^{(\text{tes})}$. The dashed guidelines are added only for measure of slow decays.

E.3 Solving the ss-OAFP equation with Fixed $\{Q_n\}$

To test whether the origin of numerical instability in integration of the ss-OAFP system is *only* from the large change in independent variables due to the factor $(-E)^\beta$ in 4ODE (1.7a) - (1.7d), the present appendix shows a result of solving the 4ODE and Q -integral for fixed coefficients $\{Q_n\}$. As test coefficients, we used the Chebyshev coefficients for the reference solutions (depicted in Figure 3). We found that, for the fixed $\{Q_n\}$, the Chebyshev coefficients of spectral solutions show very stable behaviors (Figure E.31); coefficients $\{F_n\}$, $\{G_n\}$, $\{I_n\}$ and $\{J_n\}$ reach order of 10^{-15} around at $n = 90$ and show flattenings even at large index ($n \approx 1000$) that are due to the rounding error. Also, Figure E.32 compares the values of c_1 and c_4 at different degrees $n = 10, 20, \dots, 900$ to the corresponding values at $n = 1000$. The relative error in c_1 and the value of $|v_I(x = -1)|$ reach machine precision around at $n = 400$ while the error in c_4 reaches order of 10^{-13} at $n = 1000$. The relative error in c_1 flattens at order of 10^{-13} that appears on degrees $70 \leq n \leq 300$. This result would reflect the fact that the minimum absolute value of test coefficients $\{Q_n\}$ is order of 10^{-13} and to gain more accurate solution one needs more Gauss-Chebyshev nodes near the endpoints.

The result of the present appendix is important to consider the cause of the numerical instability. The difference between the 4ODE with fixed $\{Q_n\}$ and those with unfixed may appear in equation (A.6b). In the equation as $x \rightarrow -1$

the differentiations of v_F , v_Q and v_J becomes significant compared to the rest of factors and terms. For fixed v_Q , one can determine v_F in the equation while v_J is determined from equation (2.14a). In case of non-fixed v_Q , as one can see the form of the Q -integral, the value of the integral is undetermined beyond $E \approx -0.06$ at which $(-E)^\sigma$ reaches machine precision. This infers v_Q must be also further determined as $E \rightarrow 0$ with an extra equation. Hence, for non-fixed v_Q equation (A.6b) becomes an underdetermined problem at $E < -0.06$; a possible remedy would be to enhance machine precision.

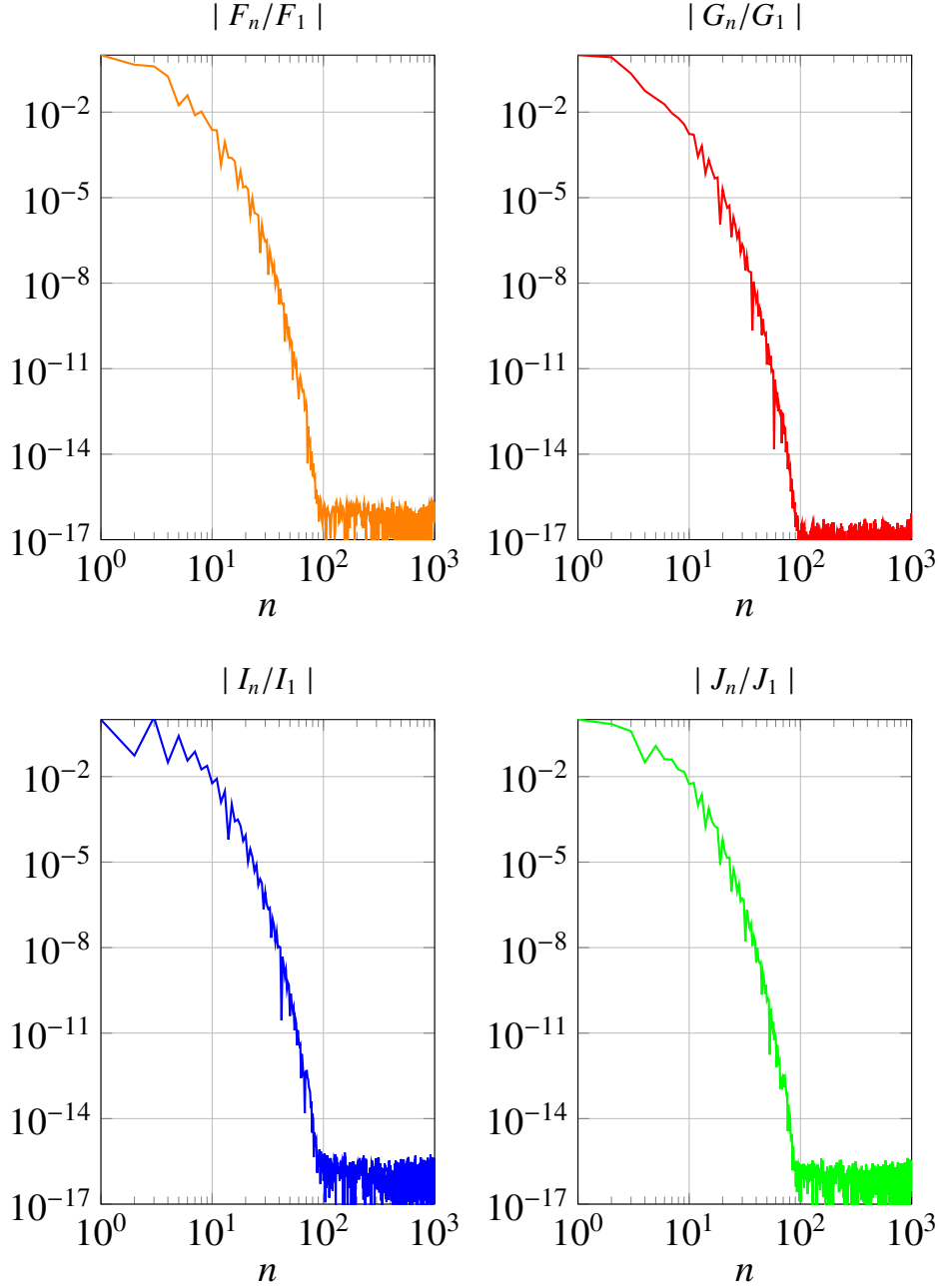


Figure E.31: Absolute values of Chebyshev coefficients for regularized functions for which ss-OAFP system (only 4ODE and Q -integral) was solved with fixed $\{Q_n\}$ on the whole domain ($\mathcal{N} = 1000$, $L = 1$, $F_{BC} = 1$).

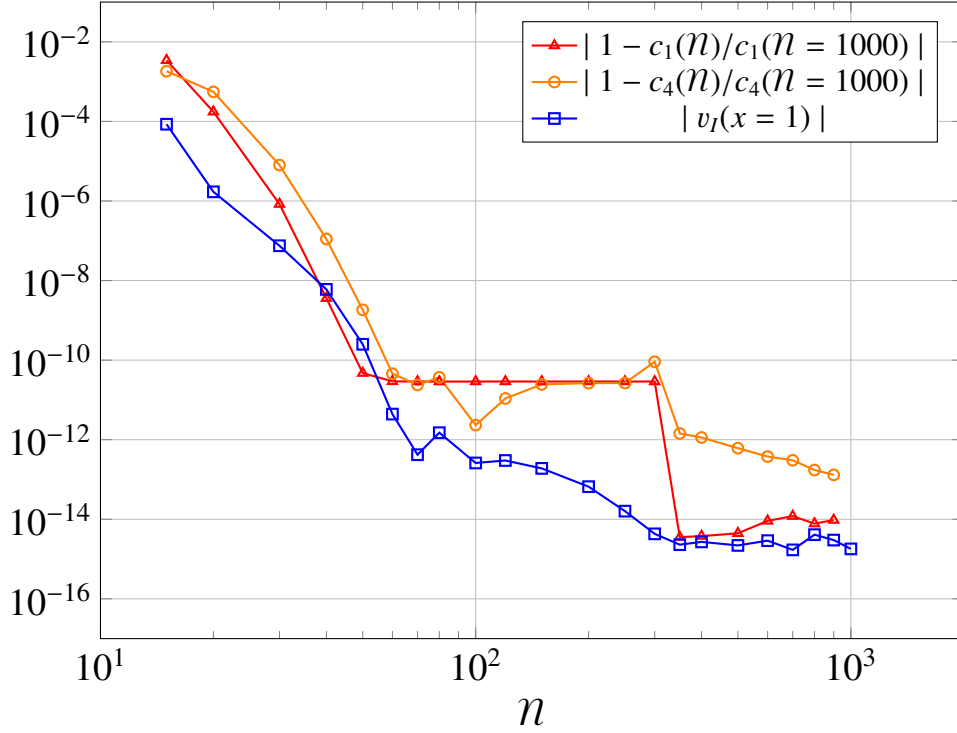


Figure E.32: Relative error in c_1 and c_4 and the value of $|v_I(x = -1)|$ obtained by numerical integration of the 4ODE and Q -integral for the fixed $\{Q_n\}$. c_1 and c_4 are compared to their values at $n = 1000$.

Appendix F Relation between the reference- and Heggie-Stevenson's solutions

The reproduced HS's solution in Section 6.3 is not satisfactory due to the limited available degrees n , hence the present appendix tests variants of modified independent variables aiming to detail a distinct condition to systematically find the reference solution and the HS's solution even for high degree of polynomials. For this appendix, we employed formulations similar to the formulation of (Heggie and Stevenson, 1988). Appendix F.1 shows the results that we obtained by solving the ss-OAFP system after modifying the regularization of variables v_R , v_I , v_G , and v_J and Appendix F.2 after modifying that of v_F . The latter modification provided the reference- and HS's solutions with reasonable accuracy by controlling E_{\max} . However, the available degrees of polynomials are limited in the same way as in Section 6.3. This motivated us to apply to the ss-OAFP system combinations of modified variables employed in Appendix F.2 and Section 6.3 (Appendix F.3). This combination reproduced the HS's and reference- solutions even for high (~ 200) degree of polynomials.

F.1 Modifying the regularization of variables v_R , v_I , v_G , and v_J in the ss-OAFP system

We first examined formulations similar to (Heggie and Stevenson, 1988)'s formulation but they were not useful, rather they increased the condition number for the 4ODEs and Q -integral. First, we introduced the following modified independent variables

$$v_R^{(m2)}(x) \equiv (0.5 + 0.5x)^\nu v_R(x), \quad (\text{F.1a})$$

$$v_I^{(m)}(x) \equiv (0.5 + 0.5x)^\beta v_I(x), \quad (\text{F.1b})$$

$$v_G^{(m)}(x) \equiv (0.5 + 0.5x)^\beta v_G(x), \quad (\text{F.1c})$$

$$v_J^{(m2)}(x) \equiv (0.5 + 0.5x)^b v_J(x). \quad (b \geq 0) \quad (\text{F.1d})$$

If one applies all the modified functions to the ss-OAFP model, the new system is very similar to the HS's formulation. We found the whole and truncated-domain- solutions for the ss-OAFP system with the modified functions using the procedure of Section 3.2 after we tested many different combinations of the modified variables. The first three modified independent variables ($v_R^{(m2)}$, $v_I^{(m)}$ and $v_G^{(m)}$) did not change the results almost at all compared to the reference solution. On one hand, the fourth modification ($v_J^{(m2)}$) provided very high condition numbers. For $b = 1$, we found a spectral solution on whole domain and it is almost identical to the reference solution, while the condition number was high $\sim 10^{11}$. For $b > 1$, the Newton method was hard to work due to higher condition numbers on whole domain. On one hand, we found solutions on truncated domain with $b = \beta$ near $E_{\max} = -0.225$. These numerical parameters are close to those used in HS's work. However, the condition number is still high ($\sim 10^{13}$). Solutions with high condition numbers (close to a reciprocal of machine precision) are generally less trustful (e.g. Section 3.3 of Walter, 2014). Also, as done in (Heggie and Stevenson, 1988), we had to shorten the size of Newton step to less than 0.1 to find those solutions using Newton iteration method, which costed an unfeasible CPU time.

F.2 Modifying the regularization of variable v_F in the ss-OAFP system

We employed the following modification that provides a sensible condition to find the both HS's and reference-solutions only by controlling E_{\max}

$$v_F^{(m)} = \ln \left(\exp[v_F] \left[\frac{1+x}{2} \right]^\beta \right). \quad (\text{F.2})$$

We solved the ss-OAFP system for $v_F^{(m)}$ and unmodified variables v_S , v_Q , v_G , v_I , v_J and v_R using the procedure of Section 3.2. In a similar way to the $v_R^{(m)}$ -formulation (Sections 6.2 and 6.3), the spectral solution based on $v_F^{(m)}$ -formulation is close to the HS's solution for small E_{\max} while it also can be close to the reference solution for small E_{\max} (See Table F.9 in which $(v_F^{(m)}, v_R)$ is the corresponding result). Due to the logarithmic endpoint singularity of $v_F^{(m)}$, the Chebyshev coefficients $\{F_n^{(m)}\}$ for $v_F^{(m)}$ show slow decays for both large- and small- E_{\max} (Figure F.33). A more distinct slow decay appears in Chebyshev coefficients $\{I_n\}$ for v_I especially when E_{\max} is large (Figure F.34). Interestingly, the value of $v_I(x=1)$ is still order of 10^{-4} for large E_{\max} that is the same order as the value given by the modified function $v_R^{(m)}$ in Sections 6.2 and 6.3. This infers that the HS's solution may be obtained when a numerical scheme has a low accuracy and E_{\max} is small (≈ -0.225). This condition occurred to our spectral solutions when we intentionally included the non-analytic and non-regular properties in the solutions and so Chebyshev coefficients decayed slowly. The modified function $v_F^{(m)}$ provides the HS's solution only for small \mathcal{N} , hence one may further be able to find the HS's solution with larger \mathcal{N} by controlling the singularities in independent variables.

F.3 Combination of modified variables ($v_R^{(m)}$, $v_F^{(m)}$) to find the HS's solution with high degree of Chebyshev polynomials

Double modification ($v_R^{(m)}$, $v_F^{(m)}$) provides a proper feature of ss-OAFP solutions in the sense that one can obtain the reference- and HS's solutions for high degrees ($\mathcal{N} = 80 \sim 200$). The results of Appendix F.2 shows that slowing the rapid decay in Chebyshev coefficients is also a key to find the both HS's and reference solutions based on a single formulation. Hence, we combined the two formulations of Appendix F.2 and Section 6.3. As expected, we found the HS's and reference- solutions only by controlling the value of E_{\max} based on double modification ($v_R^{(m)}$, $v_F^{(m)}$). This double modification provided spectral solutions that can reach high degree, such as $\mathcal{N} = 200$ for $E_{\max} = -0.225$, while it also provided a spectral solution close to the reference solution for $E_{\max} = -0.04$ and $\mathcal{N} = 80$ (Table F.9). One may conclude that the HS's solution can be found around for small $E_{\max} (\approx -0.225)$ with low accuracy ($v_I(x=1) = \mathcal{O}(10^{-4})$) while the reference solution can be found for large $E_{\max} (\approx -0.05)$ with high accuracy (at least $v_J(x=1) = \mathcal{O}(10^{-6})$). Also, the Chebyshev coefficients $\{F_n\}$ and $\{I_n\}$ show a distinctive difference between the two solutions. The coefficients $\{F_n\}$ decay in different fashions depending on the combination of modifications for v_F and v_R (Figure F.33) while the absolute values of $\{I_n\}$ stall approximately at $10^{-4} \sim 10^{-5}$ for $E_{\max} \approx -0.25$ and at $10^{-6} \sim 10^{-7}$ for $E_{\max} \approx -0.05$ (Figure F.34). The latter would well reflect the fact that $\{I_n\}$ is directly associated with v_I and β that are more stable against numerical parameters compared to c_4 , accordingly v_F .

function	n	E_{\max}	β	c_1	c_4	$ v_I(x=1) $
$(v_F^{(m)}, v_R)$	15	-0.24	8.181	9.1014×10^{-4}	3.516×10^{-1}	3.3×10^{-4}
$(v_F, v_R^{(m)})$	15	-0.24	8.1731	9.1023×10^{-4}	3.524×10^{-1}	2.1×10^{-4}
$(v_F^{(m)}, v_R^{(m)})$	200	-0.225	8.175860	9.1018×10^{-4}	3.523×10^{-1}	2.9×10^{-4}
$(v_F^{(m)}, v_R)$	70	-0.00525	8.1783712	9.0925×10^{-4}	3.304×10^{-1}	2.2×10^{-6}
$(v_F, v_R^{(m)})$	200	-0.04	8.178371129	9.0925×10^{-4}	3.301×10^{-1}	4.9×10^{-7}
$(v_F^{(m)}, v_R^{(m)})$	80	-0.04	8.1783683	9.0926×10^{-4}	3.301×10^{-1}	8.9×10^{-7}

Table F.9: Eigenvalues and $|v_I(x=1)|$ for combinations of $v_R^{(m)}$ and $v_F^{(m)}$. The upper three rows are the data that reproduced the HS's eigenvalues while the lower three rows are the data that reproduced three significant figures of the reference eigenvalues. In the modified ss-OAFP systems, the variables v_S, v_Q, v_G, v_I and v_J are not modified

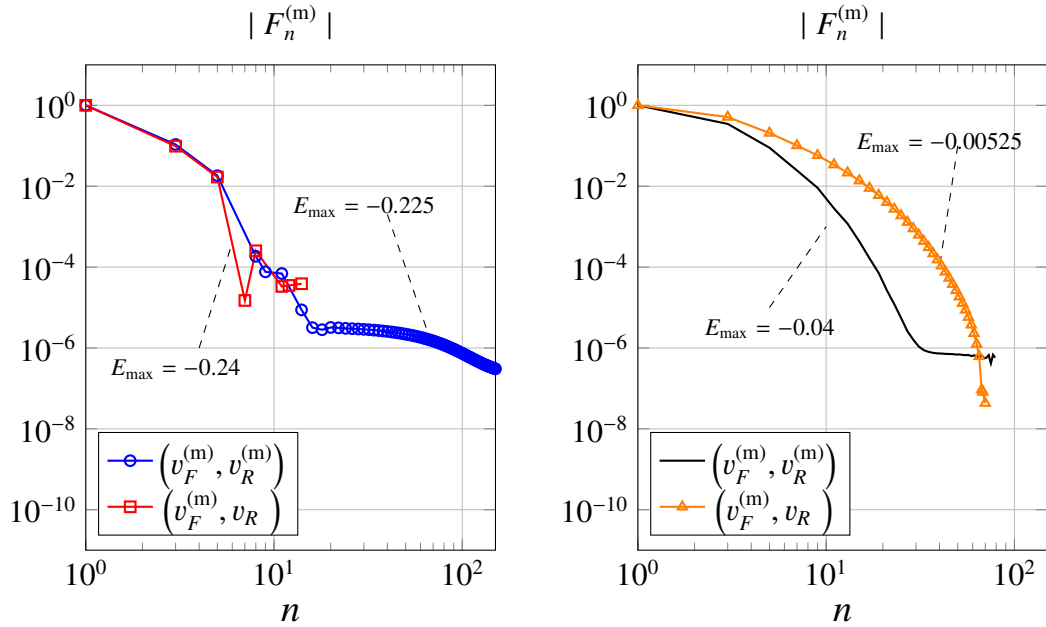


Figure F.33: Absolute values of Chebyshev coefficients $\{F_n^{(m)}\}$ for $v_F^{(m)}$. In the modified ss-OAFP system, v_S, v_Q, v_G, v_I and v_J are not modified. The maximum values E_{\max} of the truncated domains are also depicted in the figure.

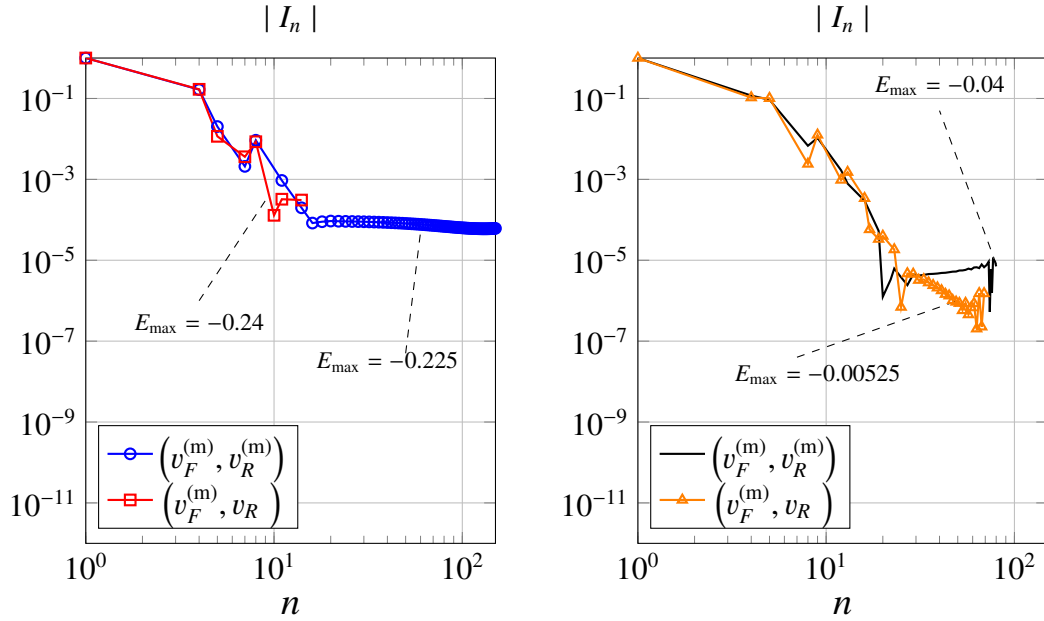


Figure F.34: Absolute values of Chebyshev coefficients $\{I_n\}$ for v_I . In the modified ss-OAFP system, v_S, v_Q, v_G, v_I and v_J are not modified. The maximum values E_{\max} of the truncated domains are also depicted in the figure.

- Antonov, V. A., 1985. Most probable phase distribution in spherical star systems and conditions for its existence. Symposium - International Astronomical Union 113, 525–540.
 URL <https://doi.org/10.1017%2Fs007418090014776x>
- Baumgardt, H., Heggie, D. C., Hut, P., Makino, J., may 2003. Parameters of core collapse. Monthly Notices of the Royal Astronomical Society 341 (1), 247–250.
 URL <https://doi.org/10.1046%2Fj.1365-8711.2003.06407.x>
- Baumgardt, H., Hut, P., Heggie, D. C., nov 2002. Long-term evolution of isolated n-body systems. Monthly Notices of the Royal Astronomical Society 336 (4), 1069–1081.
 URL <https://doi.org/10.1046%2Fj.1365-8711.2002.05736.x>
- Bhrawy, A., Alofi, A., jan 2012. A jacobi–gauss collocation method for solving nonlinear lane–emden type equations. Communications in Nonlinear Science and Numerical Simulation 17 (1), 62–70.
 URL <https://doi.org/10.1016%2Fj.cnsns.2011.04.025>
- Binney, J., Tremaine, S., 2011. Galactic Dynamics. Princeton university press.
- Boyd, J. P., 2001. Chebyshev and Fourier Spectral Methods. Courier Corporation.
- Boyd, J. P., oct 2008. Evaluating of dawson’s integral by solving its differential equation using orthogonal rational chebyshev functions. Applied Mathematics and Computation 204 (2), 914–919.
 URL <https://doi.org/10.1016%2Fj.amc.2008.07.039>
- Boyd, J. P., may 2013. Rational chebyshev series for the thomas–fermi function: Endpoint singularities and spectral methods. Journal of Computational and Applied Mathematics 244, 90–101.
 URL <https://doi.org/10.1016%2Fj.cam.2012.11.015>
- Căruntu, B., Bota, C., jul 2013. Approximate polynomial solutions of the nonlinear Lane–Emden type equations arising in astrophysics using the squared remainder minimization method. Computer Physics Communications 184 (7), 1643–1648.
 URL <http://dx.doi.org/10.1016/j.cpc.2013.01.023>
- Cody, W. J., Paciorek, K. A., Thacher, H. C., jan 1970. Chebyshev approximations for dawson’s integral. Mathematics of Computation 24 (109), 171–171.
 URL <https://doi.org/10.1090%2Fs0025-5718-1970-0258236-8>
- Cohn, H., dec 1979. Numerical integration of the fokker-planck equation and the evolution of star clusters. The Astrophysical Journal 234, 1036.
 URL <https://doi.org/10.1086%2F157587>
- Cohn, H., dec 1980. Late core collapse in star clusters and the gravothermal instability. The Astrophysical Journal 242, 765.
 URL <https://doi.org/10.1086%2F158511>
- Giersz, M., Spurzem, R., jul 1994. A comparison of direct n-body integration with anisotropic gaseous models of star clusters. Monthly Notices of the Royal Astronomical Society 269 (2), 241–256.
 URL <https://doi.org/10.1093%2Fmnras%2F269.2.241>
- Gilbert, I. H., jun 1968. Collisional relaxation in stellar systems. The Astrophysical Journal 152, 1043.
 URL <https://doi.org/10.1086%2F149616>
- Goodman, J., may 1984. Homologous evolution of stellar systems after core collapse. The Astrophysical Journal 280, 298.

- URL <https://doi.org/10.1086%2F161996>
- Heggie, D. C., Stevenson, D., jan 1988. Two homological models for the evolution of star clusters. *Monthly Notices of the Royal Astronomical Society* 230 (2), 223–241.
URL <http://dx.doi.org/10.1093/mnras/230.2.223>
- Hénon, M., Feb. 1961. Sur l'évolution dynamique des amas globulaires. *Annales d'Astrophysique* 24, 369.
- Ito, Y., Jan 2018a. A convergent kinetic theory of collisional star clusters (i) a self-consistent 'truncated' mean-field acceleration of stars. arXiv e-prints, arXiv:1801.04903.
- Ito, Y., Aug 2018b. A generalized Landau kinetic equation for weakly-coupled probability distribution of N-stars in dense star cluster. arXiv e-prints, arXiv:1808.10294.
- Ito, Y., Mar. 2020a. Self-similar orbit-averaged Fokker-Planck equation for isotropic spherical dense clusters (ii) Physical properties and negative heat capacity of pre-collapse core. arXiv e-prints, arXiv:2003.13179.
- Ito, Y., Mar. 2020b. Self-similar orbit-averaged Fokker-Planck equation for isotropic spherical dense clusters (iii) Application to Galactic globular clusters. arXiv e-prints, arXiv:2004.00747.
- Ito, Y., Poje, A., Lancellotti, C., jan 2018. Very-large-scale spectral solutions for spherical polytropes of index $m \lesssim 5$ and the isothermal sphere. *New Astronomy* 58, 15–28.
URL <https://doi.org/10.1016%2Fj.newast.2017.07.003>
- Jeans, J. H., jan 1902. The stability of a spherical nebula. *Philosophical Transactions of the Royal Society A: Mathematical, Physical and Engineering Sciences* 199 (312-320), 1–53.
URL <http://dx.doi.org/10.1098/rsta.1902.0012>
- Luciani, J. F., Pellat, R., jun 1987. On the antonov criterion for gravothermal instability. *The Astrophysical Journal* 317, 241.
URL <https://doi.org/10.1086%2F165272>
- Lynden-Bell, D., Eggleton, P., jul 1980. On the consequences of the gravothermal catastrophe. *Monthly Notices of the Royal Astronomical Society* 191 (3), 483–498.
URL <http://dx.doi.org/10.1093/mnras/191.3.483>
- Mason, J., Handscomb, D., sep 2002. Chebyshev Polynomials. Informa UK Limited.
URL <http://dx.doi.org/10.1201/9781420036114>
- Meylan, G., 1987. Studies of dynamical properties of globular clusters. iii-anisotropy in omega centauri. *Astronomy and Astrophysics* 184, 144–154.
- Meylan, G., Heggie, D., feb 1997. Internal dynamics of globular clusters. *Astronomy and Astrophysics Review* 8 (1-2), 1–143.
URL <https://doi.org/10.1007%2Fs001590050008>
- Parand, K., Shahini, M., 2010. Rational Chebyshev collocation method for solving nonlinear ordinary differential equations of Lane-Emden type. *International Journal of Information and Systems Sciences* 6, 72.
- Pavlík, V., Šubr, L., dec 2018. The hunt for self-similar core collapse. *Astronomy & Astrophysics* 620, A70.
URL <https://doi.org/10.1051%2F0004-6361%2F201833854>
- Polyachenko, V. L., Shukhman, I. G., Apr. 1982. Collisions in Spherical Stellar Systems. *Soviet Astronomy* 26, 140–145.
- Spitzer, L. S., jan 1988. *Dynamical Evolution of Globular Clusters*. Walter de Gruyter GmbH.
URL <http://dx.doi.org/10.1515/9781400858736>
- Szell, A., Merritt, D., Kevrekidis, I. G., aug 2005. Core collapse via coarse dynamic renormalization. *Physical Review Letters* 95 (8).
URL <https://doi.org/10.1103%2Fphysrevlett.95.081102>
- Takahashi, K., 1993. Self-similar solutions of the orbit-averaged fokker-planck equation: Application of the generalized variational principle. *Publications of the Astronomical Society of Japan* 45, 789–793.
- Takahashi, K., 1995. Fokker-planck models of star clusters with anisotropic velocity distributions i. pre-collapse evolution. *Publications of the Astronomical Society of Japan* 47, 561–573.
- Takahashi, K., Inagaki, S., 1992. Application of the generalized variational principle to self-similar solutions for the evolution of star clusters. *Publications of the Astronomical Society of Japan* 44, 623–631.
- Walter, É., 2014. *Numerical Methods and Optimization*. Springer International Publishing.
URL <https://doi.org/10.1007%2F978-3-319-07671-3>
- Xiang, S., sep 2013. On convergence rates of fejer and gauss–chebyshev quadrature rules. *Journal of Mathematical Analysis and Applications* 405 (2), 687–699.
URL <https://doi.org/10.1016%2Fj.jmaa.2013.04.027>